USE OF SATELLITE DATA IN MONITORING AND PREDICTION OF RAINFALL OVER KENYA

By

Gilbert Ong'isa Ouma

Department of Meteorology

Faculty of Science

University of Nairobi

A thesis submitted in partial fulfillment of the requirements for the degree of Doctor of Philosophy in Meteorology, University of Nairobi, Kenya

AUGUST, 2000

DECLARATION

This thesis is my original work and has not been presented for a degree in any other University

Signature 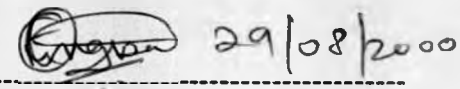 29/08/2000

Gilbert O. Ouma

This thesis has been submitted for examination with our approval as University Supervisors

Signature  35/8/00

Professor Laban A. Ogallo

Department of Meteorology

University of Nairobi

Signature 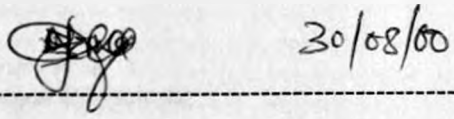 30/08/00

Dr. Nzioka J. Muthama

Department of Meteorology

University of Nairobi

TABLE OF CONTENTS

Abstract

Skillful monitoring, prediction and early warning of the extreme weather events is crucial in the planning and management of all rain dependent socio-economic activities. They are also vital for the development of effective disaster preparedness strategies. Prediction methods depend on availability of long period, high quality data with good spatial coverage. Real and near real time data are also useful as initial conditions for the integration of prediction models. Thus, high quality data with good spatial and temporal coverage is fundamental for any research and applications. Unfortunately, limitation of rainfall data is a serious problem in many parts of the world, especially in the developing countries.

This study investigated the viability of satellite derived data in providing alternative rainfall information and hence enhancing rainfall monitoring, prediction and disaster preparedness in Kenya. The data sets used in the study included observed daily rainfall, dekadal Cold Cloud Duration (CCD) and pentad Total Precipitable Water (TPW) data together with the reanalysis data from ECMWF.

The various methods that were used to achieve the objectives of the study included data quality analyses, S-mode Principal Component Analysis (PCA) together with correlation and regression analyses. The regression models used included simple linear, stepwise and canonical regression approaches. The skills of the developed models were further investigated during anomalous wet and dry periods. Meteorological conditions that could be associated with the decreased or increased skill of the regression models during the anomalous periods were also investigated.

The results obtained from the quality control tests indicated that all data used in the study were of good quality. The S-mode PCA solutions delineated eleven regions for March-April-May (MAM), June-July-August (JJA) and December-January-February (DJF) seasons, while only nine were delineated for the September-October-November (SON) season from the

rainfall data. The number of significant PCA modes was higher for the dry seasons of JJA and DJF as compared to those from the wet seasons of MAM and SON. However, these components extracted relatively low percentage of total variance in the observed rainfall and hence the development of regression models concentrated on the wet seasons of MAM and SON. Although the duration of the satellite-derived data available was shorter, the regions derived from this data set were generally consistent with those obtained using the rainfall data.

The results from correlation analyses showed significant linear relationships between rain gauge rainfall and only CCD data. The results of ANOVA tests on the linear regression models indicated that the developed models had reasonable skill in estimating rainfall from CCD data. Results from stepwise regression analyses of rain gauge rainfall, CCD and the three layers of TPW data indicated that the additional variance explained by the inclusion of TPW data were generally low. It was, however, evident that, in some regions, the inclusion of TPW in the estimation models was of added value. The examinations of the skill of the models during anomalous dry and wet periods revealed better performance during the anomalous seasons. The composites of the meteorological conditions showed that for the anomalous dry seasons, a westerly component exists in the equatorial winds (surface to 800 mb layer) that interferes with the supply of moisture from the Indian Ocean and lead to a reduction in the amount of moisture available inland. During anomalous wet seasons, the southeasterly flow inland is very strong enhancing the moisture influx from the Indian Ocean.

The last part of the study examined the more complex Canonical Correlation Analysis (CCA) in the development of estimation and forecasting models. The results from the CCA indicated significant year to year variations in the skills for the estimated areal observed rainfall from satellite-derived data. A comparison of the CCA models results to those of the stepwise regression revealed that the CCA models performed considerably better during the

SON season in estimating the areal observed rainfall. The results from the forecasting models revealed that the canonical correlation coefficients based on CCD data were all not statistically significant in all locations and seasons. Results obtained from analyses of TPW data, however, indicated some skill in forecasting of rainfall with SON season registering higher canonical correlation coefficients.

This study has, for the first time, regionalized Kenya into seasonal climatological homogeneous zones using satellite-derived data. It has also developed statistical models based on satellite-derived data that can be used to estimate areal rainfall for the derived climatological zones. The study further highlights the vital need to use distinct CCD temperature thresholds for rainfall estimation for individual climatological zones and seasons. Finally, it is the first time that a study has used CCA technique for the estimation of areal rainfall from satellite-derived data in Kenya. CCA predictors were also derived for areal rainfall forecasting. The complex CCA approach improved skills in the rainfall estimates during some seasons that had relatively poor skills with the other methods.

In conclusion, the study has for the first time provided some useful information regarding the enormous potential use of satellite-derived data in the estimation of 10-day areal rainfall for specific regions in Kenya. The results from the PCA regionalization show that the satellite-derived data can be used to delineate large-scale spatial anomalies in the rainfall over the study region. Accurate delineation of these anomalies is vital in drought monitoring, flash flood forecasting and general preparedness against extreme weather events.

TABLE OF FIGURES

LIST OF TABLES

LIST OF ACRONYMS AND SPECIAL TERMS

1D-VAR	One Dimensional Variation
ADMIT	Agricultural Drought Monitoring Integrated Technique
AIC	Akaike's Information Criterion
ANOVA	Analysis of Variance
ASALS	Arid and Semi-Arid Lands
BIAS	Bristol/NOAA Interactive Scheme
CCA	Canonical Correlation Analysis
CCD	Cold Cloud Duration
CCR	Cloud Cleared Radiance
CFA	Common Factor Analysis
CL	Confidence Level
CST	Convective Stratiform Technique
CWV	Column Water Vapor
DJF	December-January-February
DMSP	Defense Meteorological Satellite Project
EBBT	Equivalent Black Body Temperature
ECMWF	European Centre for Medium-range Weather Forecasts
EOF	Empirical Orthogonal Functions
EPI	ESOC Precipitation Index
ERA	ECMWF Re-Analysis
ESA	European Space Agency
ESMR	Electrically Scanning Microwave Radiometer
ESOC	European Space Operation Centre
GARP	Global Atmospheric Research Program

GATE	GARP Atlantic Tropical Experiment
GMS	Geostationary (Geosynchronous) Meteorological Satellite
GOES	Geostationary Operational Environmental Satellites
GOES-E	GOES East
GPI	GOES Precipitation Index
GSCAT2	Goddard Scattering Algorithm version 2
GTS	Global Telecommunications System
HIRS	High Resolution Infrared Radiation Sounder
INSAT	Indian Satellite
IR	Infrared
ISCCP	International Satellite Cloud Climatology Project
ITCZ	Inter Tropical Convergence Zone
JJA	June-July-August
JKIA	Jomo Kenyatta International Airport
K-L	Kullback-Liebler
MAM	March-April-May
METEOSAT	Meteorological Satellite
MSE	Mean Square Error
MSG	METEOSAT Second Generation
MSU	Microwave Sounding Unit
NASA	National Aeronautics and Space Administration
NCAR	National Center for Atmospheric Research
NESDIS	National Environmental Satellite Data and Information Service
NESS	National Environmental Satellite Service
NOAA	National Oceanic and Atmospheric Administration

NOAA-SRL	NOAA Satellite Research Laboratories
NVAP	NASA Water Vapor Project
NWP	Numerical Weather Prediction
OF-HPP	Owen Falls Hydroelectric Power Plant
PCA	Principal Component Analysis
PCs	Principal Components
PCT	Polarization-Corrected Temperature
PM	Passive Microwave
POT	Percent-Of-Total
RCSSMRS	Regional Centre for Services in Surveying, Mapping and Remote Sensing
SHARP	Short Term Automated Radar Prediction
SMMR	Scanning Multi-channel Microwave Radiometer
SSM/I	Special Sensor Microwave/Imager
SON	September-October-November
SST	Sea Surface Temperature
SSU	Stratospheric Sounding Unit
TIROS	Television Infrared Observation Satellite
TOVS	TIROS Operational Vertical Sounder
TPW	Total Precipitable Water
UTH	Upper Tropospheric Humidity
VIS	Visible

CHAPTER ONE

INTRODUCTION

1.0 Introduction

One of the major forcing mechanisms of the general circulation is the tropical convection with its attendant release of latent heat. Good knowledge of its space-time variability, and detailed monitoring of its day to day evolutions are crucial for the proper understanding of the dynamics of the global climate system and improvement of prediction skills.

In equatorial Africa, as in all other tropical regions, one of the most important climatic elements is rainfall due to its large spatial and temporal variability. This high variability has a major impact on the socio-economic activities of the countries within this region since their economies depend mainly on the rain-fed agriculture. Agriculture and the associated industries are also the major employment sectors in the region. Extreme rainfall anomalies like droughts and floods often have far reaching socio-economic impacts in the region including a decrease in food production and agricultural exports, famine, mass migration of people and animals, environmental refugees, loss of life and property among many other socio-economic miseries. Skillful prediction of the onset, duration, amount, intensity, and cessation of rainfall expected during any season is crucial in the planning and management of agricultural activities and, by extension, economies of these countries. Skillful prediction of rainfall would also be useful in early warning of any impending extreme rainfall events, and enable proper disaster preparedness policies to be adopted in time, in order to avoid the post disaster relief policies that are common in the region.

A good example of the need for emergency mitigation policies was witnessed in Kenya during the extreme floods that were associated with the 1997/98 El-Niño phenomenon. Over 80% of Kenya may be classified as arid and semi arid lands (ASALs) that have very high year to year rainfall variability. During the period 1996 – 1997, for instance, the region experienced a prolonged drought that forced the government of Kenya to declare a National Famine Disaster Emergency. Extreme floods, associated with El-Niño phenomena, soon followed in 1997 – 1998 and these caused heavy damage to the country's infrastructure, and loss of human and animal life. This was followed by another drought that started in 1999 and persisted into the year 2000 in many parts of Kenya. The 1999-2000 drought was considered as one of the worst in the century. During the times of such national disasters, resources meant for other development projects are diverted to the management and mitigation of the effects of these rainfall-related problems. Such extreme events are capable of seriously depressing the economy of many developing nations.

For proper planning and management, disaster management policies are required if the impacts of meteorological disasters that are very common in Kenya are to be minimized. The disaster preparedness component requires, among others, effective early warning system, which can provide good lead-time warning of any potential disasters. Such early warning systems are derived from various prediction models, which are integrated using initial condition data. Data for defining the initial conditions and the development of the prediction models must be of good quality, and must have good spatial and temporal coverage. The study of the processes and the development of the predictive models also require long periods of such data. Data insufficiency is a serious problem in many parts of the world and, especially, in the developing countries.

Accurate measurement and monitoring of precipitation is therefore important in the planning and management of all water-use activities. Long period, high quality data with good spatial density are also required in order to study the past rainfall evolutions and help to improve prediction models

for rainfall. All prediction models attempt to use various ways to extrapolate the future from the available information about the past and the present.

Standard rain gauges are the most accurate means of measuring rainfall at a point since they give a reading of the actual rain collected at that point. However, they give accurate information only at single point locations since, by their nature, they measure what is trapped in the container. Tropical air masses are generally unstable with strong components of micro and meso scale circulations that are closely teleconnected with the global general circulation. Regional features, like topography and the existence of large water bodies, also have significant modification on the space-time patterns on rainfall over Kenya. The topography of the study region, Kenya, as is shown in Figure 1.1, is very complex and this enhances the spatial variability of rainfall whose measurement may only, therefore, be adequately done using a very dense network of rain gauges. However, the rain gauge network available in this region is relatively sparse especially over remote areas. Furthermore, the cost of development and maintenance of a dense rain gauge network would be extremely expensive for a developing country like Kenya. Using rain gauges is further compounded by the interrelated factors of wind, siting and gauge design.

Many efforts have therefore been made to find alternative methods of rainfall monitoring both in space and time. These problems have led to the exploration of the potential use of ground-based weather radar and satellite-based techniques as alternative methods of estimating rainfall. For example, attempts have been made to estimate rainfall using the weather radar based on the transmitted microwave radiation into space and then monitoring the backscattered microwave energy. The strength of the backscattered radiation depends on the raindrops in the path of the transmitted radiation. An empirical relationship is developed that is then used to convert the backscattered radiance into a measure of rainfall.

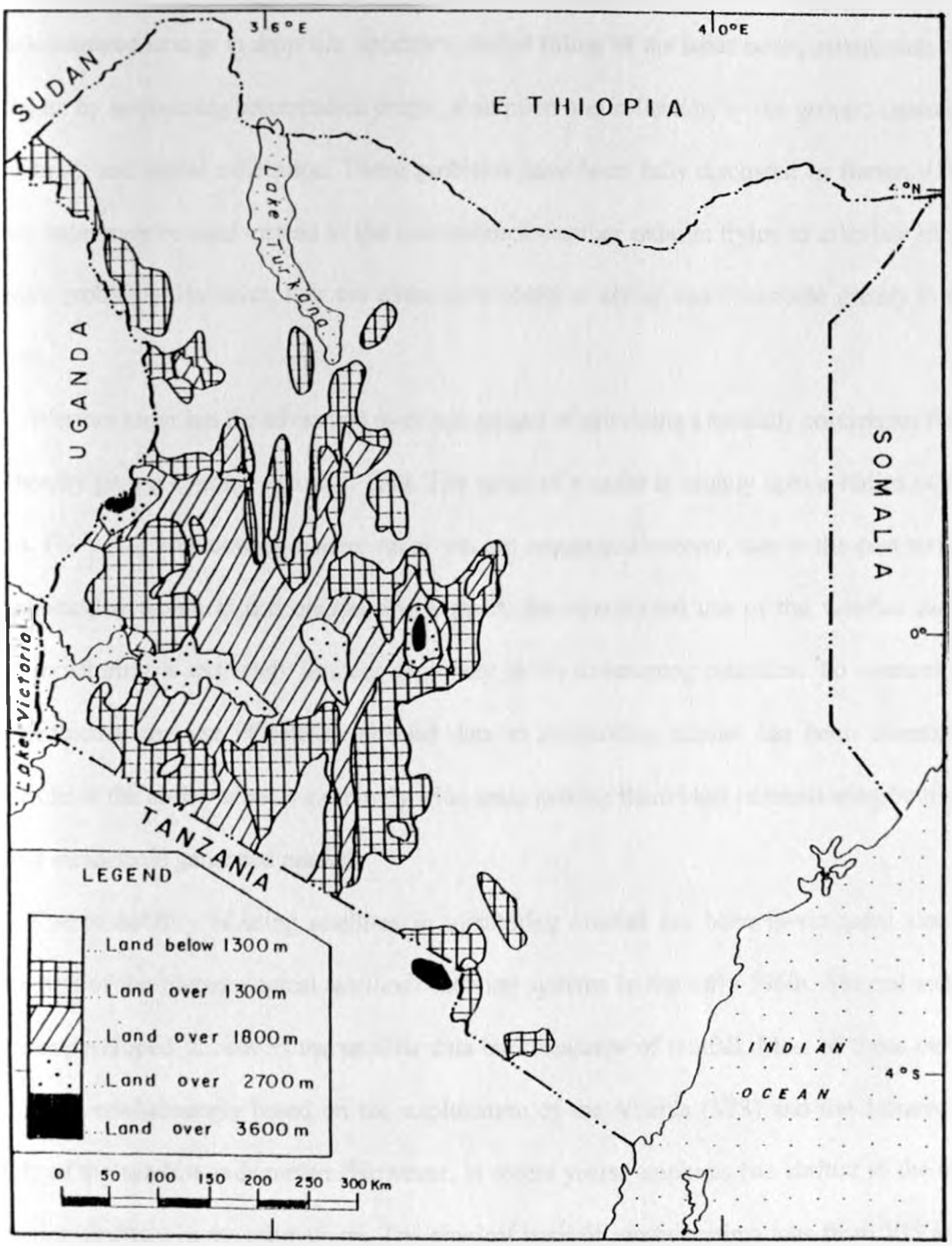

Figure 1.1: Relief map of Kenya (Source: Kenya Meteorological Department Research Report. No. 8/79)

However, the weather radar has some problems relating to the proper relationship between the back-scattered energy to drop size spectrum, partial filling of the radar beam, attenuation of the radar beam by intervening precipitation drops, absorption and reflection by the ground (anomalous propagation), and signal calibration. These problems have been fully discussed in Battan (1973). Doppler radar may be used instead of the conventional weather radar in trying to alleviate some of the above problems. However, they are even more costly to set up and contribute greatly to noise pollution.

Weather radar has the advantage over rain gauges of providing a spatially continuous field of view thereby giving continuos flow of data. The range of a radar is usually upto a radius of about 200 km. For wider area coverage, more radar sets are required. However, due to the cost and need for sophisticated technical and engineering support, the operational use of the weather radar in rainfall monitoring is extremely limited, especially in the developing countries. To overcome the above problems, the use of satellite-derived data in monitoring rainfall has been investigated. Satellites have the ability to view extremely wide areas making them ideal in monitoring both large-scale and meso-scale generated rainfall.

The probability of using satellites in monitoring rainfall has been investigated since the inauguration of the meteorological satellite observing systems in the early 1960s. Several methods have been developed to convert the satellite data into measures of rainfall. Most of these methods have been overwhelmingly based on the exploitation of the Visible (VIS) and the Infrared (IR) channels of the satellite radiometers. However, in recent years, emphasis has shifted to the use of microwave windows in the estimations. The physical basis of rainfall estimations from VIS and IR imagery depend on the supposition that inference of rain falling out of the base of a cloud may be made from the analysis of the cloud-top characteristics which are monitored by the satellites. In the VIS imagery, the brightest clouds, which are more reflective because of their thickness, may be the

most likely to precipitate while in the IR imageries the clouds with the coldest tops, and therefore those with the highest tops, are the most likely to precipitate. The disadvantage of using techniques dependent on VIS and IR images is the physical indirectness of the relationship between the characteristics at the top of the clouds and the processes that are taking place at their bases. The characteristics considered are just proxies of the temperature and liquid content of the clouds (Kidd and Barrett, 1990).

Imagery from selected passive microwave (PM) windows can be used to provide information of alternative or additional value for rainfall monitoring purposes. It was demonstrated, using data from the pioneering instrument ESMR (the Electrically Scanning Microwave Radiometer) on Nimbus-5 as early as in mid-1970s, that naturally emitted PM radiation in particular frequencies, from the earth's lower atmosphere and surface can be measured and analyzed to give pictures of instantaneous rainfall intensities. This was found to be true at least over sea surfaces. It has now been shown that PM radiation is valuable for rainfall monitoring purposes over both land and sea areas (Kidd and Barrett, 1990). The physical basis of monitoring rainfall through PM radiation windows is dependent on the fact that PM radiation at certain frequencies are attenuated mainly by rain drops in the atmosphere. Techniques using PM therefore depend on a physical relationship between the liquid water in the clouds and the final precipitation rather than proxy information in their estimation procedures.

However, the applications of the satellite-derived methods in the monitoring of rainfall also have problems that create errors in the estimates. The VIS channels can only be used during daytime while the IR channels are likely to give erroneous measurements during periods of large-scale subsidence due to the inherent problems in the IR radiative transfer equation. The microwave channels are, at the moment, only useful over large water bodies since the emissivity of land and clouds are comparable. Additionally, all satellite procedures are hampered by the surface resolutions

of the satellites. The footprints of most satellites are at least 5 km (as in the case of METEOSAT). The next generation satellites, like METEOSAT Second Generation (MSG) set to be launched in the year 2002, are going to solve this problem with better resolutions.

Inspite of the above mentioned problems, satellite-derived methods of estimation of rainfall give very useful additional precipitation information, especially in areas with sparse rain gauge observation network. They also provide near-real time precipitation data. However, they have to be calibrated using other available rainfall observations ("ground truth"). Measurements of rainfall from rain gauges and/or weather radar are usually used as "ground truth" in these cases. This study looks at the possibilities of using satellite derived data in rainfall monitoring and forecasting over Kenya. The details of the objectives of the study are in the next section.

1.1 The Objectives of the Study

The overall objective of the study is to investigate the viability of using satellite derived data as a means of enhancing rainfall monitoring and forecasting over Kenya. This objective will be achieved by addressing the following specific objectives:

(i) Regionalization of the study region into homogeneous climatic zones based on 10-day rain gauge and satellite-derived records. The delineated zones from the different sets of data will be compared.

(ii) The development of empirical functions for the relationships between various types of satellite data and rain gauge rainfall for each of the homogenous rainfall zones based on (i).

(iii) Investigation of the skill of the derived models during anomalous wet/dry seasons.

(iv) The study of the evolution of 10-day/seasonal rainfall and general circulation patterns, in order to identify the systems that could be associated with the low or high skills of the satellite derived estimates during anomalous wet/dry years.

(v) Determination of the relationships between the rain gauge and satellite-derived records in attempts to derive potential predictors of rain gauge rainfall records from satellite-based data.

1.2 Justification for the Study

Extreme rainfall anomalies like floods and droughts, in Kenya usually result in untold suffering of the people leading to loss of life and massive damage to property and infrastructure. It is, therefore, imperative that timely and accurate weather forecasts and climate prediction be made for the study region in order to reduce the vulnerability of the society to climate related disasters. Accurate weather forecasts and climate prediction require adequate and accurate observations as inputs in either the conventional forecasting procedures or the numerical forecasting techniques. One of the problems encountered in the region is lack of an adequate set of observations for use in forecasting.

Furthermore, the economy of the study region, Kenya, is highly dependent on agriculture and hence rainfall dependent. The existing station network used in rainfall measurements is highly concentrated in the densely populated and most accessible areas, but sparse in the remote areas, which unfortunately cover over 80% of the country. Rainfall data are also required in the planning and management of all rainfall dependent activities such as water resources, hydropower resources, building and construction, agricultural activities, among many others. The study attempts to augment the existing station network to give timely and spatially representative coverage for better forecasts, and hence enhance the use of rainfall information in sustainable national development efforts.

The study region includes the world's second largest fresh water lake, Victoria. The lake is of great economic importance in the region. It provides a livelihood to a large percentage of the region's populace through fishing activities. It is also used for transportation in the transfer of

goods between the three East African states (Kenya, Uganda and Tanzania) and beyond. Most importantly, the lake is the source of river Nile on which the Owen Falls HydroElectric Power Plant (OF-HPP) is built. The OF-HPP plant supplies electricity to all three East African States. To sustain the current industrial development in the region, a considerable extra amount of energy is required. Fortunately, there exists the potential for expanding the OF-HPP and, currently, an extension is under construction to generate an extra 200MW.

The planning for hydroelectric power stations require an accurate estimation of the volume of water that will be used. In the case of the OF-HPP, an accurate estimation of the volume of water in the lake is important. The volume of water in the lake depends on the amount of rainfall received around its catchment (about 20%) and the actual amount received over the lake (about 80%) (Yin and Nicholson, 2000). The amount received in the catchment is usually estimated from the rain gauges installed in the area. However, the amounts over the lake are usually more difficult to quantify since the conventional methods of measuring rainfall are not readily available. Accurate estimates from satellite records would, therefore, be of immense value for the planning of the power generating stations over the region and help in the Kenya government's policy of industrialization.

The national water development plan lays strategies for the provision of tap water to every Kenyan. Such a dream cannot be achieved without good network of historical rainfall databases, which may also be used to compute the risk of some hydrological decisions.

With most of the high potential areas being highly populated, many people are currently being forced to move to the ASALs that cover over 80% of the country. Others are being forced to migrate to the urban centers. The national long-term development plan has addressed long term development of the ASALs and large cities as some of the key challenges to Kenya in the future. Data is the key limitation in assessing the vulnerability of such development plans. The data and

other information from this study can be used to fill some of this gap, and also in enhancing national early warning efforts in Kenya for extreme rainfall anomalies.

1.3 The Study Region

This section defines the physical location of the study region and gives an overview of the climatology of its rainfall.

1.3.1 Location of the Study Region

The study region is located within latitudes 5^0 N to 5^0 S, and longitudes 34^0 E to 42^0 E, and covers the whole of Kenya. It is situated within the Eastern African States, and is bounded by Uganda to the west, Tanzania to the southwest and south, Indian Ocean to the south and southeast, Somalia to the east, and Sudan and Ethiopia to the north. A map showing the location of the study region in Africa is given in Figure 1.2 while the list of stations is provided in Table 2.1.

1.3.2 Rainfall Climatology of the Study Region

Being in an equatorial region, the rainfall of the area is expected to be associated with synoptic scale circulation patterns like the convergent low-level winds in the Inter Tropical Convergence Zone (ITCZ) surface locations. However, superimposed on the synoptic-scale circulation patterns are meso-scale systems induced by regional factors such as complex topographical patterns, the existence of many large inland lakes and the proximity of the Indian Ocean (Ogallo, 1983; Basalirwa *et al.*, 1999).

Studies have shown that a higher percentage of annual rainfall over most of the study area is experienced during the MAM season (Okoola, 1996). However Camberlin and Wairoto (1997) show that the southeasterly lowlands receive most of its rainfall during the SON season. The mean annual rainfall map of the study region is shown in Figure 1.3.

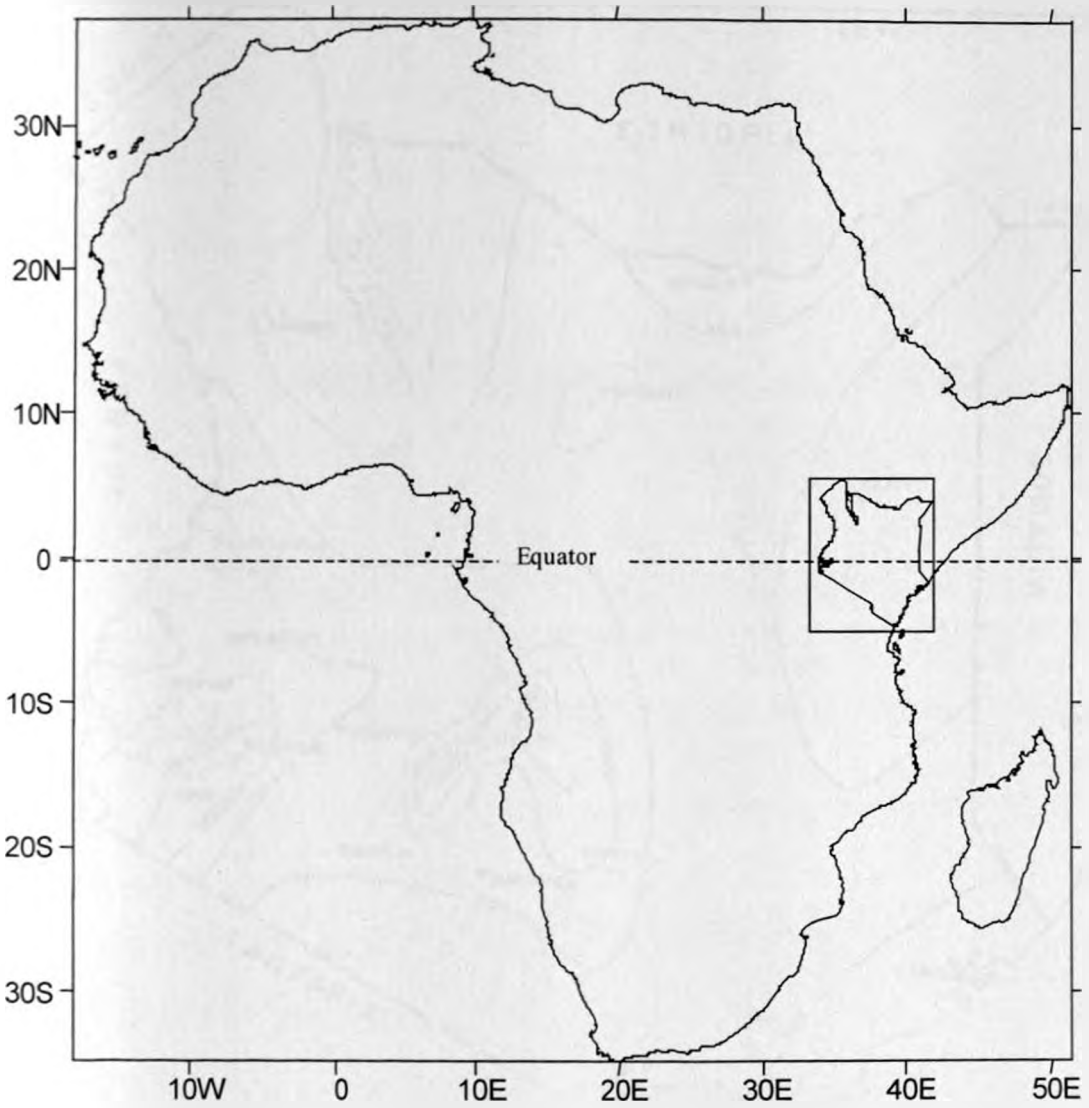

Figure 1.2: The location of the study area with respect to the continent of Africa

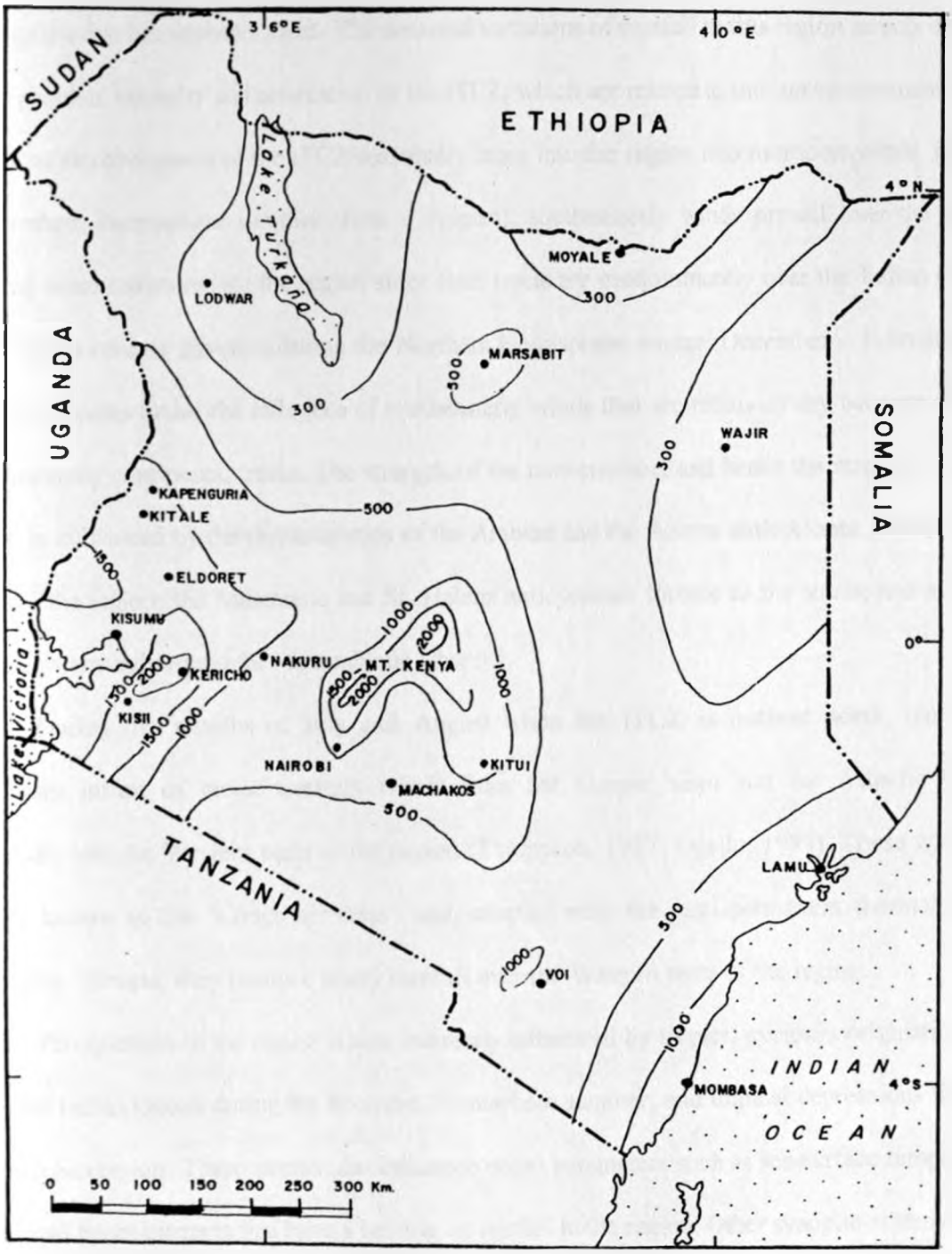

Figure 1.3: Mean annual rainfall map of the study area (Okoola, 1996)

Several large-scale and synoptic-scale features influence precipitation in the study region. The most important of these features is the ITCZ that is a broad low-pressure belt in which the trade winds of the two hemispheres meet. The seasonal variations of rainfall in this region largely depend on the position, intensity and orientation of the ITCZ, which are related to the sun's movements. The north - south movements of the ITCZ seasonally bring into the region two monsoon winds. During the Northern Hemisphere summer (June – August), southeasterly winds prevail over the region bringing some moisture into the region since their tracts are predominantly over the Indian Ocean. These winds reverse direction during the Northern Hemisphere winter (December – February) and the region comes under the influence of northeasterly winds that are relatively dry because of their predominantly continental tracks. The strength of the convergence, and hence the strength of these winds, is influenced by the characteristics of the Arabian and the Azores anticyclones located to the north of the region; the Mascarene and St. Helena anticyclones located to the south; and a trough located within and around the Mozambique Channel.

During the months of July and August when the ITCZ is furthest north, there is a maximum influx of moist westerly winds from the Congo basin and the Atlantic Ocean, especially into the Western parts of the region (Thompson, 1957; Ogallo, 1989). These winds are locally known as the "Congo air mass" and, coupled with the semi-permanent thermal trough over Lake Victoria, they produce heavy rainfall over the Western parts of the region.

Precipitation in the region is also indirectly influenced by tropical cyclones originating from southern Indian Ocean during the Southern Hemisphere summer, and tropical depressions from the Arabian Sea region. These storms also influence ocean parameters such as sea-surface temperatures (SST) and ocean currents that have a bearing on rainfall in the region. Other synoptic systems which control rainfall of the region include the Easterly waves, the Sub-Tropical Jetstreams, the East African low level jetstream, Tropical Easterly Jetstream and remnants of extra-tropical weather

systems (e.g. fronts) that are forced further south or north into the region. A discussion on the characteristics of some of the extra-tropical systems and their effects on the region's rainfall maybe found in Fremming (1970) and Njau (1982).

There are large spatial and temporal variations in climate over the study region caused by several regional features. These features include large inland lakes, like lakes Victoria, Nakuru and Turkana, and topographic features including several mountain ranges (Kenya, Abadares, and Elgon) and the Great Rift Valley that runs north to south through the study region. These physical features induce significant modifications in the general wind patterns over the region creating variations in the rainfall (Ogallo, 1989).

The following section reviews some of the literature that is relevant to the study.

1.4 Literature Review

Since the inauguration of the meteorological satellite observing systems in the early 1960s, several authors have investigated the possibility of monitoring rainfall from satellite altitudes. This section takes a look at the work that has already been done in line with this study. The review covers even areas different from the study region since not a lot of this line of research has been undertaken over this region.

Many methods have been developed in trying to convert the satellite data into estimates of rainfall. Martin and Scherer (1973) have reviewed some of the methods developed earlier. Barrett and Martin (1981) give an update of these methods in their review of those in use upto the end of 1970s. The earlier techniques of estimating rainfall from satellite data were mainly based on data from Visible (VIS) and Infrared (IR) channels. However in recent years, more emphasis has been laid on the use of Passive Microwave (PM) channels since these give data that have a more direct relationship with rainfall than does VIS- or IR-derived data. The satellite rainfall estimating methods

can be broadly classified as cloud indexing, life history, bispectral and cloud model, and passive microwave methods. In the next sections, these individual classes of methods are reviewed.

1.4.1 Cloud indexing methods

The cloud indexing methods use cloud indices, for example the fractional area covered by raining clouds, derived from VIS and/or IR images to estimate rainfall. The algorithms developed for these methods are generally simple and can be run on most of the available desktop personal computer systems. The requirements, in terms of computer software and hardware are minimal. Therefore, they have been applied to a wide range of climatic conditions as defined by latitudinal zones and/or continental or maritime characteristics.

Two of the most applied families of cloud indexing methods have their origins in the Applications Group of the National Environmental Satellite Services (NESS) of the National Oceanic and Atmospheric Administration (NOAA), and the Applied Climatology Laboratory of the Department of Geography, University of Bristol, United Kingdom. The NESS technique basically uses the convective cloud area as the index for the estimation of rainfall (Follansbee, 1973). The method maybe expressed as:

$$R = \frac{(K_1 A_1 + K_2 A_2 + K_3 A_3)}{A_0} \qquad (1)$$

Where R is the estimated rainfall, A_0 the area under observation, A_1, A_2, A_3 are areas of A_0 covered by the three most important types of rain producing clouds (cumulonimbus, cumilocongestus and nimbostratus), and k_1, k_2, k_3 are empirical coefficients to be determined. The Bristol method

originally used cloud type, which depends on climatological and synoptic considerations, cloud area and the altitude in estimating rainfall (Barrett, 1980). The Bristol method assumes:

$$R = f(c, i(A)) \quad (2)$$

Where R is the rainfall accumulated over a period at grid intersections or in selected sizes of grid squares, c the cloud area, i the cloud type, and A the altitude.

Wu *et al.* (1985) developed a pattern recognition technique that extracts cloud indices from VIS and IR images or IR images only to estimate rainfall. The indices were based on radiance and texture features of the clouds. Radiance features were global measurements of the 20 X 20 km grid elements containing information about the overall characteristic of the radiance within the grid element, while the texture features were measurements that concern the spatial distribution of the radiances. When a grid contains radiances that vary little, the dominant properties of that grid are the radiance feature, whereas when the grid has a wide variety of radiances, the dominant property of that area is texture. This led to the recognition of three rain-rate groups (0 – no rain, 1 – light rain, and 2 – heavy rain).

Muruyama *et al.* (1986) formulated a regression method for estimating monthly rainfall amounts using high-cloud amount derived from the Geostationary Meteorological Satellite (GMS) in the tropical western Pacific as an index. The high-cloud amounts were determined 6-hourly from the number ratio of cloud pixels with equivalent blackbody temperature (EBBT) lower than climatic 400 mb temperature within a 1-degree latitude - longitude area using GMS IR data. Using the mean fractional coverage of cloud colder than 235K in a 2.5° X 2.5° box as an index from the Geostationary Operational Environmental Satellites (GOES) IR data, Arkin and Meisner (1987)

derived estimates of large space- and long time-scale convective precipitation. These estimates are known as the GOES Precipitation Index (GPI) and were developed for the Western Hemisphere. They calculated this index as a product of the mean fractional coverage of cloud colder than the threshold temperature, the length of the averaging period in hours and a constant of 3 mm h^{-1}. That is,

$$GPI=3F_c t \tag{3}$$

Where GPI is in millimeters, F_c is the fractional cloudiness (a dimensionless number between 0 and 1), and t is the length of the period (hours) for which F_c was the mean fractional cloudiness.

Callis and LeComte (1987) similarly used the percentage of convective cloud cover, considered to be producing rainfall, deduced from four images each day to produce daily estimates of rainfall for the Sahel region of Africa. Chiu (1988) showed that fractional rain area of clouds as an index in estimating rainfall accounted for a large part of the area rainfall variance in the Global Atmospheric Research Program (GARP) Atlantic Tropical Experiment region (GATE). His work was improved upon by incorporating data from a network of rain gauges alongside the initially used radar data as "ground truth" by Short *et al.* (1989). Mitchel and Smith (1987) developed a model for estimating rainfall by applying statistical discriminant analysis on indices derived from cloud-top parameters to determine the best combinations of the cloud indices that best classify rain versus no-rain occurrences within the Cooperative Convective Precipitation Experiment (CCOPE) Mesonet region. Some of the parameters used included the coldest cloud-top temperatures (to represent the convectively active cloud region), largest absolute temperature gradients (found in the vicinity of cloud updrafts), largest temperature laplacian (gives cloud towers within the area of convection)

among many others. Similarly Negri and Adler (1987a,b) derived several indices from cloud parameters using both VIS and IR images to estimate rainfall over the Florida Peninsular.

Turpeinen *et al.* (1987) validated the European Space Operation Center (ESOC) Precipitation Index (EPI) by comparing satellite data with observed rainfall from five African countries including Ivory Coast, Kenya, Senegal, Morocco and Tunisia. The EPI is a cloud coverage index, counted every three hours and summed over five days, based on the IR channel. They used an index similar to Arkin and Meisner (1987) but included Upper Tropospheric Humidity (UTH) as an additional feature. The objectives were to convert the fractional cloud cover (given by EPI) into rainfall in the five geographical locations, and to investigate the importance of humidity in the determination of accumulated precipitation. European Space Agency (ESA) Meteorological Satellite (METEOSAT) and rain gauge data for the period 3 October to 26 December 1985 were used. Using the UTH, three indices were developed. EPI-moist (UTH: 75%-100%), EPI-normal (UTH: 40%-75%) and EPI-dry (UTH: 0%-40%). The results for Kenya indicated that all three indices could be used to estimate accumulated precipitation with considerable precision. However, these results must be treated cautiously due to certain constraints in the study. First, the sampling period was too short. Second, the choice of the countries may not have been ideal. Tunisia experiences little convective rainfall, while many stations in Kenya and Morocco are located at high altitudes where orographic effects play an important role. Finally, the UTH has a limited accuracy due to its calibration against radiosonde data.

However, these cloud-indexing methods rely upon subjective cloud type identification in sample areas by an experienced meteorologist. This is labour intensive and also allows for the introduction of extra errors.

1.4.2 Life-History methods

Life-History methods depend on the premise that significant precipitation comes mostly from convective clouds and these convective clouds can be distinguished in the satellite images from the other clouds. These clouds can be recognized and the amount of rainfall from them can be estimated largely from the changes that occur within them. These changes, therefore, need to be closely monitored and hence it is important to use sequences of images from geostationary satellites (short intervals between consecutive images) in order to follow the growth and decay of the convective clouds. An example of these changes is the convective cloud area during the various stages of development.

Purdom (1981) proposed the study of the development of mesoscale systems as an aid to very short-range weather forecasting. The mesoscale developments were studied through the information on cloud developments and patterns received from geostationary satellite data combined with radar, surface and upper-air conventional observations. The clouds and cloud patterns observed represent the integrated effect of ongoing dynamic and thermodynamic processes in the atmosphere. With this information, he was able to make short-range weather forecasts. Martin and Howland (1986) also developed a method that similarly produces forecasts by using measurements on cloud developments from satellite information. The cloud measurements were taken at grid points at fixed time intervals within a day using both VIS and IR imagery to estimate daily rainfall in the tropics.

Doneaud *et al.* (1987) made a preliminary investigation into the usage of the Area-Time-Integral (ATI) technique on satellite data. They applied the technique on the GOES rapid scan satellite data alongside radar information over Bowman (Southwestern North Dakota) to estimate the total rain volumes over fixed and floating target areas. The basis of the approach is the existence of a strong correlation between the radar echo area coverage integrated over the lifetime of

a storm and the radar estimated rain volume. The lifetime of a storm is ascertained by using GOES data to track convective clouds.

Dugdale *et al.* (1987) used the total duration taken by raining clouds derived from IR images in estimating 10-day total rainfall amounts for the Sahel region. This technique involves the identification of raining clouds by use of a temperature threshold and keeping track on how long that particular cloud stays over a certain area. These durations are then totaled-up to give the 10-day period that the raining cloud stayed over the region. This is what is used as a proxy of rainfall. Ouma *et al.* (1995) used a similar approach to estimate 10-day rainfall amounts for southern Tanzania. They found that using the Cold Cloud Durations (CCD) as a proxy gave reasonable estimates of that region's rainfall. They derived regression equations for retrieval of rainfall using optimum threshold temperature of -50^{0}C.

Scofield (1987) developed the National Environmental Satellite Data and Information Service (NESDIS) operational convective precipitation estimation technique for estimating half-hourly convective rainfall amounts by analyzing changes in two consecutive (half-hourly) satellite images. This technique estimates rainfall following three steps. The first step involves location of the active portion of the thunderstorm system. The active portion of a convective system is the area of strong updrafts that coincides with heavy sector of the thunderstorm cluster under the spreading anvil. The second step involves the computation of half-hourly rainfall estimate from cloud-top temperature and cloud growth or divergence aloft, the overshooting tops, thunderstorm cluster or convective cloud-line merger, and the saturated environment. Finally, these half-hourly convective rainfall estimates from the second step are summed up and multiplied by a moisture correction factor for the actual estimate. This technique was initially designed for deep convective systems that occur in tropical air masses with high tropopauses. It is affected by cloud base level, the height of the tropopause, and orography.

Mishra *et al.* (1988) used 3-hourly Indian geostationary multi-function Satellite (INSAT-1B) data in a scheme to estimate heavy convective rainfall over India during the monsoon season. They adopted the Scofield (1987) scheme and tailored it for the Indian subcontinent during the monsoon season. The scheme takes into account the convective cloud structure, cloud growth in space and time, and the prevailing environmental conditions.

However, these life-history methods rely on the successful tracking of convective clouds through their life spans. Some convective systems have relatively short life spans that may be missed out between consecutive images from the satellites, leading to an underestimation of rainfall.

1.4.3 Bi-spectral and cloud model methods

The other group of methods is the bi-spectral and cloud model methods. Bi-spectral methods use VIS and IR images simultaneously to map the extent and distribution of precipitation. IR images give information about the temperature and, indirectly, the heights of the tops of the clouds, whereas the VIS images provide information on the thickness, geometry and the composition of the clouds. The bi-spectral methods use dual thresholds on both the VIS and IR data simultaneously to identify the raining clouds. Some cloud indexing and life history methods also belong to this group of techniques. These methods are based on bivariate frequency distributions.

Several bi-spectral satellite rainfall estimation methods have been developed. Austin (1981) used VIS and IR images from Geosynchronous Meteorological Satellite (GMS) and GOES-E archived at 30-minute intervals, and the corresponding radar data from McGill Radar Weather Observatory in an attempt at short-range forecasting of precipitation. The radar information, converted to rain rates using SHort term Automated Radar Prediction (SHARP) procedure, were used as the "ground truth" in defining raining and non-raining clouds. The fundamental algorithm consisted of obtaining two bivariate frequency distributions from the VIS and IR images, collocated

with simultaneous radar data inorder to discriminate between raining and non-raining clouds. The "ground truth" helped in defining the dual thresholds for both VIS and IR data.

Cherna *et al.* (1985) used bivariate frequency distribution on VIS and IR images collocated with simultaneous radar data to discriminate between thunderstorm and non-thunderstorm areas or between rain and non-rain areas. Tsonis and Isaac (1985) while delineating instantaneous rain areas in the mid-latitudes while using GOES data employed a similar approach. They also tried to distinguish between four classes of rain-rates namely no rain, light rain, moderate rain and heavy rain classes. Barrett and D'Souza (1986) integrated three time daily pairs of METEOSAT VIS and IR images, and three night-time IR only images using the Agricultural Drought Monitoring Integrated Technique (ADMIT) to determine rain/no rain boundaries across the whole continent of Africa. They plotted VIS and IR digital counts in the VIS/IR two-dimensional space and used double thresholding technique to determine the rain/no rain boundaries.

The bivariate models have the advantage of effectively isolating the cirrus and stratus components of the IR and VIS imageries. The information from VIS channels discards the cirrus component while IR information removes the stratus component to reduce the over-estimation that normally arises from these non-raining clouds when IR or VIS channels are used individually.

The convective cloud model methods incorporate models of convective processes in their development. Satellite data is used to estimate the convective parameters of the convective clouds. Gruber (1973) applied Kuo's (1965) parameterization scheme over a grided area in estimating rainfall in the regions of active precipitation. The parameters were estimated using satellite data. Wylie (1979) used the Simpson and Wiggert (1969) one-dimensional cloud model to estimate rain in the Global Atmospheric Research Program (GARP) Atlantic Tropical Experiment (GATE) and Montreal regions by calculating the stability factors. The incorporation of the cloud model was found to substantially improve the satellite estimates of rain in the region. Adler and Negri (1988)

developed the Convective-Stratiform Technique (CST) to estimate both tropical convective and stratiform precipitation (produced under anvils of mature and decaying convective systems) using IR images. The method defines convective cores, and assigns rain-rate and rain-area to the features based on the IR brightness temperature and the cloud model approach of Adler and Mack (1984). The one-dimensional cloud model accounts for ambient temperature, moisture and shear conditions.

All the methods discussed above use the VIS and IR channels in acquiring information. The VIS channels are only useful during daylight hours and also misclassify stratus clouds as rain clouds due to their high reflectivity, while the IR channels usually wrongly classify the cirrus clouds due to their low temperatures. Further, these channels give information that lead to indirect schemes of rainfall retrieval because they provide cloud information that can only be used as proxy to rainfall. Due to these problems, research into alternative channels to retrieve information started and hence the use of PM channels was introduced. The next sections review the research that has been done using the PM channels.

1.4.4 Passive microwave methods

The final group of satellite rainfall estimations are those that use PM windows in obtaining satellite data for rainfall estimations. These estimation techniques are called direct since they are based on observations of the radiative effects of precipitation-sized hydrometeors (Arkin and Meisner, 1987). They use observations of radiation at frequencies that are not affected by cloud droplets or by the gaseous contents of the atmosphere. At microwave frequencies, the major source of attenuation is due to precipitation-sized particles (Grody, 1984). Within the microwave spectrum, raindrops may absorb, emit or scatter radiation, producing changes in the brightness temperature relative to clear or cloudy conditions. The dominant attenuation process seems to be determined by the nature and the quantity of both liquid droplets and ice particles. Together, these are a reflection

of the rainfall processes at work within a cloud (Kidd and Barrett, 1990). Monitoring the brightness temperature would, therefore, give a good approximation of the rainfall received from such a cloud. However, microwave emissions from the underlying surface usually affects this brightness temperature. The radiation from the underlying surface depends on the temperature and emissivity of the surface. Over the oceans, the emissivity is relatively low and constant providing a predictable background signal. Over land, however, both the temperature and emissivity are highly variable due to nature of the of land surface. This makes the microwave background signal over land highly variable. It is, therefore, easier to monitor rainfall using microwave data over the oceans than over land surface backgrounds (Arkin and Ardanuy, 1989).

Passive microwave rain-rate retrieval methods are based on one of three approaches, emission-, scattering- and combination of emission and scattering-based methods (Hong *et al.*, 1997). In the next sections, PM-based methods that fall under the various rainfall retrieval approaches are reviewed.

1.4.4.1 Emission-Based Methods

The emission-based methods use the fact that absorption and emission by liquid cloud drops and raindrops cause rapid increases of brightness temperatures over a radiometrically cold background, such as the ocean. Most emission-based approaches rely on integration of the equation of radiative transfer for hypothetical models of raining atmosphere to predict the brightness temperature for a given rainfall rate. These methods are normally successful against a surface background of low emissivity, such as the oceans, with rainfall standing out as a "warm" area against a cold background. The principal drawbacks of these emission-based methods are that they saturate at relatively low rainfall rates and also show substantial sensitivity to the assumed freezing level. Lower frequency channels are used for these approaches.

(Wilheit *et al.*, 1973) demonstrated that the data from the Electrically Scanning Microwave Radiometer (ESMR) system carried on Nimbus 5 could be qualitatively interpreted as indicating the presence or absence of rain above an unspecified threshold intensity. Allison *et al.* (1974) found that rain rate could at least be crudely estimated from this data. Wilheit *et al.* (1977) managed to develop a theoretical model for calculating microwave radiative transfer in raining atmospheres and used this to estimate rainfall from PM data.

Barrett *et al.* (1987) investigated the possibility of using PM data in support of their Bristol/NOAA Interactive Scheme (BIAS) for improved satellite rainfall monitoring. BIAS is an interactive scheme that uses VIS and IR imagery from polar orbiting or geostationary satellites, synoptic weather reports from conventional stations, and vertical motion and precipitable water charts to estimate rainfall. In this study, they overlaid the BIAS results with PM information obtained using all three approaches of PM methods. The usefulness of PM data in rainfall monitoring was clearly demonstrated by this study.

Barrett *et al.* (1989a) investigated the effect of combining the conventional rain gauge observations, passive microwave satellite data, and radar observations in rainfall monitoring. Their areas of interest included Kenya and the British Isles. There were three objectives for the project over Kenya. The first objective was the examination of the performance of scanning multi-channel microwave radiometer (SMMR) rainfall algorithms over a tropical area. Kenya was chosen as representative of tropical regions. The second objective was the determination of VIS and IR thresholds, through a more physically direct method by using hourly rain gauge and weather radar data collected simultaneously with METEOSAT VIS and IR data. The final objective was to examine the performance of the convective stratiform technique (CST) developed by Adler and Negri (1988) over this tropical region. The CST has been briefly discussed in earlier sections. They used METEOSAT data, hourly recorded rainfall data from

nine automatic rainfall stations, analog weather radar observations from ground based radar located at Jomo Kenyatta International Airport (JKIA), and SMMR data for the period 20th April to 3rd May 1987.

The results from SMMR studies proved inconclusive, mainly due to lack of sufficient data to test a variety of rain conditions. However, the background signals from the lakes were detected and established. The examination of VIS/IR data in conjunction with ground based weather radar imagery provided new insights into the pattern of rainfall in the area. Most of the rain in the region fell from small rapidly moving convective cells seen on sequences of radar imagery, but were often sub-pixel sized and were not therefore resolved as individual elements by the infrared radiometers. Because of higher spatial resolutions of the textual features, and shadows, the VIS imagery were found useful in distinguishing the convective cores. However, this imagery is only available during the day light hours.

The CST results were very encouraging. Most major convective elements and their associated stratiform rainfall were correctly located and identified. However, the rain area assigned was, in some cases, smaller than the areas indicated by the radar echoes and VIS imagery. Many smaller convective elements were also missed and Barrett *et al.* (1989a), therefore, concluded that the CST can be tuned more finely to produce more accurate results in this environment. Unfortunately, the technique requires weather radar observations or hourly recording rain gauges. These are not readily available over all of Kenya and hence studies in this direction have been hampered. A similar study was done over the British Isles and the surrounding areas with better results mainly due to the availability of weather radar observations (Barrett *et al.*, 1989b)

A review of other methods developed using passive microwave data in rainfall monitoring during the period upto 1989 has been given by Arkin and Ardanuy (1989). Using observations of

a three-month period beginning September 1987 from Special Sensor Microwave/Imager (SSM/I) at 19.30 GHZ, Tjemkes *et al.* (1991) developed an algorithm to retrieve precipitable water content over global oceans. They utilized measurements of the polarization state or the radiation felt at the top of the atmosphere given the polarization state at the sea surface. The results were compared with rawinsonde observations, which occurred within a kilometer radius and within the same day of SSM/I observations. The correlation between the two independent values of precipitable water was found to be very good. However, this scheme does not distinguish between liquid and precipitable water and this may lead to large errors in instantaneously retrieved precipitable water due to liquid water content contamination.

Greenwald *et al.* (1993) modified the method of Tjemkes *et al.* (1991) by taking into account the temperature and moisture profile effects on the estimate of the emission temperature of the atmosphere. Their primary goal was to develop and validate a simple physical scheme that can be used to retrieve cloud liquid water from SSM/I observations on a global basis over the ice-free oceans. This method was however found to be disappointing for tropical regions. While comparing the column water vapour (CWV) information derived from both television infrared observation satellite (TIROS) operational vertical sounder (TOVS) and SSM/I, Stephens *et al.* (1994) applied the scheme of Greenwald *et al.* (1993). The results of the comparison show that both sets of data give comparable estimates. Hong *et al.* (1997) developed a physical-statistical approach that uses an emission-based method to retrieve instantaneous rain rates and computes monthly rainfall. The method employs a maximum likelihood estimate method on a limited rain-rate dynamic range. The beam filling error is corrected by multiplying by a factor of 1.8 generated from simulation studies of GATE data. The results indicated that the method performs well in the tropics.

1.4.4.2 Scattering Based Methods

The scattering-based methods use the fact that scattering by ice hydrometers in the upper parts of clouds causes brightness temperature decreases over land or ocean. The assumption is that a larger amount of ice at cloud top is associated with heavier rainfall. The scattering-based approaches are generally empirically based statistical relationships between satellite-measured brightness temperatures and surface rain obtained from coincident ground-based radar measurements or automatic recording rain gauges. Higher frequencies (typically higher than 37GHZ) are used inorder to get as much scattering information as possible. Difficulties in using scattering-based techniques arise primarily in situations devoid of deep convective precipitation.

Grody (1991) developed a simple algorithm to classify precipitation and snow cover using the SSM/I observations. He introduced a scattering index, based on 19, 22 and 85 GHz channels, that is used to identify precipitation or snow cover using their scattering characteristics. Weng *et al* (1994) evaluated two sources of error in the monthly rainfall estimates from the SSM/I observations. These errors were due to poor temporal sampling of the instrument and due to different averaging methods for converting instantaneous small-scale rain rates to climate scale products. They used the SSM/I algorithm that was used by the NOAA satellite based on the classification procedure developed by Grody (1991). This procedure uses a scattering index to identify the scattering signal at 85 GHz. from precipitation over land and ocean. It has been briefly reviewed in earlier parts of this section.

The estimates of monthly global precipitation, from a single technique, are not very reliable. Huffman *et al.* (1995) combined satellite-based estimates, rain gauge analysis, and numerical weather prediction (NWP) model precipitation information in a bid to get more reliable global monthly precipitation estimates. For the microwave estimates they used the Goddard

Scattering Algorithm, version 2, (GSCAT2) (Adler *et al.*, 1994) in which a simple regression relation is applied to the 86 GHz. horizontal polarization channel to infer precipitation rate. Results show that this method compares favorably with the other state of the art microwave techniques in retrieving rainfall.

1.4.4.3 Emission and Scattering-based Methods

The emission/scattering-methods use a multi-channel, statistical-physical rain-rate retrieval approach. They establish the statistical relationships between multi-channel brightness temperatures and rain rates based upon data generated by a cloud radiative model for a wide range of conditions. The model simulates various atmospheric parameters, cloud structures and microphysics, and surface characteristics, and then computes their associated brightness temperatures in each of the available channels. This requires the solution of the radiative transfer equation for every observed datum and assumptions about the structure of the rain clouds, which are usually unknown.

Mugnai and Smith (1988) investigated the impact of time-dependent microphysical structure of clouds on the transfer to space of PM radiation at several frequencies. This was in order to explore the feasibility of using multi-channel PM retrieval technique for the estimation of precipitation from space-based platforms. They concluded that due to the considerable variability and inhomogeneity of the microphysical and structural characteristics of precipitation clouds, it is necessary to use multi-channel PM precipitation retrieval techniques. In this way, the various characteristics of a precipitating cloud will be taken care of leading to a more accurate retrieval.

In an attempt to improve satellite rainfall retrievals using the SSM/I observations, Liu and Curry (1992) used a radiative transfer model that combines emission and scattering. In the model,

three types of rain clouds were included, two of the types having both liquid and ice hydrometeors. The results showed that combining SSM/I data at 19.35 and 85.5 GHz could retrieve wider rainfall range than either emission- or scatter-based algorithms alone. Besides this advantage, using these two wavelengths also results in the relationship between a linear function of 19.35 and 85.5 GHz. brightness temperature, and rainfall rate being closer to linearity than the relationship between brightness temperature of a single channel and the rainfall rate. Ferriday and Avery (1994) used a vertically structured, plane-parallel and horizontally infinite cloud model similar to that of Liu and Curry (1992) in PM remote sensing of rainfall from SSM/I observations. They developed an inversion scheme for converting brightness temperatures to rain rate that is relatively simple to apply, globally applicable and easily calibrated.

Weng and Grody (1994) developed a method combining several retrieval algorithms to measure different ranges of liquid water in the atmosphere. This composite algorithm uses all SSM/I frequencies to measure the liquid water for low stratus clouds as well as for highly convective systems, and is based on data sets simulated from the radiative transfer model. The calibration was done using ground-based radar observations. They realized that brightness temperatures at 19.35 and 22.235 GHz are capable of retrieving high amounts of liquid in convective clouds, whereas brightness temperatures at 85.5 and 22.235 GHz can be used to retrieve low amount of liquid in the stratus or stratocumulus clouds.

Although there are several techniques available to identify areas of rain from PM measurement observations, the conversion to an instantaneous rain rate is difficult because of the inhomogeneity of rain field in the relatively large microwave footprints. This problem is compounded by scarcity of validation data, especially over the oceans. Ferraro and Marks (1995) empirically derived the rain rate retrieval coefficients for SSM/I rain algorithms developed at NOAA-Satellite Research Laboratories (NOAA-SRL). They used both scattering- and emission-

based algorithms for rain retrieval and used ground-based radars for ground truth. Employing an algorithm that uses an 85 GHz approach over land and a blended scattering/emission component over oceans, Ferraro (1997) generated an 8-year monthly global data set from SSM/I measurements.

Extracting rainfall from over both land surfaces and water bodies at the same time is difficult due to the effects of background emissivities at microwave frequencies. To enhance the precipitation signal by minimizing the effects of surface emissivity, Kidd (1998) used a Polarization-Corrected Temperature (PCT) algorithm. The algorithm has a constant value, theta, which is determined according to the prevailing meteorological conditions. Theta also controls the threshold chosen to delineate rain from no-rain. As theta increases, the rain/no-rain threshold also increases. The PCT algorithm has the advantage of being able to retrieve rainfall over land, sea, and most importantly, coastal areas. Furthermore, using PCT at 85, 37 and 18 GHz provides information about height distribution of hydrometeors within the cloud system. Although the PCT at 85 GHz is strongly affected by thick cirrus clouds, it is very sensitive to light precipitation and is, therefore, ideal for rain/no-rain delineation.

From the literature review above, it can be noted that not a lot of work has been done over the East African region as regards estimating rainfall from satellite information. It can also be noted that the more direct method of estimating rainfall is based on PM channels. The validation for the methods based on PM channels require ground-based radars or automatic recording rain gauges. Both of these are not very available in the East African region. It is the aim of this study to use appropriate satellite-derived data to estimate rainfall over some parts of the East African region, bearing in mind the limitations mentioned above.

CHAPTER TWO

DATA AND DATA QUALITY CONTROL

2.0 Introduction

A discussion of the data used in the study is undertaken in this chapter. The data include rain gauge recorded rainfall information, Cold Cloud Duration derived from METEOSAT satellites, and Total Precipitable Water derived from a combination of data from radiosonde, Special Sensor Microwave/Imager (SSM/I) and TIROS Operational Vertical Sounder (TOVS) data, and wind derived from ECMWF reanalysis data.

2.1 Rainfall Data

Daily rainfall data from sixty stations distributed over the study region were used in the study. Table 2.1 gives the list of names, locations in latitudes and longitudes, and altitudes of the stations used in the study while Figure 2.1 show their spatial distribution. The data period covered January 1st 1982 to December 31st 1995. The sixty stations were chosen from about two thousand Kenyan rainfall stations. A criterion for the selection of stations was less than 10% missing data during the period considered for the study. Some synoptic stations were not considered in the study because the rainfall cards, from where the daily records were extracted, were missing. The data were obtained from The Kenya Meteorological Department, Nairobi.

Simple data quality control procedures were performed on the data to ascertain their internal, temporal and spatial consistency. Single mass curves (Ogallo, 1982, 1987) were used to test for the homogeneity of the data. The missing data were estimated using the correlation and regression techniques. This was done using the station most highly correlated to the station with missing data.

Table 2.1: List of Stations used in the study

S/NO.	STN. NO.	STN. NAME	LAT.	LONG.	ALT(m)
1	8534000	Lokichogio	4° 15'	34° 21'	1133
2	8536000	Sabarei	4° 21'	36° 54'	467
3	8635000	Lodwar	3° 07'	35° 37'	553
4	8637000	North-Horr	3° 19'	37° 04'	560
5	8639000	Moyale	3° 32'	39° 03'	1217
6	8641000	Mandera	3° 56'	41° 52'	362
7	8641001	Rhamu-Mandera	3° 56'	41° 14'	327
8	8735009	Lokichar	2° 20'	35° 40'	833
9	8740000	El wak	2° 47'	41° 57'	400
10	8835004	Kapenguria	1° 14'	35° 07'	480
11	8836000	Maralal	1° 06'	36° 42'	550
12	8839000	Habba-Swein	1° 01'	39° 28'	217
13	8840000	Wajir	1° 45'	40° 04'	267
14	8934096	Kakamega	0° 17'	34° 46'	1400
15	8935020	Kabarnet	0° 30'	35° 45'	2233
16	8935181	Eldoret	0° 03'	35° 17'	2318
17	8737003	Isiolo	0° 02'	37° 35'	1207
18	8937065	Meru	0° 05'	37° 39'	1667
19	8940003	Liboi	0° 22'	40° 52'	300
20	9034001	Kisii	-0° 41'	34° 46'	1933
21	9034025	Kisumu	-0° 06'	34° 35'	1256
22	9034049	Mbita	-0° 25'	34° 13'	1433
23	9034100	Rongo	-0° 45'	34° 36'	1533
24	9035046	Chemelil	-0° 04'	35° 09'	1344
25	9035128	Sorget	-0° 02'	35° 32'	2600
26	9035155	Londiani	-0° 08'	35° 35'	2533
27	9035279	Kericho	-0° 22'	53° 21'	2387
28	9036020	Nakuru	-0° 17'	36° 04'	2023
29	9036062	Naivasha-K	-0° 49'	36° 16'	2012
30	9036081	Naivasha-Vet	-0° 39'	36° 25'	2012
31	9036271	Aberdare	-0° 29'	36° 45'	1010
32	9037112	Embu	-0° 41'	37° 20'	1267
33	9038008	Kitui	-0° 56'	38° 04'	1150
34	9039000	Garissa	-0° 28'	39° 38'	140
35	9135001	Narok	-1° 08'	35° 50'	1733
36	9136014	Kiambu	-1° 08'	36° 47'	2000
37	9136039	Kajiado	-1° 50'	36° 48'	1900
38	9136043	Muguga	-1° 13'	36° 39'	2267
39	9136164	Dagoretti	-1° 18'	36° 45'	1967
40	9136168	JKIA	-1° 19'	37° 55'	1778
41	9137020	Machakos	-1° 18'	37° 21'	1650
42	9137099	Mbooni	-1° 38'	37° 27'	2000
43	9137143	Masii	-1° 28'	37° 27'	1467
44	9138036	Chuluni	-1° 25'	38° 02'	1267
45	9140006	Tana	-1° 28'	40° 00'	100
46	9237000	Makindu	-2° 17'	37° 50'	1093
47	9237049	Sultan-Hamud	-2° 02'	37° 23'	1343
48	9240003	Witu	-2° 23'	40° 26'	3
49	9240010	Garsen	-2° 16'	40° 07'	15
50	9240021	Mambosasa	-2° 23'	40° 31'	10
51	9337140	Kiwalwa	-3° 28'	37° 42'	750
52	9337141	Kitobo	-3° 26'	37° 38'	800
53	9338001	Voi	-3° 24'	38° 34'	612
54	9338022	Buchuma	-3° 48'	39° 57'	433
55	9339009	Kilifi	-3° 36'	39° 51'	50
56	9339036	Mtwapa	-3° 56'	39° 44'	70
57	9339038	Kaloleni	-3° 48'	39° 37'	740
58	9340002	Gedi	-3° 18'	40° 01'	100
59	9439000	DCEO	-4° 02'	39° 39'	72
60	9439021	Mombasa	-4° 02'	39° 37'	62

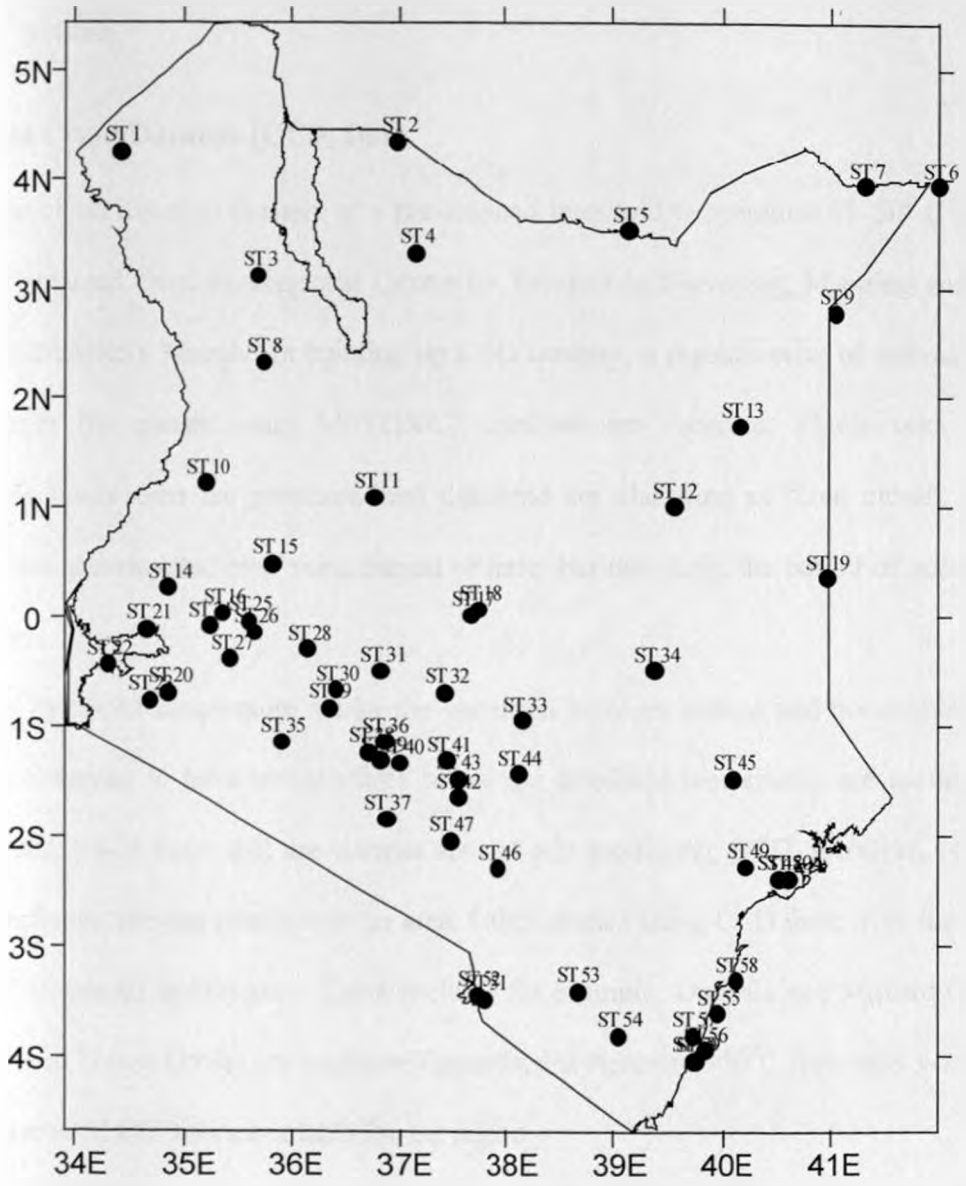

Figure 2.1: Map of the study area showing the distribution of the rainfall stations.

2.2 Satellite Data

Two types of satellite data were used in the study. These include Cold Cloud Duration (CCD) and Total Precipitable Water (TPW). A discussion of these two satellite data types follows in the next sections.

2.2.1 Cold Cloud Duration (CCD) Data

Cold cloud duration imagery at a pre-selected threshold temperature of -50^0 C (Dugdale, 1990) was obtained from the Regional Center for Services in Surveying, Mapping and Remote Sensing (RCSSMRS), Nairobi. In building up CCD imagery, a regular series of thermal infrared imagery from the geostationary METOSAT satellites are received. Pixels with apparent temperatures lower than the predetermined threshold are classified as "cold cloud" and their characteristics accumulated over some period of time. For the study, the period of accumulation was ten days.

The threshold temperature marks the transition between raining and non-raining clouds. All clouds observed to have temperatures below the threshold temperature are assumed to be raining clouds, while those that are warmer are not rain producing. CCD, therefore, is the time taken by particular raining clouds over an area. Other studies using CCD done over the area also used -50^0C threshold temperature. These include, for example, Dugdale and Milford (1987) for Zimbabwe, and Ouma (1988) for southern Tanzania. Furthermore, -50^0C threshold was the only long-term archived CCD data available for the region

METEOSAT is in geostationary orbit around the earth at about 36,000 kms. above the surface. This gives a continuos coverage of the same location on the surface of the earth hence availing 24 hours of data every day from that location. The radiometers carried aboard the METEOSAT have narrow fields of view covering an area of about 5 kms. in the thermal infrared

and water vapor channels, and about 2.5 kms. in the visible channels at the satellite subpoint. This gives the resolution of the scanners and is known as the footprint (Dugdale, 1990). The coordinates of any point on the earth's surface in relation to the satellites are derived from the northward and eastward angular displacement from the satellite subpoint of the line of sight of the satellite radiometer. Hence, any point above the surface of the earth, such as a cloud, will be attributed coordinates not corresponding to the position vertically below the cloud, but to the point on the earth's surface the radiometer would have viewed in the absence of the cloud (Dugdale, 1990). The surface position of the stations are corrected for the above parallax error using the following equations:

$$\Delta(\text{ Latitude}) = \frac{h\tan(1.1\theta)}{110} \tag{3}$$

$$\Delta(\text{Longitude}) = \frac{h\tan(1.1\phi\cos(\theta))}{110\cos(\theta)} \tag{4}$$

Where θ is the latitude, ϕ the longitude, h the height of the cloud in kilometers and Δ is the correction in degrees. The height of cumulonimbus clouds is taken as 12 km for tropical regions.

The CCD data used in the study was for the period 1989 to 1995 with a few months missing. The missing months were ignored in the analysis. 10-day data for the period 1989 to 1993 were used for algorithm development while the period 1994 to 1995 was used in validation.

2.2.2 NASA Water Vapor Project (NVAP) Total Precipitable Water

This is the second set of Satellite-derived data used in the study. Currently, atmospheric water vapour measurements are made from a variety of sources including radiosondes, aircraft

and surface observations, and in more recent years, by various satellite instruments. However, these individual sources of data have certain limitations. Radiosonde measurements are made primarily over land with limited, spatial and temporal coverage, infrared satellite techniques are only applicable in the absence of significant cloud cover, and microwave retrievals are presently feasible only over oceans. A more accurate global moisture dataset should be derived from a combination of the above measurement systems while working within the limitations of these observing systems and using advantages of each (Schurbert *et al.*, 1993). To accomplish this, the National Aeronautics and Space Administration (NASA) Water Vapour Project (NVAP) was set up and produced a 8-year (1988 - 1995) total and layered global dataset (Randel *et al.*, 1996). This dataset comprises a combination of radiosonde observations, Television and Infrared Operational Satellite (TIROS) Operational Vertical Sounder (TOVS), and Special Sensor Microwave/Imager (SSM/I) data sets. There are three primary NVAP products including total column precipitable water content (TPW), liquid water path and layered TPW. In this study, the layered TPW dataset was used.

In the following sub-sections, a brief discussion of the individual datasets used in compiling the NVAP water vapour data is given.

2.2.2.1 Radiosonde Data

The water vapour statistics used throughout scientific literature have historically been based on upper-air balloon soundings (Oort A.H, 1983). These data are still the only global ground truth available for atmospheric water vapour.

Radiosonde data from stations all over the world transmitted through the Global Telecommunications System (GTS) were decoded at the National Center for Atmospheric Research (NCAR) and supplied to NOAA. Among some 1800 stations that have reported since

1973, approximately 900 were used. This was done because the main objective was to create a useful climatological data set thus limiting the chosen stations to those having long historical records.

Using 00Z and 12Z soundings for each station, temperature, dewpoint depression, surface pressure and geopotential heights were extracted for the mandatory levels (surface, 850, 700, 500, 400 and 300 mb). Past 300 mb level, the humidity measurements are not reliable and hence the termination of the soundings at this level. From this information, dewpoint, relative humidity and specific humidity were calculated at each level with precipitable water, temperature and dew point lapse rate within each layer.

2.2.2.2 Special Sensor Microwave Imager (SSM/I) Data

The other source used to create the merged TPW data set is the SSM/I instruments flown aboard the F8, F10, F11 and F13 Defense Meteorological Satellite Project (DMSP) satellites. The SSM/I is a passive dual - polarization instrument (channels at 19.33, 22.235, 37.0, and 85.5 GHz) designed to provide measurements of rainfall, water vapour, liquid water, and near-surface wind speed over ocean surfaces and the surface characteristics of sea-ice and land. The DSMP Satellites are polar orbiters (Randel *et al.*, 1996).

A retrieval scheme based on the physical method employed by Greenwald *et al.* (1993) was used to simultaneously retrieve both total column water and integrated cloud liquid over the oceans. This scheme was an extension of the method of Tjemkes *et al.* (1991) and is based on measurements at 19.35 and 37.0 GHz. This retrieval model requires several input parameters, the first of which is sea surface temperature (SST). NVAP used monthly mean SSTs produced by NCEP on a 2^0 lat. x 2^0 long. global grid (Reynolds, 1988).

The near surface wind speed is the next input parameter using the Goodberlet *et al.* (1989) algorithm. However, this algorithm is less reliable in regions of high water vapour and hence Bates (1991) method was used instead for SSTs greater than 300K. A final input parameter is cloud top temperatures that were taken from the International Satellite Cloud Climatology Project (ISCCP) dataset.

There are three main sources of error in using the SSM/I retrievals (Randel *et al.*, 1996). The first is land contamination, which usually results in over-estimation in the retrieved quantities. NVAP used a (0.5^0 lat. X 0.5^0 long.) land-mask to prevent retrievals over land regions. Certain small islands that were not included in the land-mask were manually searched for and removed by eliminating the gridded data from these specific areas.

The second problem is due to sea ice. This is prevalent around polar coastal regions but does migrate north and south in accordance with the seasons. NVAP employed a sea ice detection routine that allowed for the removal of these bad points. This was done using sea ice detection routines of Cavalieri (1991) and Grody (1991).

The final source of error is due to precipitation contamination. For precipitating clouds, microwave retrievals of water vapour are likely to be overestimated. NVAP implemented quality control measures to detect and eliminate precipitation-contaminated retrievals.

2.2.2.3 TIROS Operational Vertical Sounder (TOVS) Data:

The NOAA/National Environmental Satellite Data and information service (NESDIS) have been making operational Satellite-based water vapour retrievals since 1978 using raw data collected from the NOAA series of operational polar orbiting satellites (Werbowtzki, 1981). Data from NOAA - 9, -10, -11 and -12 Satellites were used in compiling the NVAP data set. These satellites have a near polar sun-synchronous orbit with 102-minute period and carry aboard

the TOVS instrument package made up of the second generation High Resolution Infrared Radiation Sounder (HIRS/2), the Microwave Sounding Unit (MSU), and the Stratosphere Sounding Unit (SSU). The TOVS instrument package is used for the retrieval of atmospheric temperature, ozone and humidity (Kidder and Vonder Haar, 1995).

Measurements from all three instruments were used for the retrieval of vertical temperature and moisture profiles. The retrieval scheme was based on the radiance variance approach proposed by Smith and Woolf (1984). Radiance data from HIRS/2 and MSU channels, primarily centered on the CO_2 and O_2 absorption bands, were used simultaneously to generate temperature soundings and layered moisture in a single solution matrix (Reale *et al.*, 1989).

NVAP project used quality controled operational TOVS sounding products produced by NESDIS. These data included total and three layered TPW for approximately 25000 retrievals per day with geographical spacing of about 2^{0} lat./long. NVAP processing consisted of gridding this data into 1^{0} x 1^{0} lat./long. boxes and applying only minimal quality control during the merge process when all three data sets including radiosonde and SSM/I were compared (Randel *et al.*, 1996).

There are two problems inherent in all infrared moisture retrievals that tend to limit the dynamic range of the TOVS data. First, the inability to perform retrievals in areas of thick clouds can cause a "dry bias", and, secondly, the limitations in infrared radiative transfer theory can cause significant over-estimation of TPW in regions of large-scale subsidence (Randel *et al.*, 1996).

The noted limitations of each of the three datasets led to the NVAP project in which the three were merged to create a single dataset with better accuracy than any of the three individually. The next section looks at the merging of the three data sets into one.

2.2.2.4 Blended TPW Data

The NVAP project created the TPW blended product by first gridding the three input data sets individually into separate daily 1^0 x 1^0 lat./long. global grid maps. The SSM/I gridded analysis were then checked for missing data over the oceans and spatially filled using linear interpolation. The total column TPW blended products were created by using a weighing scheme that considered the radiosonde retrievals to be most accurate and the SSM/I retrievals more accurate than those from TOVS.

The blending process started by assuming the radiosonde points to be the truth and weighing these values at 100%. This is because the radiosondes give actual values rather than proxy values to be converted into measures of TPW. Next, the SSM/I and TOVS grids were combined together using a selected weighting of 10% TOVS and 90% SSM/I for coincident points. These weightings arose from the limitations and the possible successful elimination of the limitations for both SSM/I and TOVS datasets. Finally the blended TPW product was checked for missing data and missing regions upto 10^0 lat. x 10^0 long. were spatially interpolated. The remaining areas of missing data were filled using a temporal 3-day running average.

However, layered TPW dataset was used in this study. Two of the three input data sets, radiosonde and TOVS, contained layered information and were used to create the layered TPW dataset. The TOVS data were ordered in three layers namely surface-700, 700-500, and 500-300 mb. These were placed into 1^0 lat. x 1^0 long. grids for every layer. The radiosonde retrievals were processed into identical matching layers. This layered information was then used to "slice" the blended total column TPW product.

NVAP made two basic assumptions with respect to global water vapour distribution to "slice" the total column TPW into layers. The first assumption was that although the TOVS

column TPW is not as accurate as the SSM/I value, the fraction of total column TPW in each layer is relatively correct. The second assumption was that while the total column TPW may vary rapidly in space and time, the fraction of the total TPW in each layer changes more slowly and is a strong function of latitude and season.

The layered TPW from a combination of radiosonde and TOVS datasets were divided by the total column TPW to derive the global distribution of the percent-of-total (POT) TPW in each layer. POT is the same as the fraction of the total TPW in each layer. The POT grids were then spatially interpolated to fill in small areas of missing data and temporally interpolated using a 5-day running average to fill in larger gaps. 5-day average was used due to the slower time variability of POT. To create the layered products, the blended total TPW grids produced earlier were multiplied by the POT grids. This gave the layered products the advantage of including SSM/I information along with TOVS and radiosonde data. Details of the process of producing NVAP data set can be found in Randel *et al.* (1996).

This data was received through file transfer protocol (ftp) from the NVAP Internet website at no cost.

2.2.3 European Center for Medium-range Weather Forecasts (ECMWF) Data set

To describe the general circulation associated with the various anomalous rainfall scenarios in the study, the ECMWF Re-Analysis (ERA) project datasets and products were used. This data set was chosen because it has been used by several researchers over the study area including Mukabana (1992) to simulate the large-scale systems over Kenya, and Okoola (1996) in describing the general circulation patterns associated with various Inter-Tropical Convergence Zone (ITCZ) and rainfall anomalies. ECMWF has provided global atmospheric analyses from its archive for many years. The data assimilation system used to produce the analyses uses a

multivariate optimum interpolation analysis, a non-linear normal mode initialization and a high-resolution forecast that produces a first estimate for the subsequent analysis (Bengtsson, *et al.* 1982). The ERA data assimilation system is a special version of the ECMWF operational data assimilation system which includes an intermittent statistical (optimum interpolation) analysis with 6-hour cycling, one dimensional variational (1D-VAR) physical retrieval of TOVS cloud cleared radiance (CCR) data, and diabatic, non-linear normal mode initialization (five vertical modes). The system also includes a spectral T106 forecast model with 31 hybrid vertical levels, and a fully three dimensional semi-lagrangean advection scheme. Finally, it has a physical parameterization package that includes mean orography with a compatible parameterization of sub-grid scale orography; a four layer prognostic soil scheme with no external forcing; an interactive cloud/radiation scheme with full mode representation of cloud water content and cloud cover; and a planetary boundary layer parameterization based on similarity.

The data had a spatial resolution of 2.5° lat. x 2.5° long. The general circulation parameters derived from these records used in the study include wind fields with the associated wind derived parameters at 850, 700 and 200 mb levels. This data was obtained from ECMWF through the Department of Marine, Earth and Atmospheric Sciences at North Carolina State University.

The next chapter discusses the methods used in the analyses of the data in the study.

CHAPTER THREE

METHODS OF ANALYSES

3.0 Methodology

In this chapter, the various methods that were employed to address the overall and specific objectives of the study are discussed. The various objectives of the study were highlighted in section 1.3. These include regionalization of the study area into homogeneous climatic zones using rainfall and satellite data; the development of empirical functions for the relationships between various types of satellite data and rain gauge rainfall; identification of the systems that could be associated with the low/high skills of the satellite-derived estimates during anomalous wet and dry periods; and the development of an early warning tool based on satellite-derived products.

3.1 Regionalization

Due to the complexities of the study region, as highlighted in section 1.3.2, the mesoscale systems have significant influence on the overall climate of the region. The major meso-scale systems include complex topographical patterns and the existence of many large inland lakes that have their own strong local and regional scale circulation patterns. Their interactions with the large-scale systems are important and must be considered when looking at the distribution of rainfall, both in time and space (Mukabana and Pielke, 1996). It is, therefore, important to zone locations with similar rainfall mechanisms independently of the others with different rain forming processes. In this section, the methods, which were used to develop homogenous climate zones using daily rainfall and satellite records independently, are presented. The homogenous zones derived from the two data sets namely rain gauge and satellite-derived estimates will be

compared. The rainfall records, which are considered as ground truth for the satellite-derived estimates, were presented in section 2.1 while the models for the extraction and conversion of the various satellite-derived data are discussed in section 3.2.

Several statistical methods based on eigenvalues have been used in delineating regions into climatic zones. Among these techniques include the use of empirical orthogonal functions (EOFs) whose solutions are normally described through Common Factor Analysis (CFA) and Principal Components Analysis (PCA). A review on these methods may be found in Ehrendorfer (1987). The advantages of methods based on eigenvectors include:

(a) Their ability in the reduction of the dimension of a given data matrix by searching for a new set of uncorrelated variables accounting for most of the variance in the original data.

(b) The detection of homogenous groups of variables as in some kind of climate classification.

(c) The simplification of investigation of spatial or temporal behavior of meteorological variables, for example, periodicity, cycles, trends and prediction models through the use of relatively few representative stations for each homogenous zone.

Theory and application of eigenvalue methods is adequately covered in standard statistical textbooks, including Harman (1967), Morrison (1976) and Jolliffe (1986) among others. These techniques have been widely applied in meteorology by many authors including Lorenz (1956), Kutzbach (1967), Barring (1987, 1988) and Ogallo (1989). However, of the two techniques, common factor analysis (CFA) has rarely been used in meteorological applications.

The basic principles of EOF analysis are derived from the concept of variance. It can be shown through the calculus of variation that maximum variance in a field may be accounted for by choosing, in order, the eigenvectors associated with the largest eigenvalues of the appropriate covariance matrix. CFA assumes that the observed variable is influenced by various determinants, some of which are shared by other variables in the set, while others are not shared and are unique to the variable only. That part of a variable that is influenced by shared determinants is called common, and the remaining part is called unique. This unique part results in a variable not having a perfect correlation with itself and hence emphasis is placed on covariance between variables within the input matrix, rather than the variances. The basic factor model may be put in the form given by Harman (1967) as:

$$Z_j = \sum_{k01}^{m} a_{jk} F_k + U_j B_j \quad (j = 1,2...n) \qquad (5)$$

Where Z_j is the variable j in standardized form, F_k the hypothetical factor k, a_{jk} the standardized multi-regression coefficient, U_j the standardized regression coefficient of variable j on unique factor j, and B_j the unique factor for j variable. The value that is inserted into the principle diagonal of the input matrix in CFA, U_j, is known as the communality estimate. Using communality values usually separates the common variance (large scale map typing) from the unique and error variance (local scale systems that may affect only one station, observational and instrumental errors) in CFA (Richman, 1981). Maps from CFA would, therefore, bring out the interplay between the large-scale systems and the mesoscale systems and also include small complex regions that are results of the unique part. Such maps would be very difficult to physically explain.

However, the major problem with CFA is the determination of the unique component. This requires rigorous mathematical treatment, and hence superior computer facilities. Many studies have neglected the unique component of the variance, and that reduces the CFA to PCA. The model for PCA may then be expressed as:

$$Z_j = \sum_{k=1}^{m} a_{jk} F_k \qquad (6)$$

In this case the uniqueness is ignored and the correlation of a variable with itself is considered to be perfect (unity). That is, no account is taken of observational or instruments errors. Due to the disadvantages of CFA mentioned above, PCA was preferred in this study.

3.1.1 Principal Component Analysis (PCA)

PCA can be performed in a number of different ways depending on the manner in which the input matrix of observations is arranged (Richman, 1986). If the parameter under study (e.g. rainfall anomalies) is fixed, then it is possible to generate the correlation data matrix between locations over a set of periods (S-mode), or between periods over a set of locations (T-mode). The S-mode yields a grouping of locations in terms of the change in time while the T-mode yields a grouping of periods with similar spatial patterns (Ogallo, 1989).

The S-mode PCA was performed on the standardized dekadal anomaly rainfall data in this study to delineate the different climatic zones within the study region. In an S-mode analysis, the variables are the stations and the observations are the values at each time. The principal component loading matrix contains the correlation of each station with each component. These can be plotted on a map to depict the spatial pattern of each component that results in the climatological zoning.

Mathematically, there are as many principal components as there are stations in the data matrix. However it is typical of atmospheric data that substantial correlation exist among the original variables. This implies that there is redundant information in the data matrix, and that the first few components of the dispersion matrix will locate directions in which the joint variability of the data is greatest. Similarly, the last few components will point to directions where the data jointly exhibit very little variation. It is, therefore, possible to represent most of the information content of the data by using only the significant principal components. The next sections looks at the problem of determining the significant principal components.

3.1.1.1 Number of Significant Principal Components

PCA strives to reduce the dimensionality of a given data set by describing it completely using new variables (principal components) that have two fundamental properties namely:

(a) any two different components are uncorrelated, and

(b) each component is derived from an empirical orthogonal variable accounting for a maximum in residual total variance of the original data set (Ehrendorfer, 1987).

Each of the new variables explains a certain percentage of the variance in the original data and they all, accumulatively, explain the total variance. The number of factors considered would normally affect the configuration of the map types achieved. It is, therefore, crucial to identify only those modes that produce patterns that maybe physically interpretable as opposed to those that emerge only due to random process (noise). Several tests exist for the determination of the appropriate number of components to retain. However, after surveys by several researchers none of the methods have proved superior to the others (Richman, 1981).

In the next subsections, a brief discussion of the methods commonly used in determining the number of components to retain is presented.

3.1.1.1.1 Kaiser's Criterion

This method, developed by Kaiser (1959), is one of the simplest methods of determining the significant principal components (PCs). This method assumes that all PCs whose corresponding eigenvalues are greater than or equal to one are significant. It retains only those PCs that extract variance at least as much as the equivalent of one original variable.

3.1.1.1.2 The Scree's Method

This method plots each raw eigenvalue against the mode number producing an exponential curve that decreases as the number of modes increase. The point where the curve of the graph breaks and becomes nearly linear is the determining number of significant principal components. The principal components after this point, which have nearly equal eigenvalues, theoretically represent random noise and maybe discarded (Cattell, 1966). Cohen (1983) gives a variation of this test where the data is rotated before graphing. This gives a more distinct break in the curve.

3.1.1.1.3 The Logarithm of Eigenvalue (LEV) Method

This is a method developed by Craddock and Flood (1969) and it is a variation of the Scree test. It plots the natural logarithm of eigenvalues against the mode number. The point where the graph becomes linear is where no further PCs are retained, since the linear tail with nearly equal natural logarithms of the eigenvalues theoretically represent random noise.

3.1.1.1.4 Sampling Errors of Eigenvalues

North *et al.* (1982) uses the sampling errors of the associated eigenvalues in determining significant principal components. The aim of the method is to determine whether a sample component faithfully represents a real eigenvalue. The method assumes that the sampling errors

are of the order $(2/N)^{1/2}$, where N is the total number of observations. Dealing with first order, the shift in the eigenvectors can be shown to depend strongly on the spacing of the eigenvalues, whereas the shift of the eigenvalues does not.

If the sampling error of a particular eigenvalue, λ_a, given by $\partial\lambda_a \approx \lambda_a (2/N)^{1/2}$, is comparable to or larger than the spacing between λ_a and λ_b, a neighbouring eigenvalue, then the component associated with λ_a will be comparable to the size of the neighbouring component associated with λ_b. The above results in the rule of thumb that tests for degeneracy by examining if $\lambda_a - \lambda_b > (2/N)^{1/2}$ and retains only the principal components that satisfy the condition.

The Kaiser's criterion, Scree test and North *et al.* sampling errors test were used in this study to determine the number of principal components to retain. Using the unrotated principal components has advantages and disadvantages. The next section looks at these.

3.1.2 Rotation of the Principal Components

Unrotated solutions offer a number of potential advantages, such as their economy, ability to extract maximal variance from a data set, spatial and temporal orthogonality and pattern insensitivity to the number of principal components retained. These characteristics make unrotated solutions good candidates for situations where pure reduction of data, without the need to interpret each mode, is the objective (Richman, 1986). However, the unrotated solutions exhibit four characteristics that hamper their utility to isolate individual modes of variation. These characteristics are domain-shape dependence, sub-domain instability, sampling problems and inaccurate portrayal of the physical relationships embedded within the input data. A detailed discussion of these characteristics may be found in Richman (1986).

There are two basic classes of mode rotation, orthogonal and oblique. The orthogonal rotations rigidly rotate a predetermined number of principal components a number of degrees, to better explain the data, while retaining the orthogonality of the vectors to each other. Oblique rotations do not constrain orthogonality, thereby allowing the rotated vectors to more precisely identify the data clusters. Examples of orthogonal rotations include Quartimax, Varimax, Transvarimax, Parsimax and Equamax while oblique rotations include Quartimin, Covarimin, Oblimax and Direct Oblimin among others (Richman, 1986).

In this study, the orthogonal class of rotation, through Varimax rotation, was used in rotating the principal components. Mapping the significant rotated components then delineated the climatic zones.

3.2 Choice of Representative Records for the Homogeneous Regions

The point rain gauge records and gridded satellite data, which were used in this study, were described in chapter 2. In section 3.1 PCA method was used to group the point rainfall and gridded satellite data independently into homogenous climatological zones. Due to the high degree of space-time variability of rainfall, it is necessary to use arealy averaged rainfall records that may be taken as representative over all the climatic regions with similar rainfall characteristics. Several methods are available for areal averaging whose details may be found from many standard statistical references (Harman, 1967; WMO, 1974; Child, 1990; Basalirwa, 1991).

This section highlights the methods which were used to pick representative rainfall and satellite data for each homogenous zone. The representative data will be used in all further analyses. Three methods used in this study to pick representative records for each homogenous

group include the unweighted arithmetic mean, the principle of communality as derived from rotated PCA, and the use of PCA weighted averages.

3.2.1 Unweighted Arithmetic Mean Method

In the unweighted arithmetic mean method, the average of all the stations in a climatic zone is taken as representative of the areal rainfall for that region. Under this method arithmetic averages are computed for all homogenous regions using all stations that were clustered into the region by PCA. Time series of the generated areal averages for each region were used for searching for relations between rain gauge and satellite-derived rainfall records. One of the major problems with this method is that not all the homogenous regions have same number of stations. Even where the number of stations was the same, their spatial distributions were quite different. The regional rainfall patterns are also variable owing to the complex topography and other regional features as highlighted in section 1.3.2. The use of simple areal average method may therefore not be realistic. This method may be expressed mathematically as:

$$\overline{R} = \frac{1}{n}\sum_{i=1}^{n} X_{ij} \qquad (7)$$

Where $\overline{R}$ is the areal average rainfall, n the number of stations, and X_{ij} the observations from each of the stations, i, and for particular years, j.

3.2.2 Use of PCA Weighted Averages

Arithmetic mean method shown in equation 7 gives equal weight of 1/n to all locations within the homogenous region. Many attempts have been made to derive a realistic weighting function for each location which may be representative of the spatial differences in the mean

rainfall patterns. Such weighting functions have included the use of Thiessen polygons and the isohyetal methods. Details of these and other areal averaging methods have been given in Basalirwa (1979). In this study PCA eigenvalues were used as the weights. Under this method the eigenvalue corresponding to each location was used as a weight in equation 7, which then takes the form:

$$\overline{R} = \frac{1}{n}\sum_{i=1}^{n} \alpha_i x_i \qquad (8)$$

Where α_i are the eigenvalues corresponding to station i in each predetermined climatic zone.

The eigenvalues provide the variances explained by each corresponding station in the PCA. A summation of the eigenvalues divided by the total number of stations is equal to one. It is, therefore, logical to use the eigenvalues as a fraction of the total number of stations in weighting the corresponding stations in the averaging function. The use of PCA-derived weights in the weighting functions has been used in many recent studies due to its unique advantages over many methods. Ogallo (1980), Basalirwa *et al.* (1999) and Indeje *et al.* (2000) have used variations of this method in their studies.

3.2.3 The use of the Principle of PCA Communality

Communality, C(j), for any given location j in a homogenous zone may be expressed as:

$$C(j) = \sum_{k=1}^{m} (a_{jk})^2, (j = 1,2,...,n) \qquad (9)$$

where m is the number of significant principal components.

It has been shown by Child (1990), that *C(j)* gives a measure of the degree of interrelations amongst the various variables. The location with the highest value of *C(j)* in any homogenous region may be reflective of the location that is highly correlated with all other stations within the homogenous zone. This communality principle has been widely used to pick representative locations within each homogenous zone (Ogallo, 1980; Opere, 1998)

However, the problem with this method, as well as the method using PCA-weighted averages discussed in 3.2.2 above, is that PCA assumes orthogonality. Measures derived from PCA may therefore not be able to realistically represent the complex linkages, which are common between various locations in Kenya due to the influence of local and regional factors

The results from these three areal averaging techniques will be compared in this study. Similar methods were adopted for the homogenous zones, which were obtained from the gridded satellite-derived data.

3.3 Correlation Analysis

In the previous section we have presented the methods that will be used to delineate regions of homogenous climate. We have also presented the methods for identifying representative satellite-derived and rain gauge records for each delineated homogenous zone. This section will examine the relationships between various types of satellite data and rain gauge rainfall records for each of the homogenous zones. Correlation method will be adopted and results will form the foundation for the development of empirical relationships between the various satellite-derived information and rain gauge observations.

The satellite-derived data that were independently correlated with rain gauge rainfall records in this study are the Cold Cloud Duration and the Total Precipitable Water. The details of these records were presented in sections 2.2.1 and 2.2.2 respectively.

Correlation analysis examines the relationship between pairs of variables namely the dependent variable (Y) and the independent variable (X). The degree of relationship between the pair of variables Y and X are often quantified using correlation coefficient. The simple correlation coefficient r may be expressed as:

$$r = \frac{\sum_{i=1}^{N}(X_i - \bar{X})(Y_i - \bar{Y})}{\sqrt{\left[\sum_{i=1}^{N}(X_i - \bar{X})^2\right]\left[\sum_{i=1}^{N}(Y_i - \bar{Y})^2\right]}} \qquad (10)$$

Where r is the correlation coefficient and X_i and Y_i are i^{th} observations of variables X and Y respectively, while $\bar{X}$ and $\bar{Y}$ are the means of the variables with sample sizes N. In this study, X represents the satellite-derived data while Y represents the rain gauge recorded rainfall observations. The value of r lies between –1 and 1. The value of r equals 1 when X and Y are perfectly related, while it is zero when there is no relationship between the variables. Negative and positive values of r reflect negative (one increases as the other decreases) and positive (both increase and decrease simultaneously) relationships between X and Y. One of the major challenges of correlation analysis is the determination whether the computed value of r for any pair of variables is significantly different from zero. The following sections look at this problem.

3.3.1 Testing Statistical Significance of the Computed Correlation Coefficient

Several methods are available in most standard statistical textbooks that test the significance of correlation coefficients. Examples maybe found in Cochran (1967), Hogg and Craig (1970), Yevjevich (1972), and Clarke and Cooke (1992) among others. In this study, the student t-test, which has been widely used in studies in the region, was used to test significance of the correlation coefficient. This test may be expressed mathematically as:

$$t = \frac{r\sqrt{N-2}}{\sqrt{1-r^2}} \qquad (11)$$

where r is the correlation coefficient and N the sample size. The result of equation (11) is compared to a value from a standard t-distribution table at N-2 degrees of freedom to confirm the significance.

3.4 Regression Analysis

In section 3.3 we determined pairs of satellite-derived data and rain gauge records which were significantly correlated. Such pairs of records had statistically significant values of r. Regression analysis attempts to develop the best empirical equations that can be used to describe relationships between pairs of significantly correlated variables X and Y. Simple, multiple and canonical regression methods were used in this study.

3.4.1 Linear Regression Analysis

Simple or linear regression analysis assumes that all relationships between the dependent and the independent variables X and Y are linear. The equation that can be used to quantify the

linear relationship between X and Y is simple or linear regression equation. Under this method, the relationship between two significantly correlated variables X and Y may be represented as:

$$Y = \alpha + \beta X \tag{12}$$

where α and β are constant parameters to be estimated.

3.4.2 Multiple Regression Analysis

Relationships between rain gauge and satellite-derived data may not be strictly linear as presented in the section 3.4.1 since some of the satellite-derived data are based on various characteristics of the clouds, while rain gauges measure rainfall falling into the gauge from the clouds. Some time lead or lag may be expected between the two variables X and Y, and other variables may also significantly play a role. Under multiple regression, attempts are made to include some non-linear and, sometimes, time lead or lag relationships between Y and X. A relationship between Y and several other variables is also considered. Equation 13 gives an example of these.

In this study Y represents rain gauge recorded rainfall observations, while X_1, $X_2 \ldots X_p$ are the best p set of correlated satellite variables. A linear additive model relating a dependent Y variable to a set of p best-correlated independent variables X_1, X_2, $\ldots X_p$ may be expressed as:

$$Y = \alpha + \beta_1 X_1 + \beta_2 X_2 + \ldots + \beta_p X_p + \varepsilon \tag{13}$$

where α, β_1, $\beta_2 \ldots$ β_p are constant parameters to be estimated and ε is the residual term.

3.4.3 Canonical Correlation Analysis

Canonical Correlation Analysis (CCA) is at the top of the hierarchy of regression modelling approaches. The simple regression approach regresses one variable against another. Multiple regression attempts to relate a matrix of predictor data to a single predictand variable. In this case the predictor is made up of more than one variable. The stepwise multiple regression attempts to select, from a large set of variables, the most predictively important variables to explain a single predictand. In all the above cases, the predictand is composed of one variable. CCA is a generalization of all these approaches. It finds the optimum linear combination of the predictor data matrix that will explain the most variance in the predictand data matrix. In this case, both the predictor and the predictand are full multidimensional vectors of information.

CCA is a multivariate statistical technique that examines the strength of the linear association between two sets of random variables or geophysical fields (Cherry, 1996). It defines co-ordinate systems that optimally describe the cross covariance between two different data sets. The eigenstructure obtained is from the product of the cross covariance matrix between two data sets and its transpose. Since this product matrix describes the hindcast skill (regression coefficients squared), its eigenstructure maximizes this skill. The resulting eigenvalues are called canonical correlation coefficients and represent the levels of correlation between patterns of predictor variables and patterns of predictand variables. The sum of all the coefficients is the hindcast skill of the model.

The advantages of this method are its ability to operate on full fields of information and to objectively define the most highly related patterns of predictors and predictands. By including both space and time lag information in the predictor field, it is possible to define both space and

time evolution of the predictor data that best predicts an associated pattern of the predictand variability (Barnett and Preisendorfer, 1987).

However, the method also has several disadvantages. In highly intercorrelated data fields, the estimation of the inverse matrices needed in CCA may be impossible since the matrices may be degenerate. Further, the large number of spatial points can cause difficulties in inverting the matrices and in the eigenvalue problem. These problems may be solved by first orthogonolizing the predictor and predictand data, through a PCA analysis, and then using the orthogonal variates as input to the CCA. This would also lead to the pre-filtering of the data to eliminate noise (Barnett and Preisendorfer, 1987; Yu *et al.*, 1997). The procedure of determining the number of PCA modes to retain has been discussed in section 3.1.2. However, because the main purpose of doing the PCA is data compaction and filtering, rotation of the significant PCA modes is not necessary (Barnston and Smith, 1996).

The limitation of the number of predictors is vital to CCA. Given enough predictors, CCA, like any other regression scheme, will build a model capable of accounting for large amounts of variance in the predictand, but this apparent skill would be largely artificial. Unfortunately, limiting the number of predictors and predictands in the analyses can exclude information that is potentially useful. Therefore the choice of the number of predictors is very important. In this study, Kaiser's, Scree's test and sampling of error methods were used to identify the number of modes to retain.

Following Yu *et al.* (1997), the CCA forecast model may be derived as given in the following part. Assuming that $X_{s,t}$ denotes the predictor anomaly matrix and $Y_{r,t}$ denotes the predictand anomaly matrix, where the subscripts s and r represent space, and subscript t represent time, such that

s = 1,2...m

r = 1,2...n

t = 1,2...k

PCA on $X_{s,t}$ and $Y_{r,t}$ results in:

$$X_{s,t} = E_{s,s}T_{s,t} \tag{14}$$

$$Y_{r,t} = E_{r,r}T_{r,t} \tag{15}$$

where $E_{s,s}$ and $E_{r,r}$ represent the PCA spatial modes of the predictor and predictand matrices respectively, and $T_{s,t}$ and $T_{r,t}$ are their attendant time coefficients.

If the first i PCA modes of the predictor time series ($T_{i,t}, i < m$) and the first j PCA modes of the predictand time series ($T_{j,t}, j < n$) are retained and used as input into CCA, canonical vectors (u, v) and linear combinations $Z = u'T_{i,t}$ and $W = v'T_{j,t}$ can be determined. The following matrices are defined:

$$U' = [u_1', u_2', ..., u_q'] \tag{16}$$

$$V' = [v_1', v_2', ..., v_q'] \tag{17}$$

$$A_{q,q} = \begin{bmatrix} a_1 & & \\ & a_2 & 0 \\ 0 & & \ddots \\ & & a_q \end{bmatrix} \tag{18}$$

where a_1, $a_2 \ldots a_q$ are canonical correlation coefficients between Y and W, and $a_1 \geq a_2 \geq \ldots \geq a_q$, and q is equal to i or j, whichever is smaller.

Prediction equation at time t for lead-time l for the first j modes of predictand variable can be constructed as:

$$T_{j,t+l} = (V')^{-1} A_{q,q} U' T_{i,t} \tag{19}$$

Using the orthogonal characteristics of PCA modes, truncated equations of equations (14) and (15) can be written as:

$$T_{i,t} = [E_{s,i}]' X_{s,t} \tag{20}$$

$$Y_{r,t} = [E_{r,j}] T_{j,t} \tag{21}$$

Using equations (20) and (21), $T_{j,t+l}$ can thus be transformed back to rainfall as:

$$\hat{Y}_{r,t+l} = E_{r,j} (V')^{-1} A_{q,q} U' (E_{s,i})' X_{s,t} \tag{22}$$

Details of the mathematical derivation of CCA method may be found in several statistical references, including Barnett and Preisendorfer (1978) and Wilks (1995). The next section deals with the estimation of the parameters in the forecast models.

3.4.4 Estimation of Parameters

Major problems in applying equations 12 and 13 are encountered when trying to obtain realistic values of the unknown parameters $\alpha,\beta,\beta_1,\beta_2...\beta_p,\varepsilon$. A brief review of parameter estimation methods is given in the following sections. These include the graphical method, least squares method, method of moments and maximum likelihood method.

3.4.4.1 Graphical Method

The graphical method consists of fitting a function:

$$\hat{Y} = f(X;\alpha,\beta,...)$$

visually through the set of co-ordinate pairs. To estimate m parameters, m points on the curve are selected giving m equations to solve. This process may be simplified by trying various types of graph paper using transformed co-ordinates until a straight-line fit is possible. However, the accuracy of this method is highly subjective, limited, and depends on the experience of the researcher.

3.4.4.2 Least Squares Method

The least squares method consists of fitting a theoretical function to an empirical distribution. The sum of all the squares of the deviations of the observed points from the fitted function is then minimized. Thus to fit a function:

$$\hat{Y} = f(X;\alpha,\beta,...)$$

the sum to be minimized is:

$$S = \sum_{i=1}^{N}(Y_i - \hat{Y}_i)^2 = \sum_{i=1}^{N}(Y_i - f(X_i;\alpha,\beta,...))^2 \qquad (23)$$

where X_i and Y_i are co-ordinates of observed points, α, β, ... are parameters and N the sample size. To obtain the minimum sum of squares, equation (23) is partially differentiated with respect to the parameters as follows:

$$\frac{\partial\sum_{i=1}^{N}(Y_i - \hat{Y}_i)^2}{\partial\alpha} = 0; \frac{\partial\sum_{i=1}^{N}(Y_i - \hat{Y}_i)^2}{\partial\beta} = 0;... \qquad (24)$$

The partial derivatives, equation (24), give equations equal in number to parameters to be estimated.

3.4.4.3 Method of Moments

The method of moments utilizes either the general equation for calculation of the r^{th} moment about the origin of a distribution, P(X), given by:

$$\mu_r' = \int_{-\infty}^{\infty} x^r P(X)dx \qquad (25)$$

or the corresponding equation for central moments of the distribution given as:

$$\mu_r = \int_{-\infty}^{\infty} (x - \mu_1')^r P(X) dx \qquad (26)$$

where μ_1' is the first moment about the origin. The method of moments then relates the derived moments to the parameters of distribution.

3.4.4.4 Maximum Likelihood Method

If f(X; α, β...) is a probability density function of X, with α, β... the parameters to be estimated then the product

$$L = \prod_{i=1}^{N} f(X_i; \alpha, \beta, ...) \qquad (27)$$

is called the likelihood function of a sample of N values from a population of the continuos variable, X. The estimation of α, β, ... consists of determining their values from sample data such that the resultant value of L is as great as possible. Since the natural logarithm of L attains maximum values at a given α, β, ... as L does, the likelihood equation (27) may also be represented as:

$$\ln L = \prod_{i=1}^{N} f(X_i; \alpha, \beta, ...) = \sum_{i=1}^{N} \ln f(X_i; \alpha, \beta, ...) \qquad (28)$$

while its partial derivatives in α, β... equated to zero and called maximum likelihood equations are:

$$\frac{\partial \ln L}{\partial \alpha} = 0; \frac{\partial \ln L}{\partial \beta} = 0; \ldots \tag{29}$$

These equations, same in number as the number of parameters, allow for the computation of estimates of the parameters α, β...

In terms of efficiency, the maximum likelihood method is the best method followed by the method of moments and the least squares method. The graphical method is the least efficient. Under the regularity conditions due to Birch (1964), the parameter estimates obtained by minimizing all distance functions, as in the maximum likelihood method, the method of moments and the least squares method, are best asymptotically normal. These estimators have the following three important properties:

(a) They are consistent. That is, the estimator converges to the true value of the estimated parameter for sufficiently large sample size.

(b) They are asymptotically normally distributed.

(c) They are asymptotically efficient, in that no other estimator can have a smaller variance for sufficiently large sample size.

Due to these three properties, for a sufficiently large sample size, these three methods produce similar parameter estimates. However, the maximum likelihood method and the method of moments are more mathematically complicated and require more computer capability and time. In this study, the maximum likelihood method was used in the estimation of the parameters.

3.5 Test of the Skill of the Fitted Models

In section 3.4 we developed methods for estimating rainfall given the corresponding satellite-derived data. In this section, the ability of these methods to accurately estimate rainfall is investigated. This involves the estimation of rainfall (Y) using data for the period that is not used in the model development. These results in sets of Y values made up of the estimates and the observed. The difference between these values gives a measure of the skill of the estimation model. Several methods can be used to test for goodness of fit of the estimating model. Some of these tests include the analysis of variance (ANOVA) techniques, the Smirnov-Kolmogorov test and the Akaike's Information Criterion (AIC). These methods are highlighted in the next sections. However, details of these and other relevant methods may be found in standard statistical textbooks (e.g. Child, 1990).

3.5.1 Analysis of Variance Techniques (ANOVA)

These methods require a measuring parameter for fitting the discrete and continuous distribution function to empirical distributions. They are based on the fact that the estimators should be as close as possible to the population parameters. The differences between the observed and the estimated values give the measures of the goodness-of-fit. Three such parameters are discussed below including the mean square error, the chi-square and the F-test parameters.

3.5.1.1 Mean Square Error

The difference between the model estimated value and the actual observation could give a measure of the model skill. However, the square of this difference gives a more sensitive result and is the more often used option. The mean square error (MSE) is defined as:

$$MSE = \frac{1}{N}\sum_{i=1}^{N}(Y_i - \hat{Y}_i)^2 \tag{36}$$

where Y_i is the observed rainfall, $\hat{Y}_i$ the estimated rainfall and N the sample size.

3.5.1.2 The Chi-Square (χ^2) Test

Let a discrete variable have k mutually exclusive random events, or a continuous variable be divided into k class intervals, also of mutually exclusive events. If $f_i = 1,2...k$ are the relative frequencies of the random events or class intervals for a sample of size N, and if the discrete or continuous distribution functions have the probability mass of random events or the probability of class intervals as $p_i = 1,2...k$, then the chi-square (χ^2) parameter may be expressed as:

$$\chi^2 = \sum_{i=1}^{k}\left(\frac{N_i - Np_i}{Np_i}\right)^2 \tag{37}$$

where $N_i = Nf_i$ are the observed sample absolute frequencies, and Np_i are the expected values of absolute frequencies. This parameter will have a χ^2-distribution with (k-1) degrees of freedom for a sufficiently large N. The χ^2-test prescribes a critical value χ_0^2 for a given level of significance, so that for $\chi^2 < \chi_0^2$, the null hypothesis of a good fit is accepted, otherwise it is rejected. However, sometimes there is loss of information due to the grouping done by chi-square test and other goodness of fit methods may then be used.

3.5.1.3 The F-Test

The F-statistic used for testing the adequacy of estimation models makes use of the coefficient of determination, R^2. The coefficient of determination may be expressed as

$$R^2 = 1 - \frac{\sum_{i=1}^{n}(Y_i - \hat{Y}_i)^2}{\sum_{i=1}^{n}(Y_i - \bar{Y})^2} \qquad (39)$$

where Y_i is the observed dependent variable, $\hat{Y}$ is the value of the dependent variable estimated by the developed model, and $\bar{Y}$ is the mean of the observed values.

F-test used to test for model adequacy may then be calculated as:

$$F = \frac{R^2 / p}{(1 - R^2) / [n - (p+1)]} \qquad (40)$$

Where p is the number of parameters (one for simple linear regression), and n is the sample size.

The above calculated statistic is compared with the standard F-table values with p degrees of freedom in the numerator and [n–(p+1)] degrees of freedom in the denominator at the desired level of significance. Details of this test can be found in many standard statistical textbooks including Wilks (1995).

3.5.2 Kolmogorov-Smirnov Test

The Kolmogorov-Smirnov statistic, D, is based on the deviations of the sample distribution function F(X) from the completely specified continuos hypothetical distribution function P(X) such that

$$D_n = \max imum|F(X) - P(X)| \tag{38}$$

where D_n is the maximum difference between the two distributions and n the sample size. For a sufficiently large sample size, the value of D_n tends to be small if the actual distribution function is close to the estimating function. Tables for this test, for various values of sample size n, have been developed and are presented in many published collections of statistical tables (Yevjevich, 1972; Kite, 1978; DeGroot, 1986).

3.5.3 Hits and Alarms

Hit and Alarm rates can also be used to address the skill and reality of the fitted models. In this case the observations and the estimates are ranked and grouped into below normal, normal and above normal rainfall categories. Alarm signals correspond to all cases where the models have predicted below or above normal category while the observed is normal. Hit rate, on the other hand, refers to all correct forecasts. The percentage of hit rates can be used to reflect the skill of the model (Degene, 1999).

3.5.4 Akaike's Information Criterion

Akaike (1973) proposed the use of the Kullback-Liebler (K-L) distance (Kullback and Liebler, 1951) in the procedure for the identification of an optimal model from a class of the

estimation models. This distance may be conceptualized as a directed "distance" between two models and is a measure of the discrepancy between them. The K-L distance between the models $F(X)$ and $G(X)$ is defined, for continuos functions, as:

$$I(F,G) = \int F(X) \ln\left(\frac{F(X)}{G(X|\theta)}\right) dx \tag{30}$$

$I(F,G)$ is a measure of the information "lost" when G is used to approximate F. Using the approximating model that "loses" as little information as possible is equivalent to minimizing $I(F,G)$ over G. A relative expected K-L distance may be defined as:

$$E_y E_x \left[\ln\left(G\left(X|\hat{\theta}(Y)\right)\right)\right] = cons\tan t - E_{\hat{\theta}}\left[\hat{I}(F,G)\right] \tag{31}$$

where $\hat{\theta}(Y)$ are the estimated parameters from the data and $\hat{I}(F,G)$ the K-L distance estimated given the estimated parameter, $\hat{\theta}$.

The expression on the left-hand side of equation (31) involves what looks like the natural logarithm of the probability model for the data. That is, the conceptual $\ln\left(G\left(X|\hat{\theta}(Y)\right)\right)$ bears a strong resemblance to actual natural logarithm of the likelihood of the function. In other words,

$$\ln\left(L\left(\hat{\theta}(Y)|Y\right)\right) \equiv \ln\left(G\left(Y|\hat{\theta}(Y)\right)\right) \tag{32}$$

where Y refers to the sample data and *L(.)* is the likelihood of the estimating function. Therefore, we may estimate $E_{\cdot}E_{\cdot}\left[\ln\left(G\left(X|\hat{\theta}(Y)\right)\right)\right]$ by the maximized $\ln\left(L\left(\hat{\theta}(Y|Y)\right)\right)$ for each model. However, Akaike (1973) showed that the maximum natural logarithm-likelihood is biased upwards as an estimator of the model selection target criterion, and that this bias is approximately equal to K, the number of estimable parameters in the approximating model. Thus, an approximating unbiased estimator may be given as:

$$\hat{T} = \ln\left(L\left(\hat{\theta}|Y\right)\right) - K \tag{33}$$

where the notation $\hat{\theta} \equiv \hat{\theta}(Y)$. This result is equivalent to:

$$relative(K-L)distance = -\ln\left(L\left(\hat{\theta}|Y\right)\right) + K \tag{34}$$

The Akaike's Information Criterion (AIC) is then defined by multiplying equation (34) by two to get:

$$AIC = -2\ln\left(L\left(\hat{\theta}|Y\right)\right) + 2K \tag{35}$$

The model with minimal AIC is the best fitting model. Further details of this method may be found in Burnham and Anderson (1998).

3.5.5 Cross-Validation

After development of a prediction model, it is normally important to validate its efficiency in giving an accurate forecast. This section looks at the method used in the validation of the CCA models.

Forecasting models from CCA are developed in such a way as to give the best possible relation between the predictor and the predictand variables. Significance tests on these models are very important in the interpretation of the results. A procedure that is usually used to test the skill of the CCA models is often called cross validation (Barnett and Preisendorfer 1987; Yu *et* al., 1997).

Cross validation is a generalization of the common technique of repeatedly omitting a few observations from the data, reconstructing the model, and then making forecasts for the omitted cases (Stone, 1974). This is a non-parametric method that provides an unbiased estimate of the forecast skill (Yu *et al.*, 1997).

Assuming that the predictor and predictand data of N-time points are divided into L segments, a model is developed using the data of L-1 segments. This developed model is then used to predict the variable in the omitted segment. This process is successively repeated by changing the segment that is excluded from the model development. By doing this, N predictions are finally obtained. These predicted values are then correlated with the original N observations and the overall skill ascertained using the usual statistical tests for correlation coefficients, which were discussed in section 3.3.1.

In this study, ANOVA, the hits and alarms and the cross-validation techniques were used to determine the goodness of fit of the developed models. In the next section, the methods used to study the evolution patterns during anomalous seasons are discussed.

3.6 Rainfall Evolution Patterns during the Normal, Dry and Wet Seasons.

In sections 3.3 to 3.5 we dealt with the estimation of rainfall using satellite-derived data and assessing the skill of the satellite-derived information in estimating rain gauge recorded rainfall information. This section discusses the various methods that may be used to study the evolution of 10-day/seasonal rainfall and general circulation patterns, in order to identify the systems that could be associated with the low/high skills of the satellite-derived estimates during wet/dry seasons.

3.6.1 Identification of Anomalous Rainfall Seasons

In order to study the space-time evolution patterns of rainfall during the anomalous wet and dry seasons, it was important to first identify the major wet and dry seasons within the study period. Several methods are available for identification of years with wet, dry and normal seasons including rainfall indices and PCA T-mode.

The rainfall anomaly index involves the separation of the standardized rainfall anomalies into three categories representing excessive rainfall (wet case), deficit rainfall (dry case) and normal rainfall (normal case). To delineate the three-rainfall anomaly categories, rainfall standardized anomaly time series for the individual seasons and locations are computed in order to generate the regional rainfall anomaly indices. These indices (χ_t) may be expressed as follows:

$$\chi_t = \frac{1}{m}\sum_{j=1}^{m}\frac{(x_{tj} - \bar{x}_j)}{\sigma_j} \qquad (41)$$

where m is the total number of rainfall stations within a particular climatological region, and x_{ij} is the rainfall observation for a particular dekad for station j. The dekadal mean rainfall for station j is represented by $\bar{x}$, and σ_j is the standard deviation for the rainfall in station j. However this is a stringent index that may pick out only the very extreme cases.

Another rainfall index (R_i) that may be used to categorize the seasons utilises the observed rainfall as a fraction of the mean and maybe expressed as follows:

$$R_i = \frac{1}{m}\sum_{j=1}^{m}\frac{100X_{ij}}{\bar{X}_j} \qquad (42)$$

The rainfall indices are then ranked and appropriate values chosen to identify the dry, normal and wet scenarios.

In order to select the anomalous rainfall years, seasonal rainfall data may also be subjected to PCA in T-mode. The PCA solutions cluster together years with similar seasonal rainfall patterns. Details of PCA methodology have been discussed in section 3.1.

Percentile and quartile methods can also be used in categorizing the seasons. These involve ranking of the data and dividing it into percentiles or quartiles, depending on the data length. These methods directly compare one season with all the others under study and also take into account the skewness of historical rainfall records (Ambenje *et al.*, 1993). The season scenarios are given in table 3.1. This is the method that is used by the Nairobi based Drought Monitoring Centre for the Greater Horn of Africa region to quantify rainfall deficits and surpluses. It was the method used in this study. After identifying the years with anomalous seasons, the onset, duration and withdrawal of these seasons were determined.

Table 3.1: Classification of the dry, normal and wet seasons scenarios

Scenario Type	Range
Dry	$R \leq Q1$
Normal	$Q1 < R \leq Q3$
Wet	$R > Q3$

Note: R represents observed rainfall, Q1 and Q3 the fist and third quartiles respectively.

The next section highlights the method used in the determination of these periods.

3.6.2 Onset, Withdrawal and Duration of Rainfall Seasons

Mass curves were used to determine the onset, withdrawal and hence the duration of rainfall seasons at specific locations. Under this method, cumulative ten-day (dekad) average rainfall values were plotted against the dekad numbers giving the mass curves. The dekad of onset is the time when there is a sudden increase in rainfall values while the dekad of withdrawal is the time when there is a sudden decrease (Ogallo *et al.*, 1994). The duration of the season is derived from the onset and withdrawal dates.

Several investigations have used this method in identifying the onset, withdrawal and duration of rainfall seasons. These include Asnani (1993) for Indian Sub-continent, Alusa and Mushi (1974) and Ogallo *et al.* (1994) for East African regions, and Jollife and Sarria-Dodd (1994) for tropical rainfall.

After identifying the wet, dry and normal seasons, composites of the circulation patterns were derived. Details of the compositing method are given in the next section.

3.6.3 Composite Analysis

One of the major problems with correlation and regression methods is that they assume that variables must be related in both positive and negative phases. For example if floods occur during El Nino, droughts must occur during La Nina. This is sometimes not true in the case of some physical processes. Composite method could provide some alternative way of simplifying complex linkages. Composite analysis involves the identification and averaging of one or more categories of fields of a variable selected according to their association with "key" conditions (Folland, 1983). The "key" conditions for this study include anomaly scenarios (wet, dry and normal seasons), onset, withdrawal and duration for the respective anomaly scenarios.

Another major advantage of using composite analysis is the presentation of results in meteorological units. This makes it easier to physically interpret composite fields, especially their gradients, compared to the other statistical measures of association, which have been used in meteorology. For example, a map of non-dimensional correlation coefficient is difficult to physically interpret due to the low biasing of the correlation by random error on observation (Kendall and Stuart, 1961). The composite method is also capable of displaying some features that would otherwise be smoothed out by correlation analyses and many other basic climatological/statistical methods (Okoola, 1996).

However, studies have indicated that the results obtained from composite analysis usually agree closely with results from correlation methods (Ward, 1992). Several authors within and around the study area have used the composite analysis method. Matarira and Jury (1992) studied the meteorological structure of inter-seasonal wet and dry spells in Zimbabwe while Okoola (1998) investigated the spatial evolutions of the active convective patterns in the equatorial East

African region using outgoing long-wave radiation. Okoola (1999) also did a diagnostic study on the East African monsoon circulation using the same approach.

In this study the quartile method and the season anomaly scenarios given in table 3.1 were used to delineate wet, dry and normal years within the period of study. This was due to the relatively short length of the study period. The averages of the anomalous dry/wet categories were used as the composites for the specific variables at specific locations.

Composites were derived for winds (850 mb and 200 mb) for the seasons that were identified for each category. These would provide evolutions of circulation patterns that may be associated with the various season categories.

The next chapter presents and discusses the results obtained from the study.

CHAPTER FOUR

RESULTS AND DISCUSSION

4.0 Introduction

This chapter presents and discusses the results obtained from the various methods used in this study. These methods include PCA for regionalization and identification of representative station(s), correlation analysis for investigating the degree of relationship between the rain gauge recorded rainfall and the satellite-derived data and regression analyses for the development of models for rainfall estimation. The rest of the methods are anomaly index for the identification of anomalous wet or dry years, mass curves to identify the onset and withdrawal of the seasons, and composite analysis for the study of the evolution of the circulation parameters.

4.1 Skill of the Estimated Data and Data Quality

The methods used to estimate the missing rainfall data and to test for the quality of the data were discussed in section 2.1. These included the correlation and regression methods to estimate the data and the mass curves to test for the homogeneity of the data. Results from the mass curves of the data including the estimated missing indicated that in general only straight single lines could be fitted to rainfall records from most of the stations. Examples of the derived mass curves are shown in Figure 4.1. The results were indicative of the acceptable quality of rainfall records that were subjected to various analyses in the rest of the study.

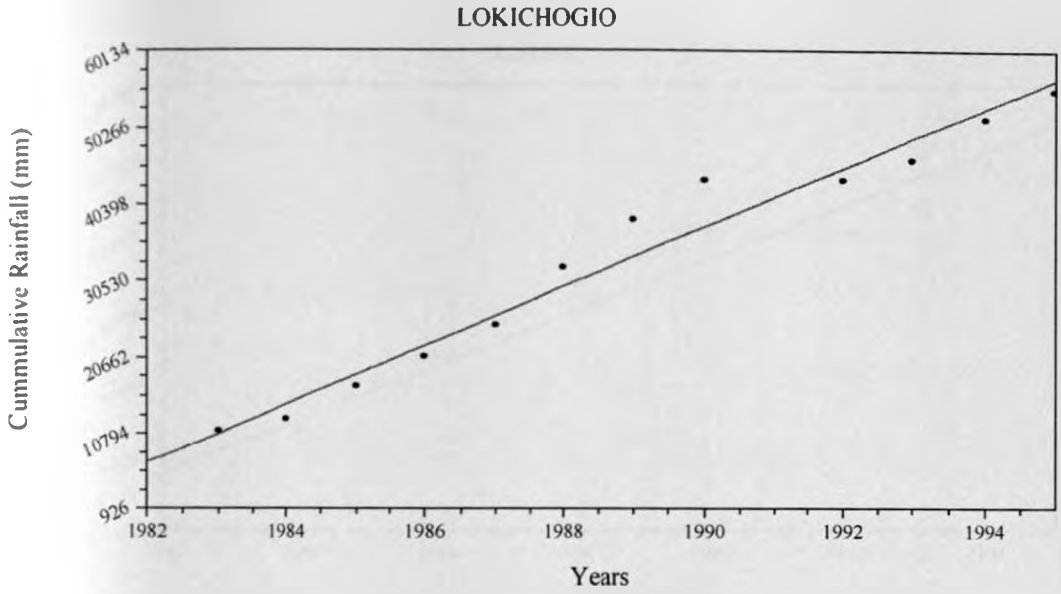

Figure 4.1(a): Mass Curve for Lokichogio Station

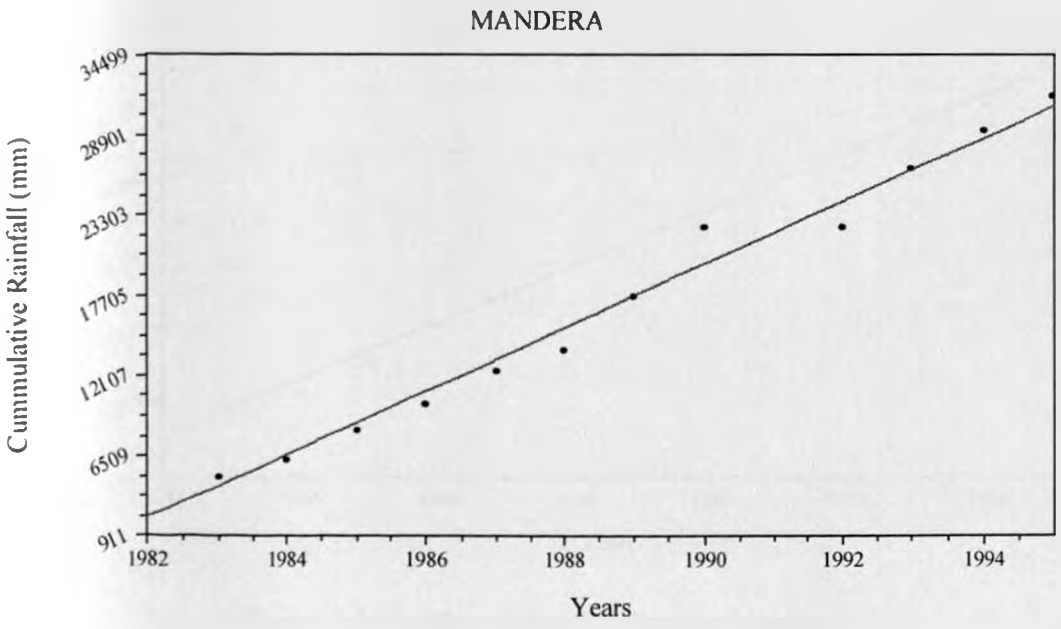

Figure 4.1(b): Mass Curve for Mandera Station

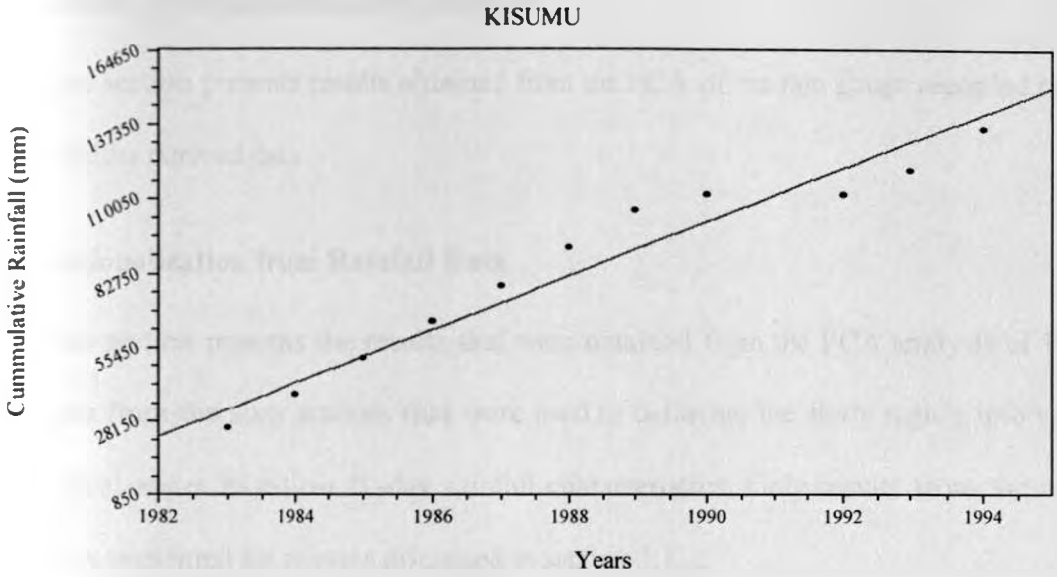

Figure 4.1(c): Mass Curve for Kisumu Station

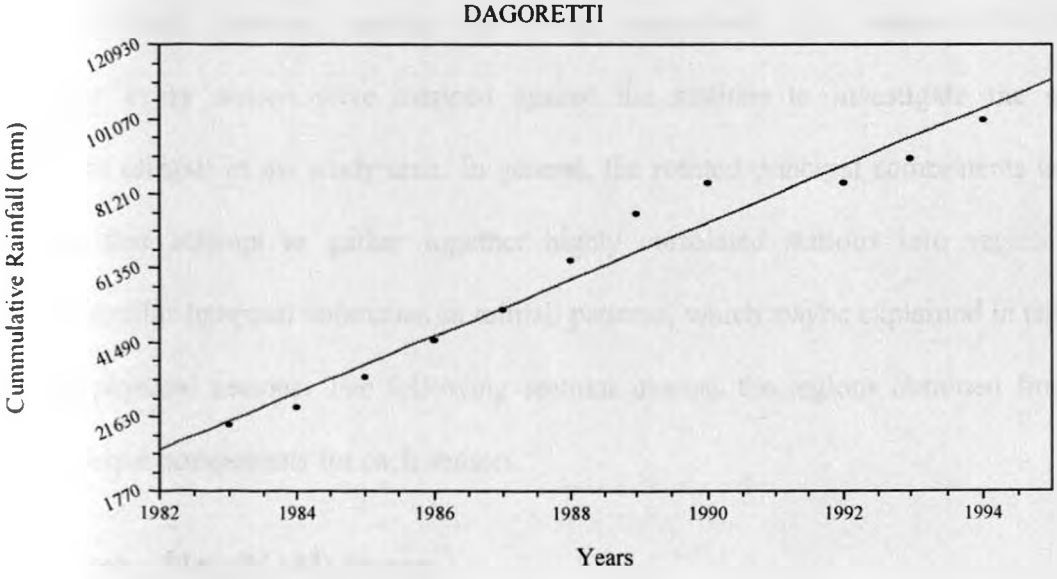

Figure 4.1(d): Mass Curve for Dagoretti Station

4.2 Results from Regionalization analyses

This section presents results obtained from the PCA of the rain gauge recorded rainfall and the satellite derived data.

4.2.1 Regionalization from Rainfall Data

This section presents the results that were obtained from the PCA analysis of 10-day rainfall data from the sixty stations that were used to delineate the study region into various climatological zones based on 10-day rainfall characteristics. Only results from the rotated solutions are presented for reasons discussed in section 3.1.2.

PCA was independently performed on the dekadal data from the four typical seasons, namely March-April-May (MAM), June-July-August (JJA), September-October-November (SON) and December-January-February (DJF). These seasons correspond to the Northern Hemisphere spring, summer, autumn and winter respectively. The rotated PCA factor loadings for every season were mapped against the stations to investigate the spatial variability of rainfall in the study area. In general, the rotated principal components usually give maps that attempt to gather together highly correlated stations into regions that experience similar temporal anomalies in rainfall patterns, which maybe explained in terms of underlying physical reasons. The following sections discuss the regions obtained from the rotated principal components for each season.

4.2.1.1 March – May (MAM) Season

This is the main rainy season for the study area. It is normally called the long rain season. During this season, the sun is directly overhead the equatorial region on its way from the Southern to the Northern Hemisphere and the ITCZ is therefore located over the study area.

Results from Kaiser's criterion, shown in Table 4.1, indicate that thirteen components, accounting for a total of 68.3% variance, were significant above noise levelswhile Scree's test declared about eight components significant as is shown in Figure 4.2. The table also shows that the sampling error test by North *et al* (1982) declared only six components significant. The six PCA components account for a variance of 54.3% of the total variance. Thus the extra seven components that were extracted by Kaiser's criterion accounts for only 14 % of the dekadal rainfall variance during the long rainfall season, while the extra two PCA modes from Scree's test can account for only 2.69% of the dekadal rainfall variance.

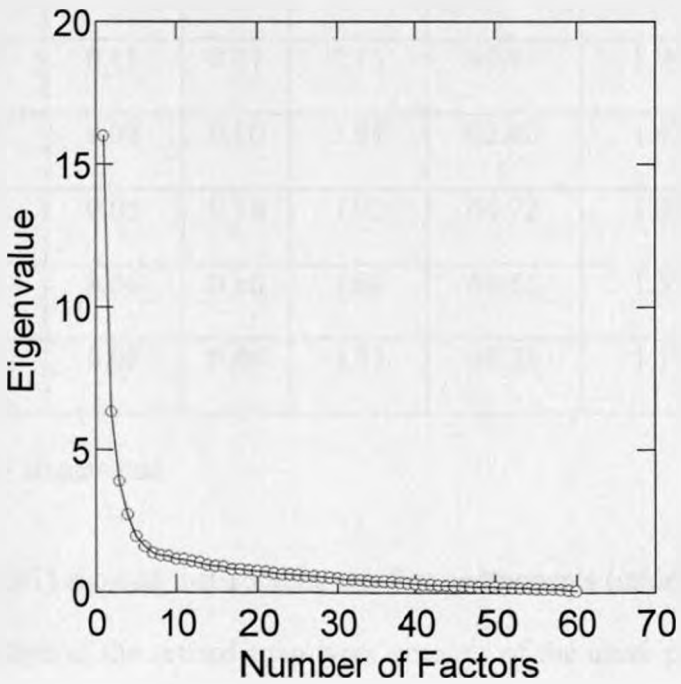

Figure 4.2: Scree's test selection of the dominant principal components for MAM season

Table 4.1: Statistical characteristics of 1982 –1995 dekadal rainfall from PCA of MAM season

Factor	Non rotated Eigenvalue	EV_{i+1}-EV_i	North's Test	Non Rotated		Rotated	
				Variance extracted (%)	Cumulated variance (%)	Eigenvalue	Variance extracted (%)
1	16.01	9.69	1.40	26.68	26.68	7.12	11.86
2	6.32	2.41	0.55	10.54	37.22	6.94	11.56
3	3.91	1.19	0.34	6.52	43.74	5.58	9.30
4	2.72	0.75	0.24	4.53	48.27	2.60	4.33
5	1.97	0.36	0.17	3.29	51.56	5.55	9.25
6	1.61	0.22	0.14	2.69	54.25	1.67	2.78
7	1.39	0.09	0.12	2.31	56.56	2.37	3.95
8	1.30	0.02	0.11	2.17	58.73	1.63	2.72
9	1.28	0.11	0.11	2.13	60.86	1.97	3.28
10	1.17	0.02	0.10	1.94	62.80	1.42	2.36
11	1.15	0.05	0.10	1.92	64.72	1.43	2.38
12	1.10	0.06	0.10	1.84	66.56	1.52	2.53
13	1.04	0.08	0.09	1.73	68.29	1.19	1.99

Note: EV = Eigenvalue

Richman (1981) showed that rotating too few components (under-factoring) is likely to result in a distortion of the rotated map types because of the usual procedures for initial component extraction which aim at removing something approximating the maximum possible variance at each step. Rotating too many factors (over-factoring), on the other hand has been shown not to have an adverse effect on the interpretation of the resultant maps (Dingman *et al.*, 1964; Cattell, 1958). The large number of significant components seems to reflect the strong influence of local and regional factors such as topography, large water

bodies and other thermally induced local/regional circulation including katabatic and anabatic circulation on dekadal rainfall patterns. Eight components that were identified by the Scree's method were, therefore, retained for rotation in this season. Only the first three significant components are presented here.

The spatial distributions of the first rotated principal component for the MAM season, which accounts for 11.9% of the total variance, were dominant around Lake Victoria and most of western and northwestern parts of the study region extending to the central sections as shown in Figure 4.3(a). This is one of the wettest parts of Kenya. The unique characteristic of the region delineated by this component may be due to the interaction between the influence of Lake Victoria, the meridional arm of the ITCZ that is often associated with incursions of the moist westerly Congo air mass, and the zonalarm of the ITCZ.

The second rotated component that accounts for a variance of 11.6% of the total variance is seen to be dominant in the coastal region as displayed by Figure 4.3(b). This component isolates a region that probably reflects the daily influence of the Indian Ocean through the Land/sea breeze circulation. The third rotated component, accounting for 9.3% of the total variance, is dominant over the southeastern lowlands capturing the topographic effects of low altitudes. This component is displayed in Figure 4.3(c). According to Burt-Banks formula (Child, 1990), significant loadings were considered as those above 0.2.

Using all the eight rotated components and comparing the spatial patterns of the dominant PCA components, eleven regions were derived for the MAM season. These regions are displayed in Figure 4.4 while the possible underlying physical reasons are given in Table 4.2.

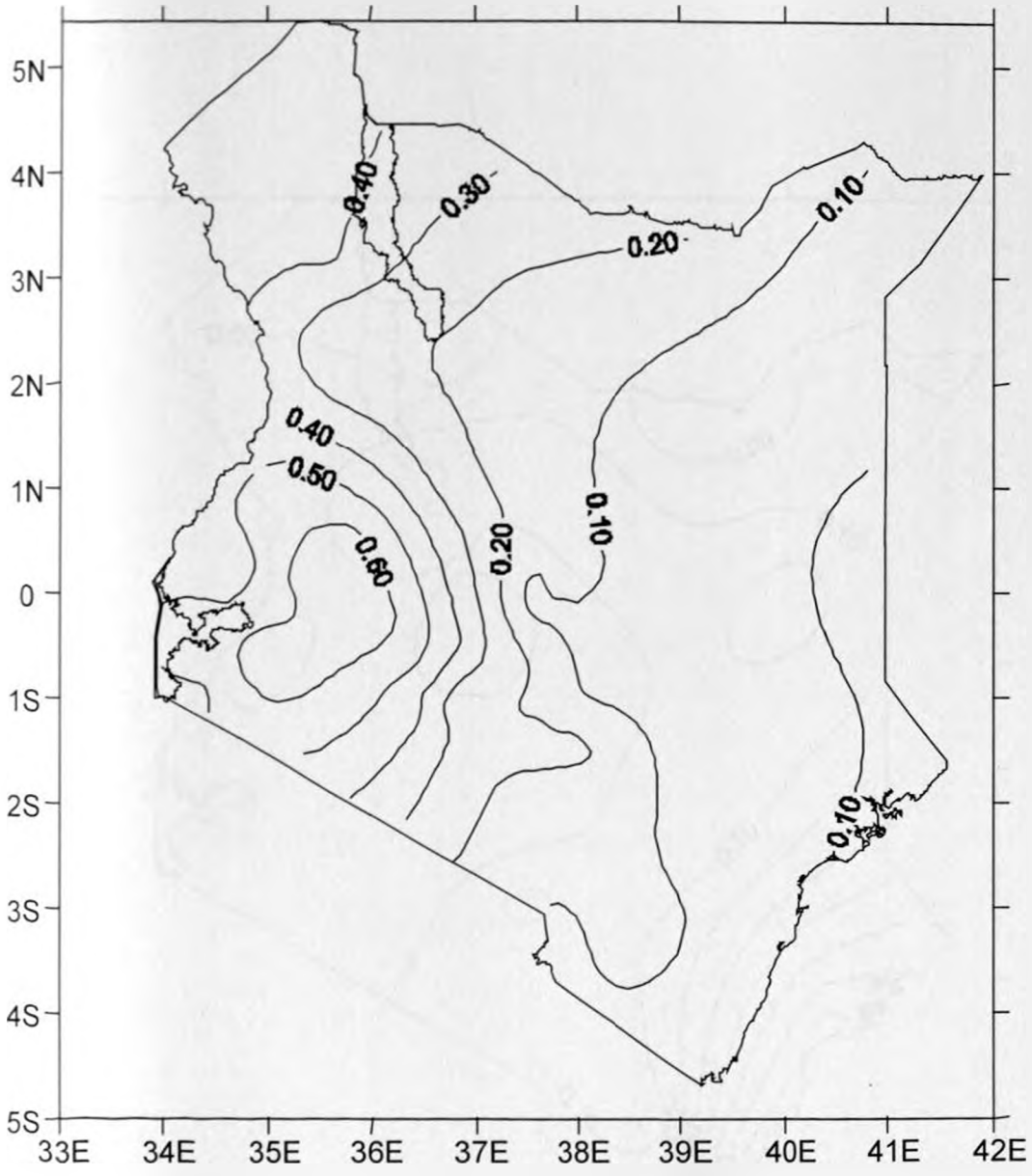

Figure 4.3(a): Spatial patterns of the first rotated principal component during MAM season.

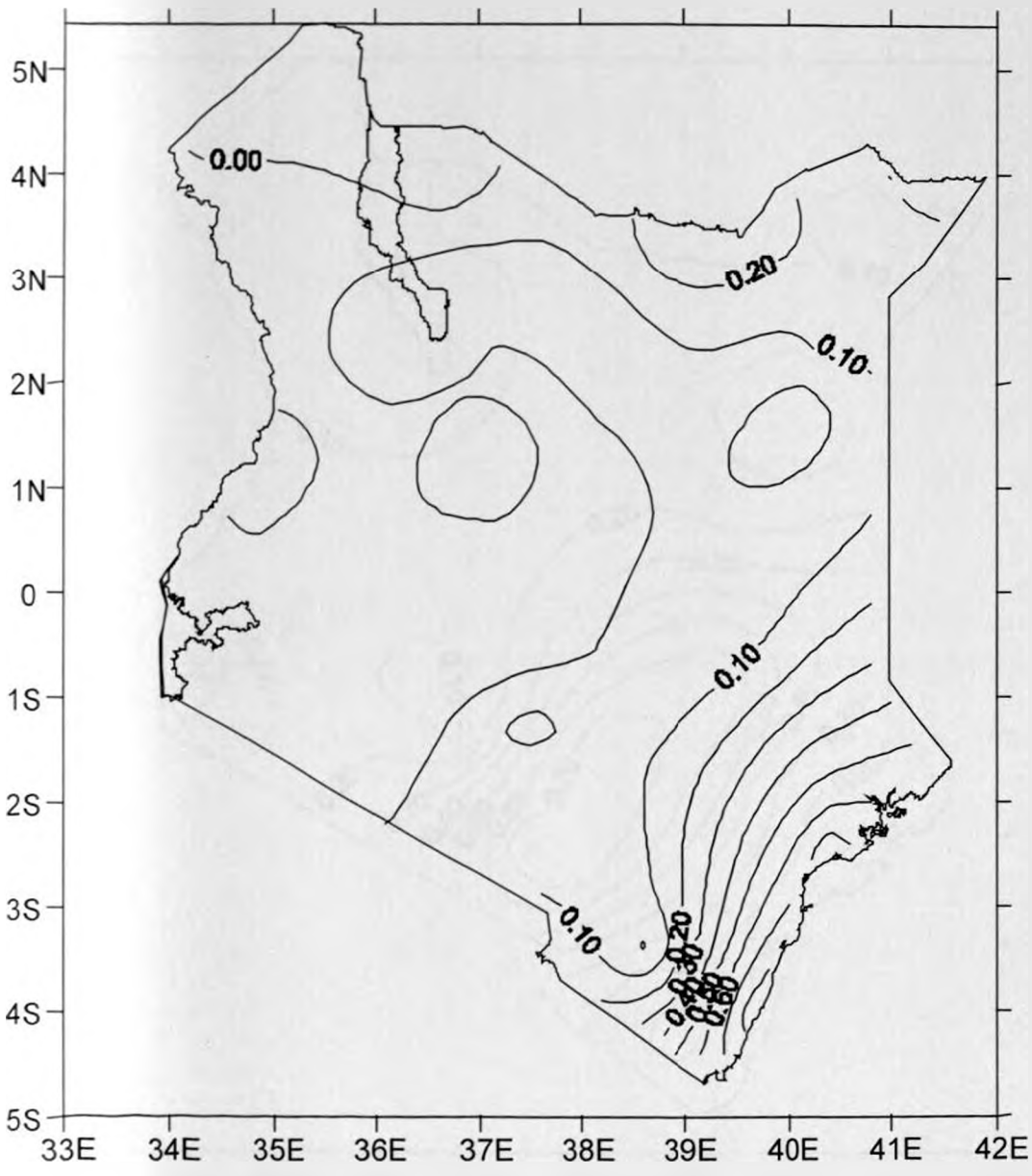

Figure 4.3(b): Spatial patterns of the second rotated principal component during MAM season.

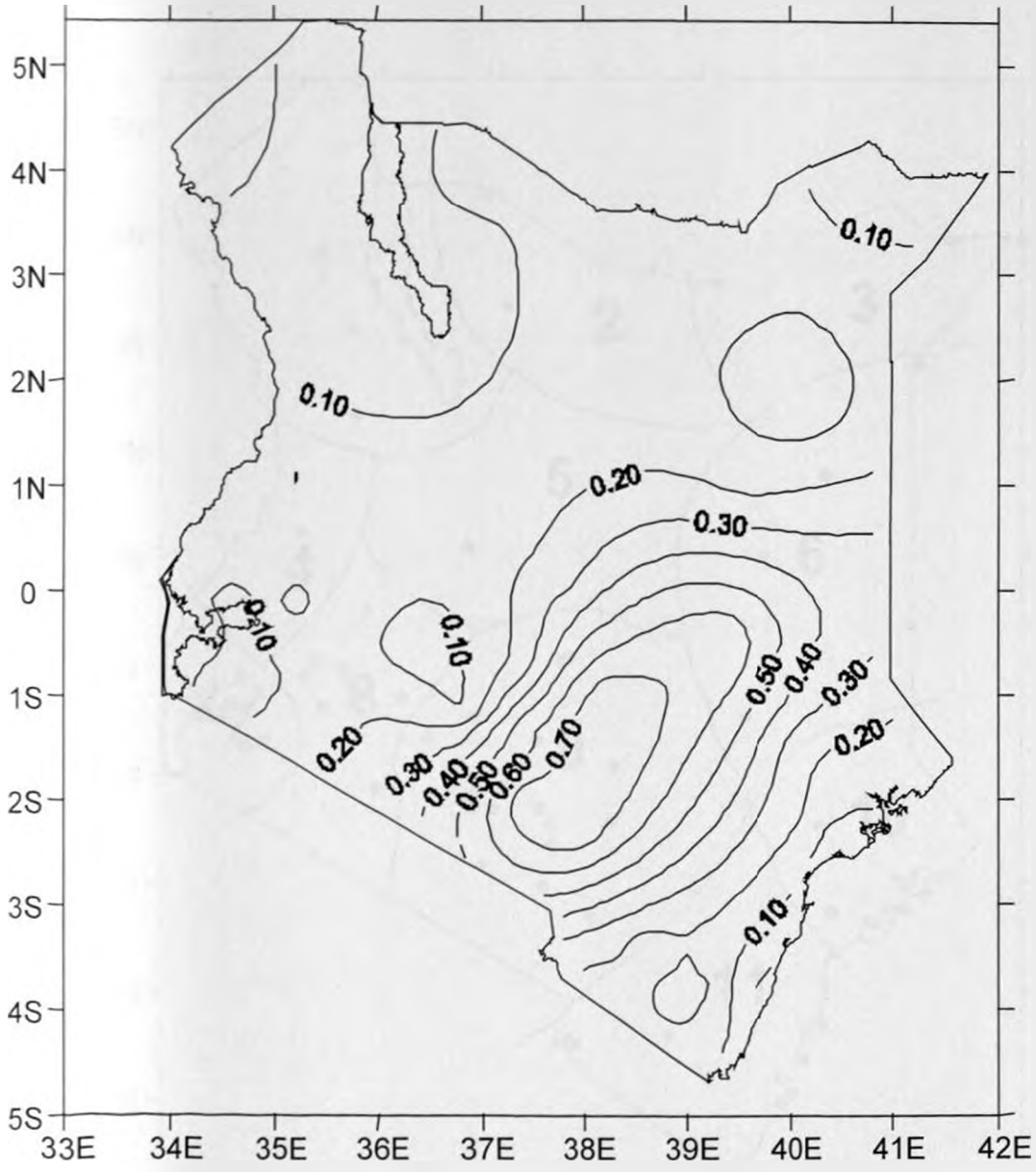

Figure 4.3(c): Spatial patterns of the third rotated principal component during MAM season.

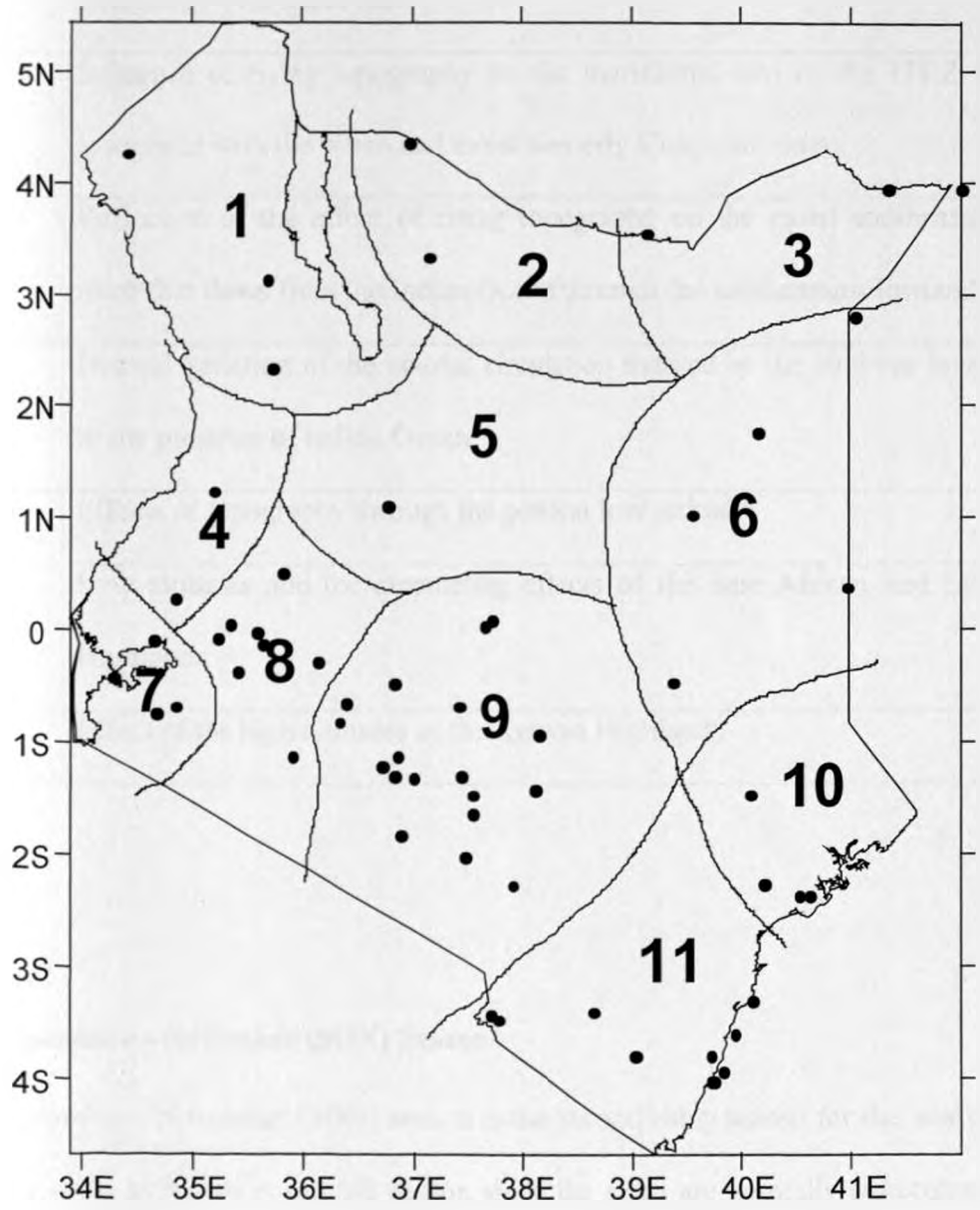

Figure 4.4: Homogenous divisions of the 60 stations derived from the MAM seasonal RPCA patterns.

Table 4.2: The possible physical reasons underlying the derived regions for MAM

REGION	POSSIBLE UNDERLYING PHYSICAL REASONS
7	Reflection of the diurnal variation of Lake Victoria circulation and its interaction with the ITCZ
4	Influence of rising topography on the meridional arm of the ITCZ usually associated with the warm and moist westerly Congo air mass
9	Reflection of the effect of rising topography on the moist southeasterly air mass that flows from the Indian Ocean through the southeastern lowlands
10 & 11	Diurnal variation of the coastal circulation marked by the land/sea breeze due to the presence of Indian Ocean
3 & 6	Effects of topography through the general low altitudes
1, 2 & 5	Low altitudes and the channeling effects of the East African and Ethiopian Highlands
8	Effect of the high altitudes of the Kenyan Highlands

4.2.1.2 September - November (SON) Season

September - November (SON) season is the second rainy season for the study area. It is locally known as the short rainfall season since the rains are normally concentrated only over the months of October and November. The ITCZ is located over the study area for the second time within the year as it moves from the Northern to the Southern Hemisphere.

The Scree's plot of the eigenvalues is given in Figure 4.5, while Table 4.3 gives the summary of the results that were obtained when dekadal rainfall records for the season were

subjected to PCA. The results show that using Kaiser's criterion, thirteen components accounting for 68.1% of the total dekadal rainfall variance were declared significant. According to Scree's test, seven components that account for 56.1% of the total variance were identified as significant. North *et al.* (1982) however declared only two components significant. The two components accounted for about 35.8 % of dekadal rainfall variance for the season.

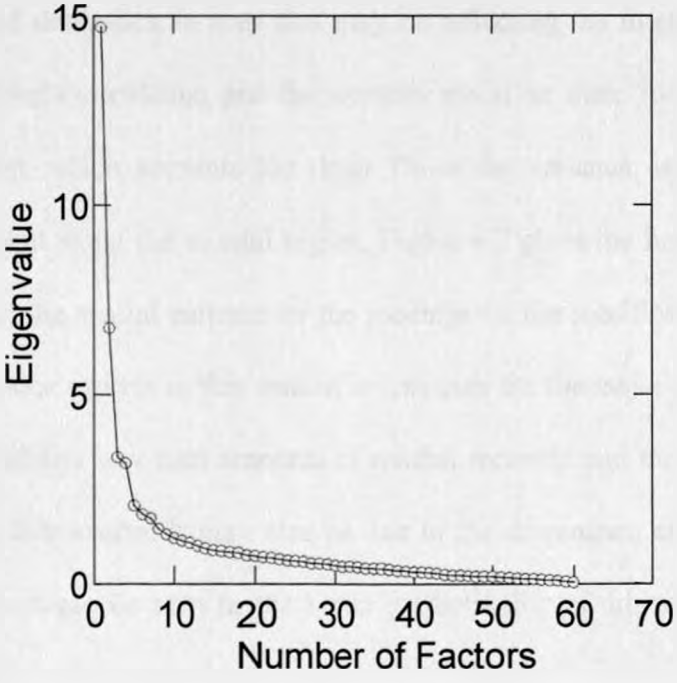

Figure 4.5: Scree's test selection of the dominant principal components for SON season

The spatial patterns of the first three dominant rotated principal components for this season are displayed in Figure 4.6. The first rotated principal component, which explains about 16% of the total variance, is shown to be relatively significant in most parts of the study region except over the Lake Victoria region. However it is highly dominant around the highlands to the southeast of the Rift Valley. This is depicted in Figure 4.6(a). This component may be capturing the homogeneity of spatial rainfall characteristic during the season that could be associated with the influence of the ITCZ. Such observations have been made in previous studies (Ogallo, 1989; Ininda, 1994; Indeje *et al.*, 2000). The spatial distribution of the second rotated component that accounts for 11% of the total variance is given in Figure 4.6(b). This component is dominant mainly to the west and northwest parts of the study region and delineates an area that may be reflecting the interactions between the ITCZ, the Lake Victoria circulation and the westerly moist air mass from the Congo Basin. The third component, which accounts for about 7% of the variance, is displayed in Figure 4.6(c) and is dominant along the coastal region. Figure 4.7 gives the homogenous zones for the season based on the spatial patterns of the loadings of the significant components. The number of homogenous regions in this season is less than for the major rainfall season. This may be due to the relative low total amounts of rainfall received and the widespread dryness experienced during this season. It may also be due to the dominance of large-scale features and teleconnections as can be seen in the better predictability of this season (Ininda, 1994; Indeje *et al.*, 2000).

Table 4.3: Statistical characteristics of 1982 –1995 dekadal rainfall from PCA of SON season

Factor	Non rotated Eigenvalue	EV_{i+1}-EV_i	North's Test	Non Rotated		Rotated	
				Variance extracted (%)	Cumulated variance (%)	Eigenvalue	Variance extracted (%)
1	14.70	7.94	1.38	24.50	24.50	9.47	15.79
2	6.76	3.40	0.63	11.27	35.77	6.63	11.04
3	3.36	0.16	0.32	5.59	41.36	4.42	7.36
4	3.20	1.12	0.28	5.33	46.69	3.06	5.09
5	2.08	0.24	0.19	3.46	50.15	1.86	3.10
6	1.84	0.09	0.17	3.07	53.22	2.33	3.89
7	1.75	0.30	0.16	2.91	56.13	2.90	4.83
8	1.45	0.11	0.14	2.42	58.55	1.86	3.09
9	1.31	0.11	0.12	2.18	60.73	2.09	3.44
10	1.20	0.06	0.11	2.00	62.73	1.99	3.31
11	1.14	0.05	0.11	1.90	64.63	1.30	2.17
12	1.09	0.09	0.10	1.82	66.45	1.55	2.58
13	1.00	0.06	0.09	1.67	68.12	1.45	2.42

Note: EV = Eigenvalue

Apart from the low value of the variance, the patterns of the homogenous zones are close to those that have been derived from monthly and seasonal rainfall values (Beltrando, 1990; Nyakwada *et al.*, 1999). Past studies have shown that the spatial distribution of rainfall anomalies is most homogenous in this season than in the others. Droughts and above normal rainfall occurrences are more widely spread over the region of study during this season than in the previous rainfall season. Thus predictability of rainfall may be higher in this season than the previous one since the first PCA mode, that may be representing a single predictor, is

significant in most parts of the region. This has been reported in some previous studies (Hastenrath *et al.*, 1993; Webster, 1994)

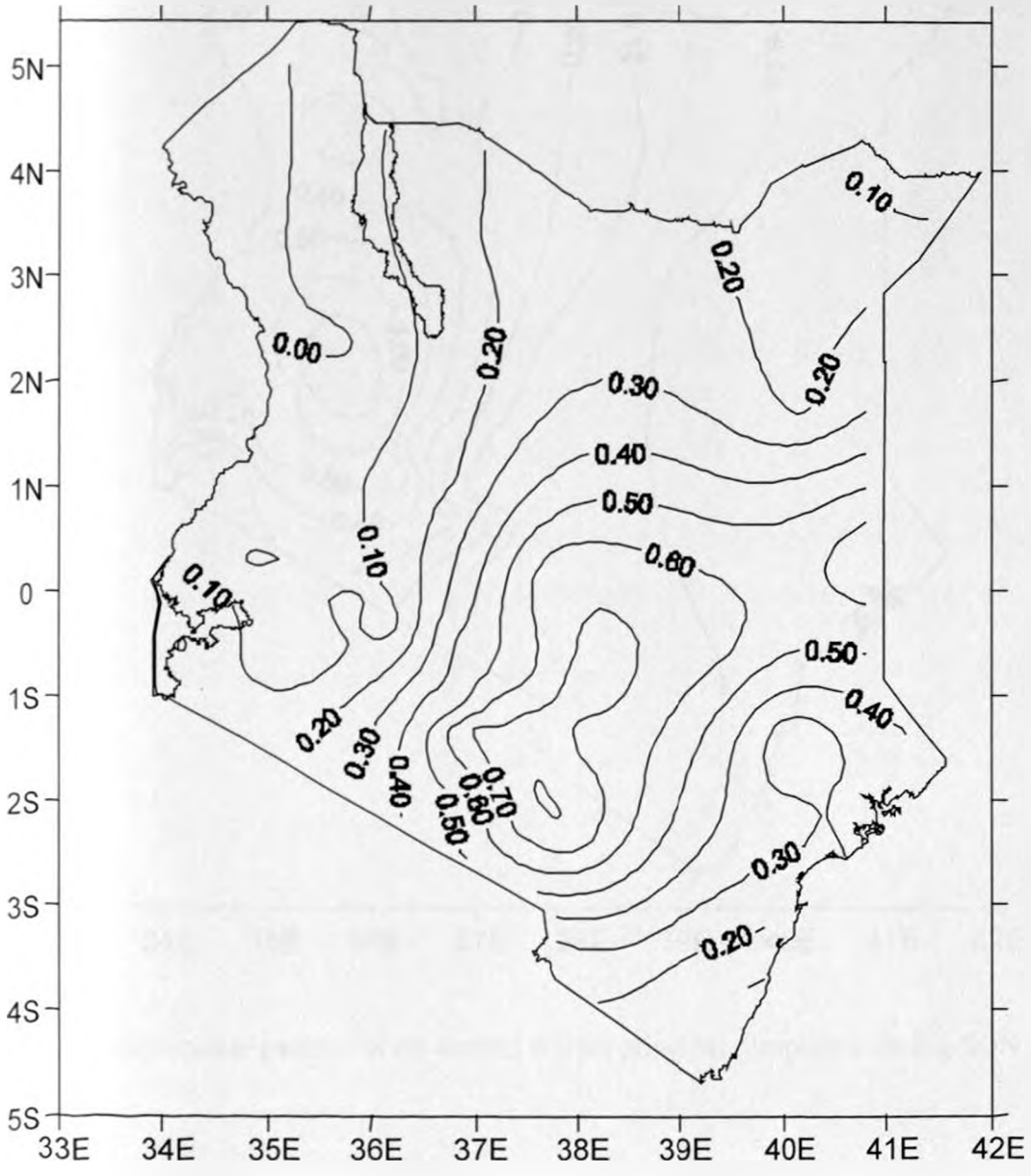

Figure 4. 6(a): Spatial patterns of the first rotated principal component during SON season.

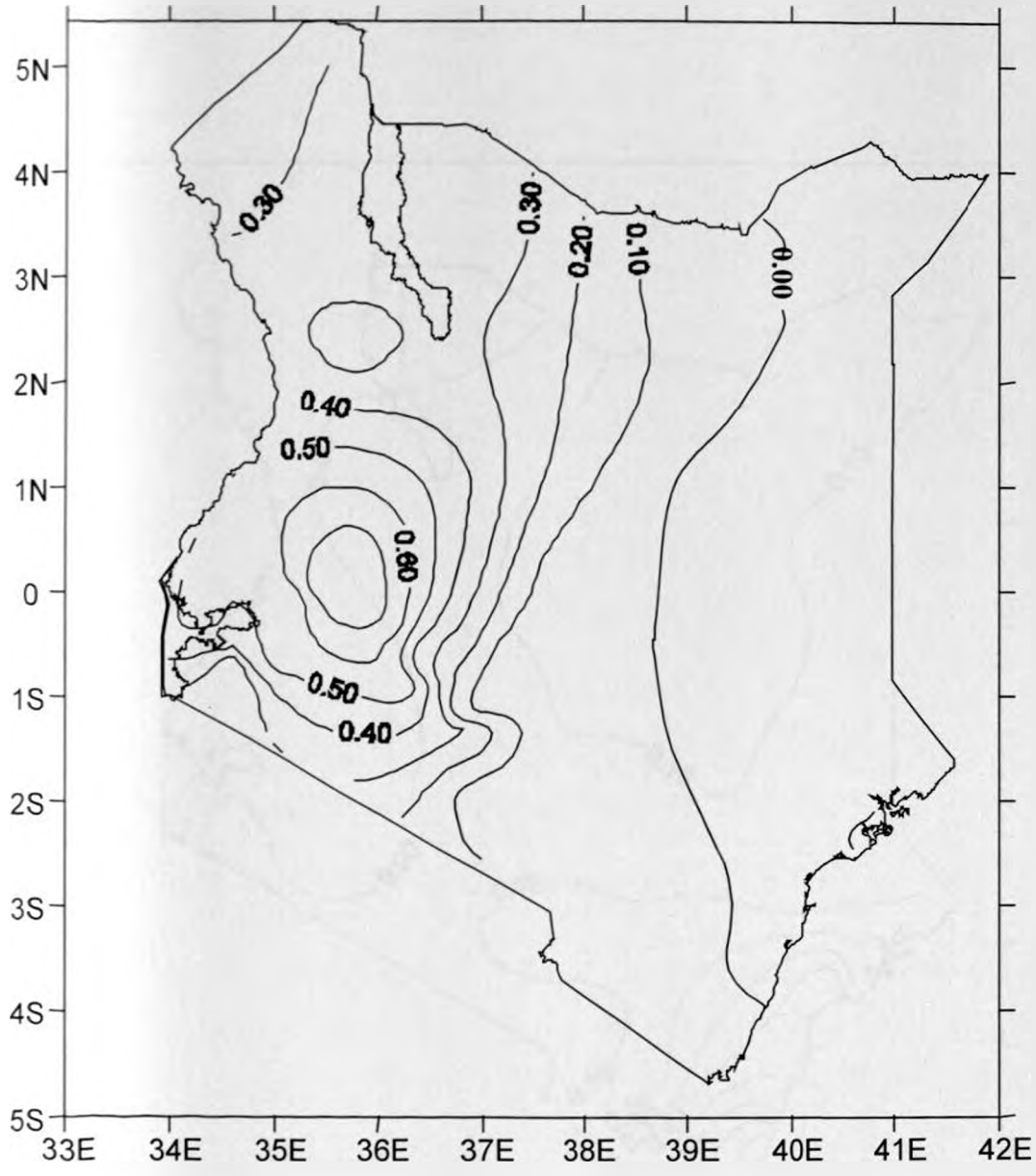

Figure 4.6(b): Spatial patterns of the second rotated principal component during SON season.

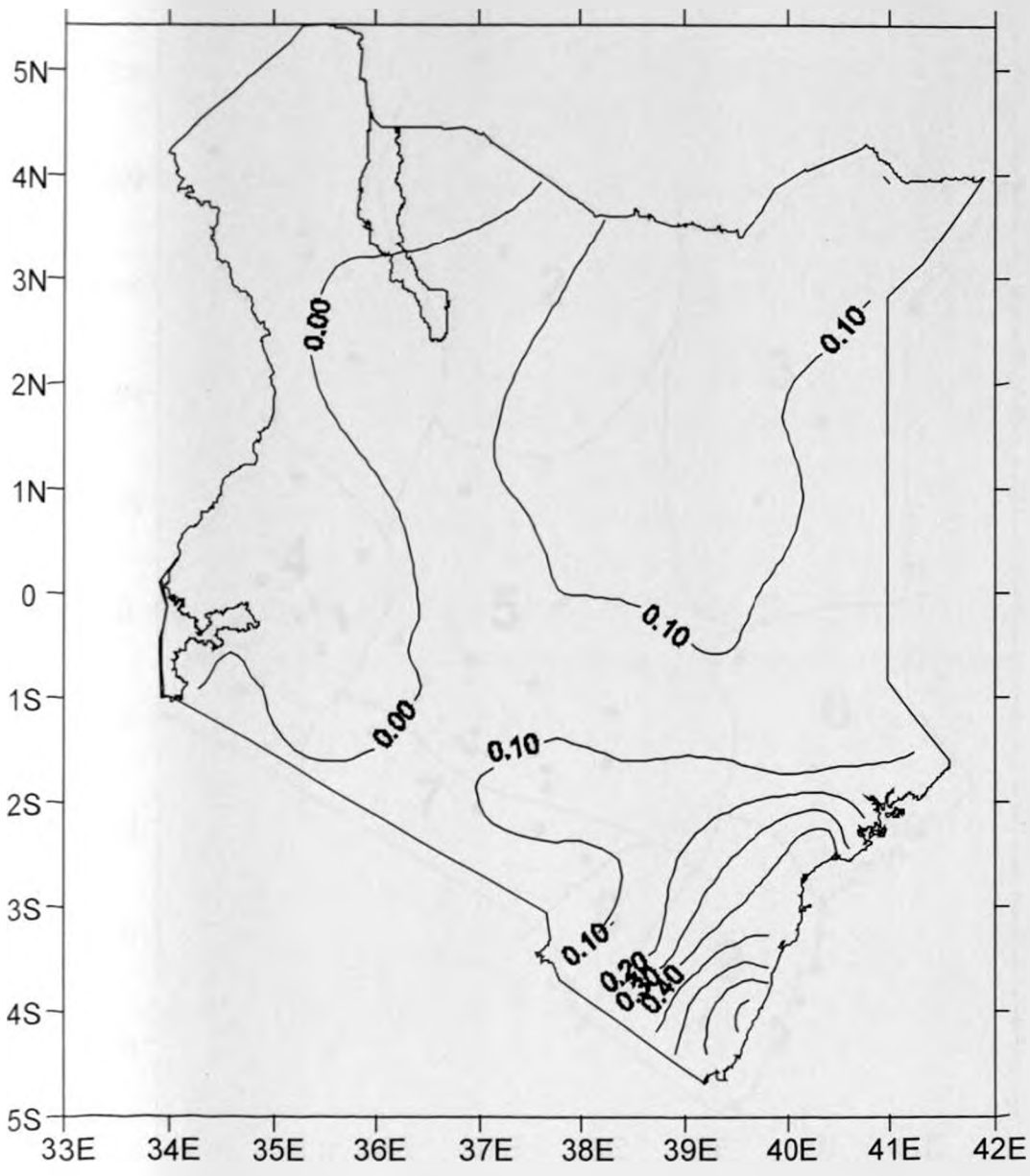

Figure 4.6(c): Spatial patterns of the third rotated principal component during SON season.

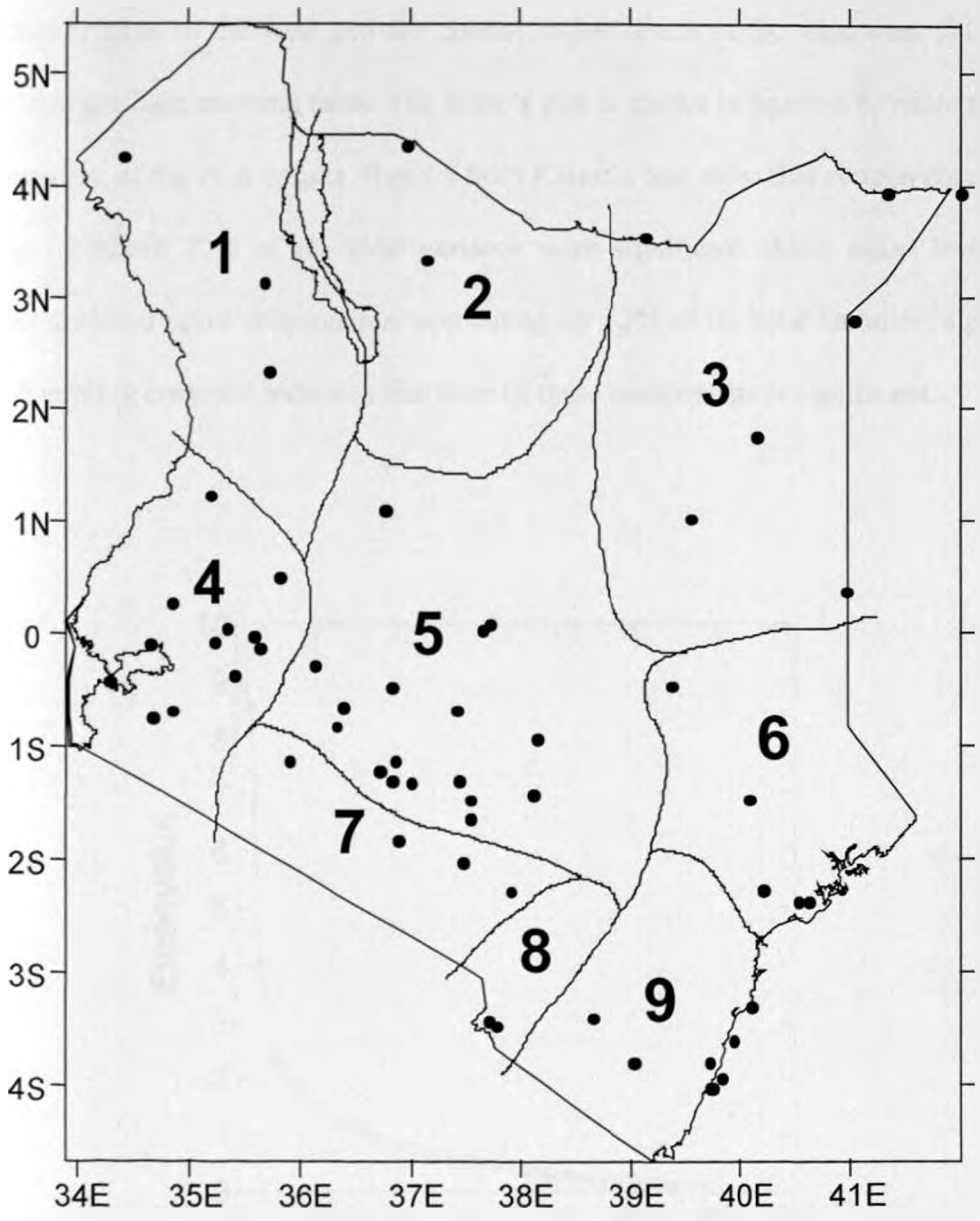

Figure 4.7: Homogenous divisions of the 60 stations derived from the SON seasonal RPCA patterns.

4.2.1.3 June – August (JJA) Season

This is the Northern Hemisphere summer season and most of the region is dry except Lake Victoria region to the west and the coastal region. Parts of the windward side of the highlands also get light morning rains. The Scree's plot is shown in figure 4.8, while table 4.4 gives a summary of the PCA results. Results from Kaiser's test show that sixteen components accounting for about 72% of the total variance were significant above noise levels. The Scree's test declared seven components, accounting for 52% of the total variance, significant while the Sampling error test indicates that none of these components is significant.

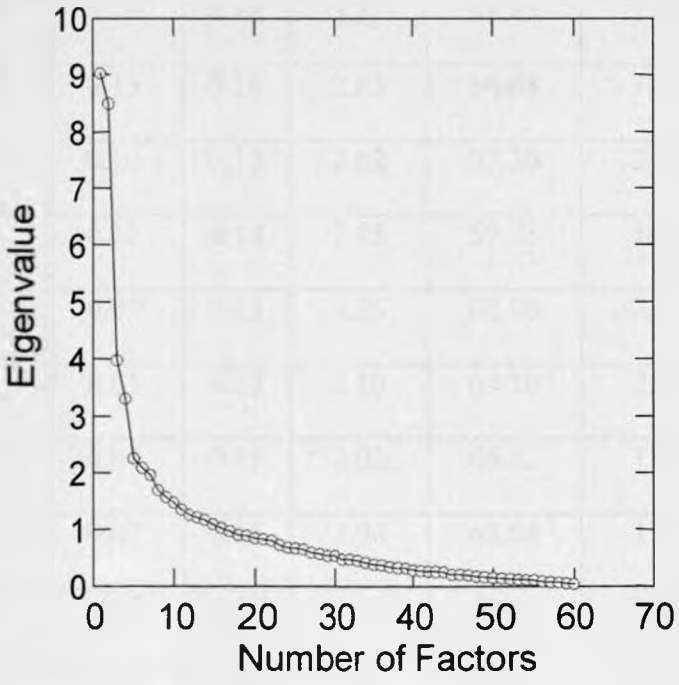

Figure 4.8: Scree's test selection of the dominant principal components for JJA season

Table 4.4: Statistical characteristics of 1982 –1995 dekadal rainfall from PCA of JJA season

Factor	Non rotated Eigenvalue	EV_{i+1}-EV_i	North's Test	Non Rotated		Rotated	
				Variance extracted (%)	Cumulated variance (%)	Eigenvalue	Variance extracted (%)
1	9.03	0.53	0.85	15.05	15.05	5.97	9.96
2	8.50	4.52	0.80	14.17	29.22	5.89	9.82
3	3.98	0.67	0.37	6.63	35.85	3.47	5.78
4	3.31	1.06	0.31	5.51	41.36	3.94	6.56
5	2.25	0.17	0.21	3.75	45.11	2.19	3.64
6	2.08	0.12	0.19	3.47	48.58	1.77	2.95
7	1.96	0.26	0.18	3.27	51.85	1.77	2.94
8	1.70	0.13	0.16	2.83	54.68	1.73	2.88
9	1.57	0.10	0.15	2.62	57.30	2.74	4.57
10	1.47	0.12	0.14	2.45	59.75	1.76	2.93
11	1.35	0.09	0.13	2.25	62.00	2.71	4.52
12	1.26	0.05	0.12	2.10	64.10	2.49	4.14
13	1.21	0.04	0.11	2.02	66.12	1.34	2.24
14	1.17	0.07	0.11	1.96	68.08	1.56	2.59
15	1.10	0.07	0.10	1.83	69.91	1.56	2.59
16	1.03	0.06	0.10	1.71	71.62	2.11	3.51

Note: EV = Eigenvalue

Figure 4.9 display the spatial distributions of the first three significant components. The first rotated component, which accounts for a variance of 9.96% of the total variance, is shown to be dominant over the coastal regions in figure 4.9(a). The second component that accounts for 9.82% of the total variance is dominant around the highlands east of the Rift Valley extending south to the area around Mount Kilimanjaro as shown in figure 4.9(b). The third component, accounting for a variance of 6.56%, is dominant in the western parts of the study area but north of Lake Victoria. This is shown in figure 4.9(c). This region is known to have a third rainfall peak within the year during this season (Davies *et al.*, 1985). It should be noted that, despite the large number of components declared significant by Kaiser's method, even the first non-rotated PCA mode accounts for only 15% of rainfall variance in this season. This may be a reflection of the highly localized nature of rainfall variation in this season. Seven components were retained for rotation. The complexity of the spatial patterns of the PCA may be due to the existence of many zero dekadal rainfall values at many locations during this season.

Using all the significant rotated components, eleven climatological regions were derived from the PCA results of the JJA season. These regions are shown in figure 4.10.

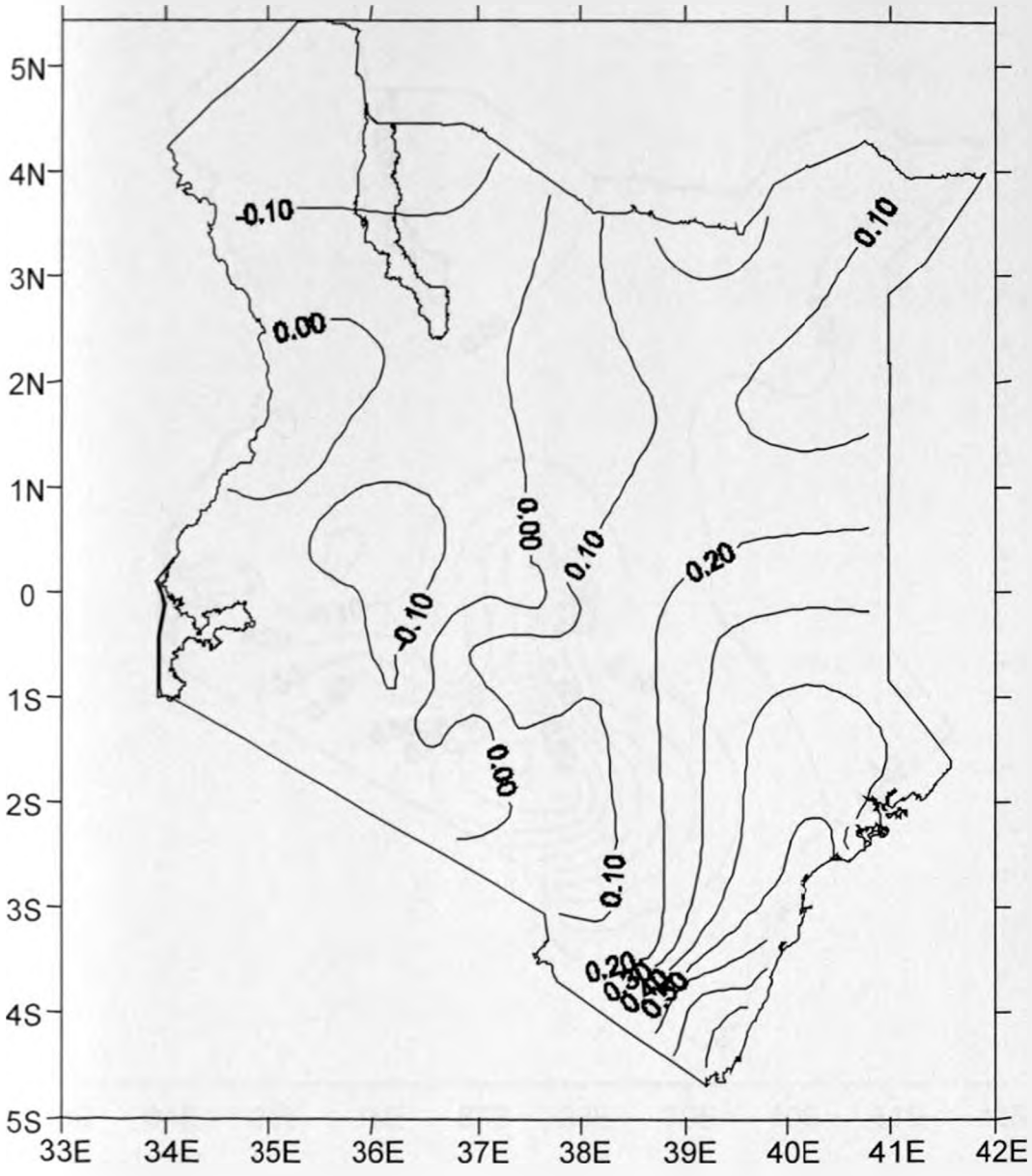

Figure 4.9(a): Spatial patterns of the first rotated principal component during JJA season.

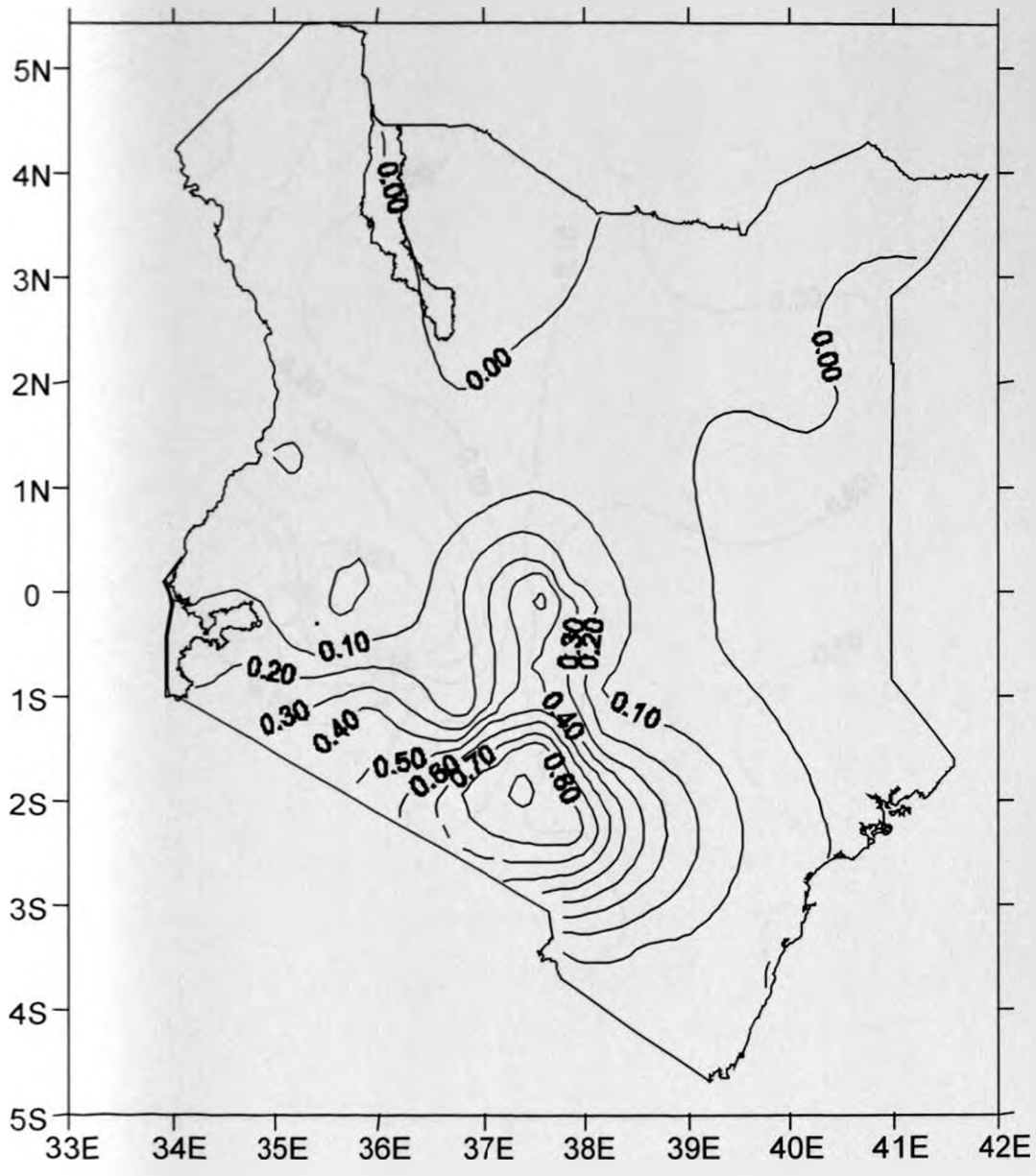

Figure 4.9(b): Spatial patterns of the second rotated principal component during JJA season.

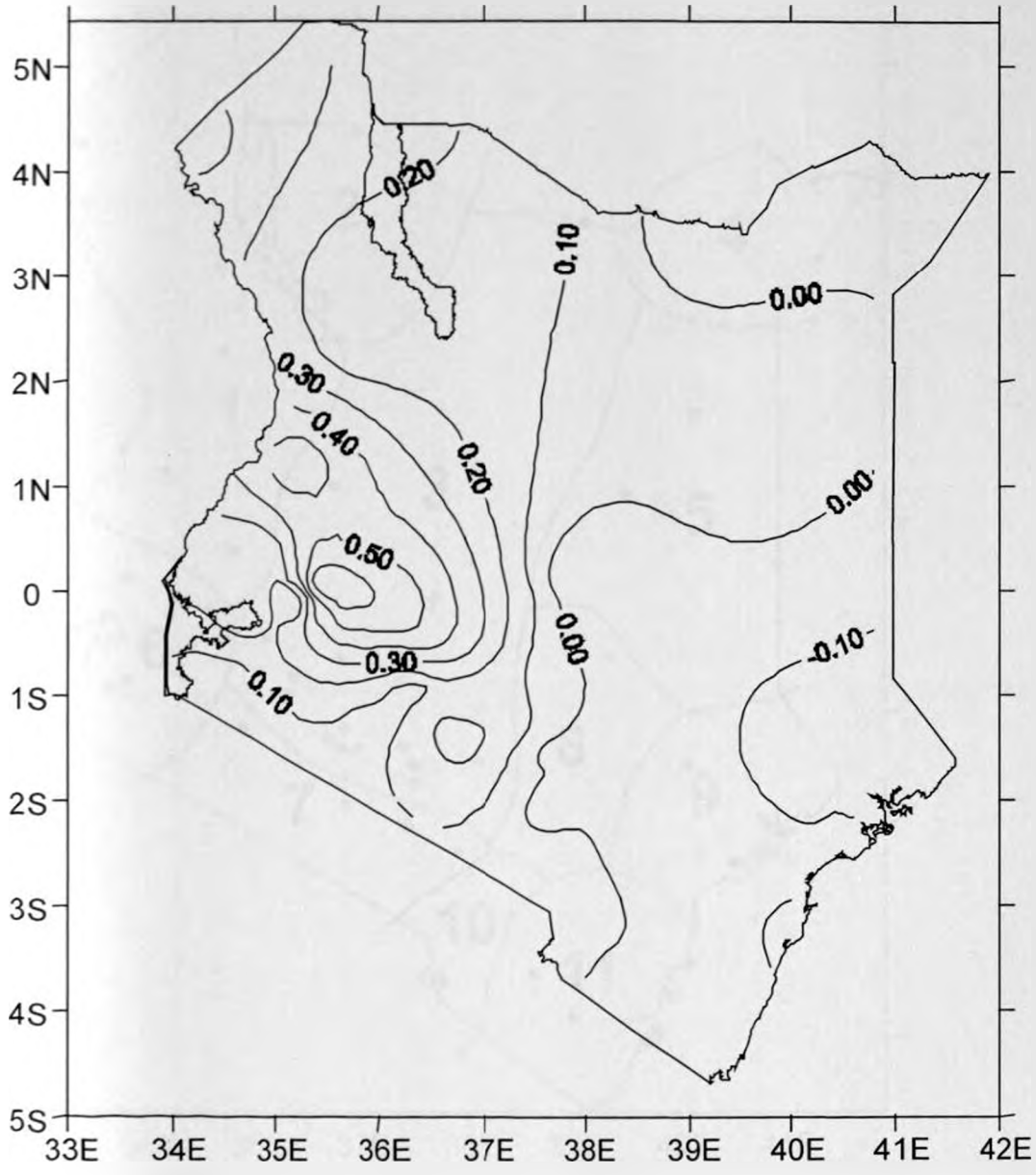

Figure 4.9(c): Spatial patterns of the third rotated principal component during JJA season.

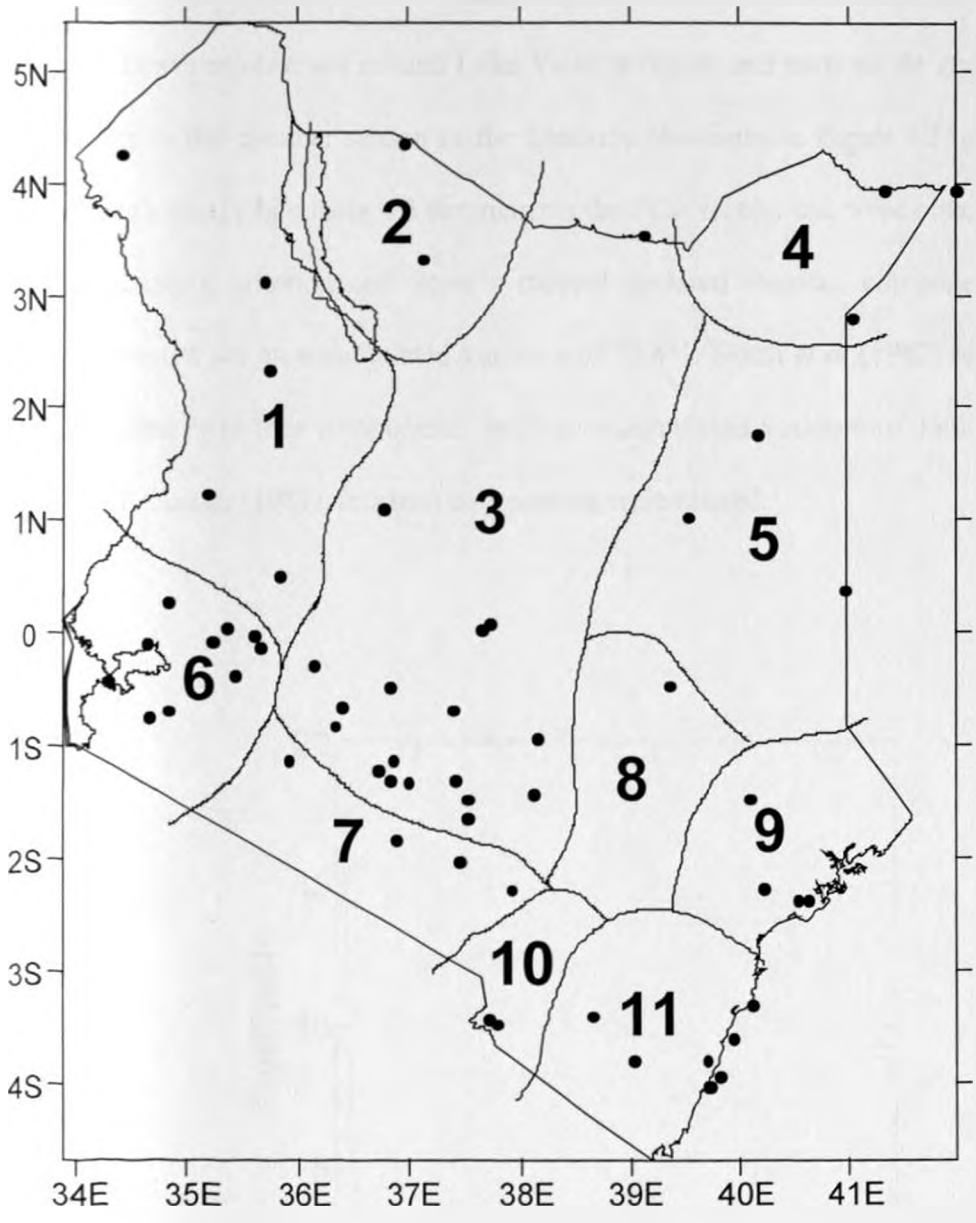

Figure 4.10: Homogenous divisions of the 60 stations derived from the JJA seasonal RPCA patterns.

4.2.1.4 December- February (DJF) Season

December- February (DJF) Season is the driest season in the area of study. Limited rainfall is however observed around Lake Victoria region and parts of the coast. This period corresponds to the summer season in the Southern Hemisphere. Figure 4.11gives the results of the Scree's test, while table 4.5 summarizes the PCA results that were obtained during this season. Kaiser's criterion and Scree's method declared fourteen components significant. These accounted for an accumulated variance of 73.4%. North *et al* (1982) test, on the other hand, declared only four components, with an accumulated variance of 33%, significant. In lines with Richman (1981), fourteen components were rotated.

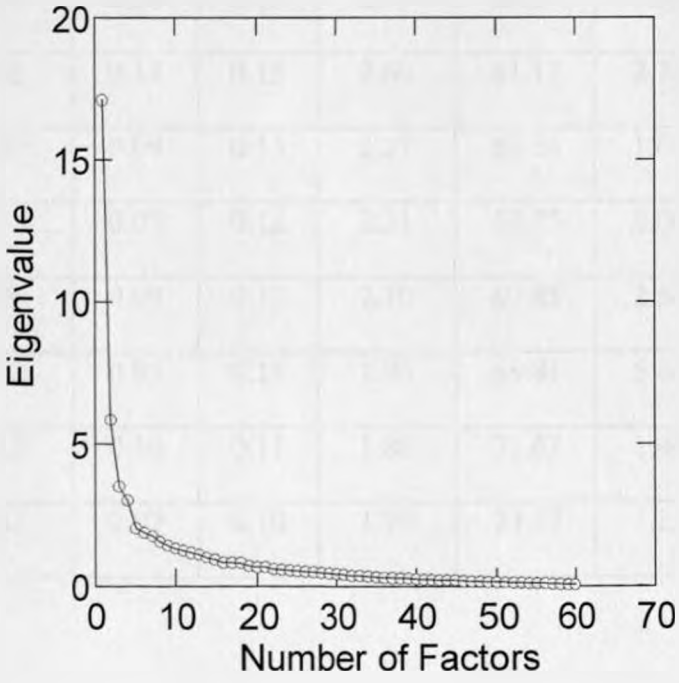

Figure 4.11: Scree's test selection of the dominant principal components for DJF season

Table 4.5: Statistical characteristics of 1982 –1995 dekadal rainfall from PCA of DJF season

Factor	Non rotated Eigenvalue	EV_{i+1}-EV_i	North's Test	Non Rotated		Rotated	
				Variance extracted (%)	Cumulated variance (%)	Eigenvalue	Variance extracted (%)
1	17.11	11.26	1.60	28.52	28.52	5.61	9.36
2	5.85	2.35	0.55	9.75	38.27	5.48	9.14
3	3.50	0.49	0.33	5.83	44.10	4.05	8.45
4	3.01	0.98	0.28	5.03	49.13	4.81	8.01
5	2.03	0.16	0.19	3.39	52.52	2.50	6.76
6	1.87	0.11	0.18	3.12	55.64	2.90	4.84
7	1.76	0.20	0.16	2.93	58.57	1.93	4.64
8	1.56	0.14	0.15	2.60	61.17	2.78	4.17
9	1.42	0.09	0.13	2.37	63.54	1.66	4.17
10	1.33	0.07	0.12	2.21	65.75	2.00	3.21
11	1.26	0.09	0.12	2.10	67.85	2.50	3.34
12	1.17	0.05	0.11	1.96	69.81	5.07	2.77
13	1.12	0.10	0.11	1.86	71.67	1.44	2.41
14	1.02	0.07	0.10	1.70	73.37	1.25	2.09

The spatial patterns of the first three dominant rotated principal components for the season are displayed in figure 4.12. The first rotated principal component, which explains about 9.4% of the total variance, is shown in figure 4.12(a) to be dominant around Lake Victoria and in the western parts of the study region.

The second rotated principal component, which accounts for 9.1% of the total variance, is dominant in the dry eastern regions of the study area and is shown in figure 4.12(b). The third rotated component, accounting for 8.5% of the total variance, is seen in figure 4.12(c) to be dominant in the region to the east of the central highlands covering the southeastern lowlands. The spatial distributions of the other components were used to get further smaller zones from the ones discussed above. For example the sixth rotated principal component, which accounts for 4.8% of the total variance, is dominant over the area around mount Kilimanjaro and helps in delineating this region.

The existence of many zero values and the localized nature of dekadal rainfall variations in this season were reflected in the complexity of the PCA solutions. It should however be noted that in some years the September - November rains extend to January-February as was witnessed in 1998. Such rains extend over the whole region. This could explain the relatively high variance that is accounted for by the first non-rotated component. It should be noted that the year to year rainfall variability of dekadal rainfall is very high in this dry season. Further it should be noted that PCA used normalized rainfall data to avoid including zero values in the input matrix. Figure 4.13 illustrates the eleven climatic zones derived from PCA of the DJF season.

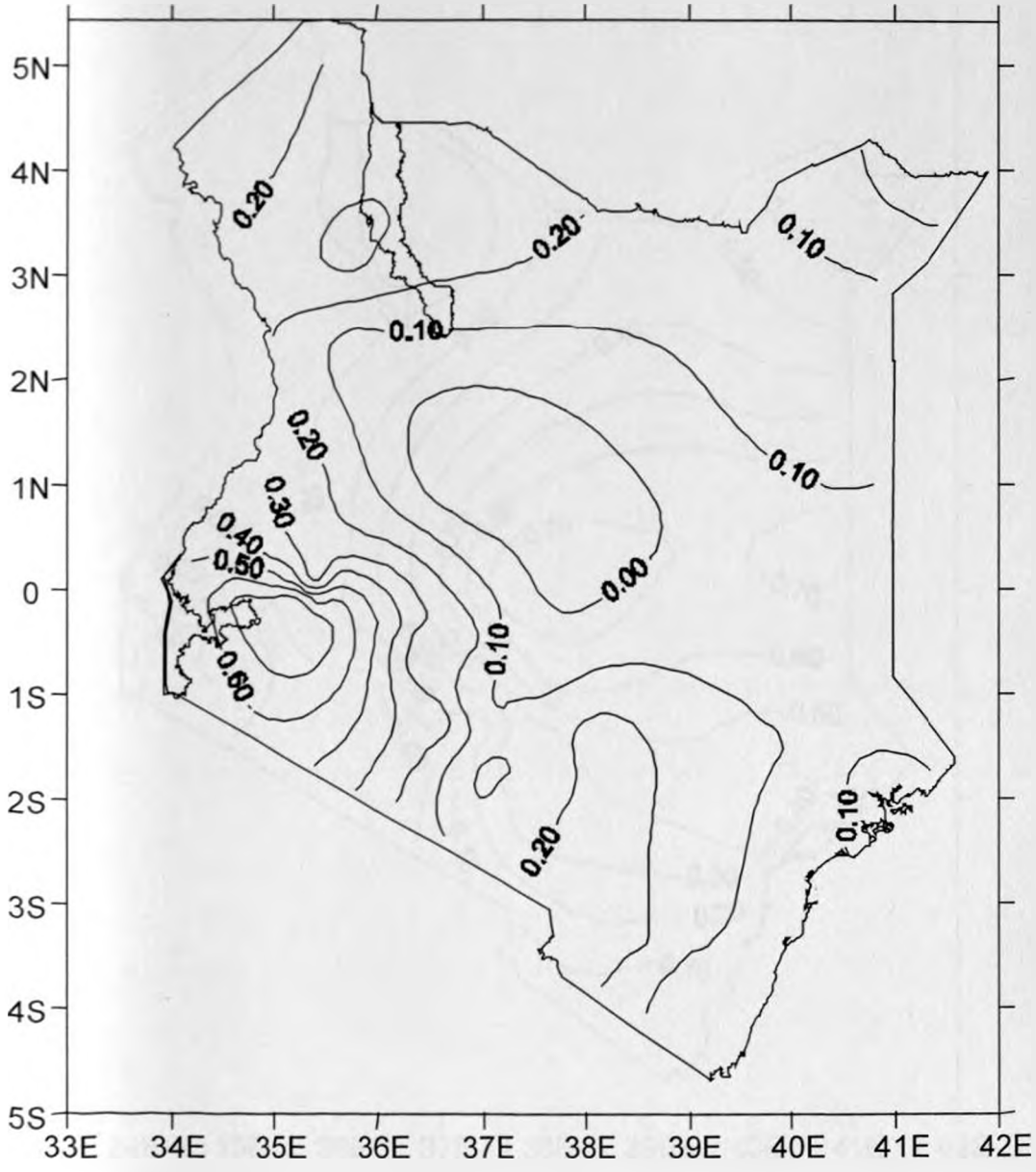

Figure 4.12(a): Spatial patterns of the first rotated principal component during DJF season.

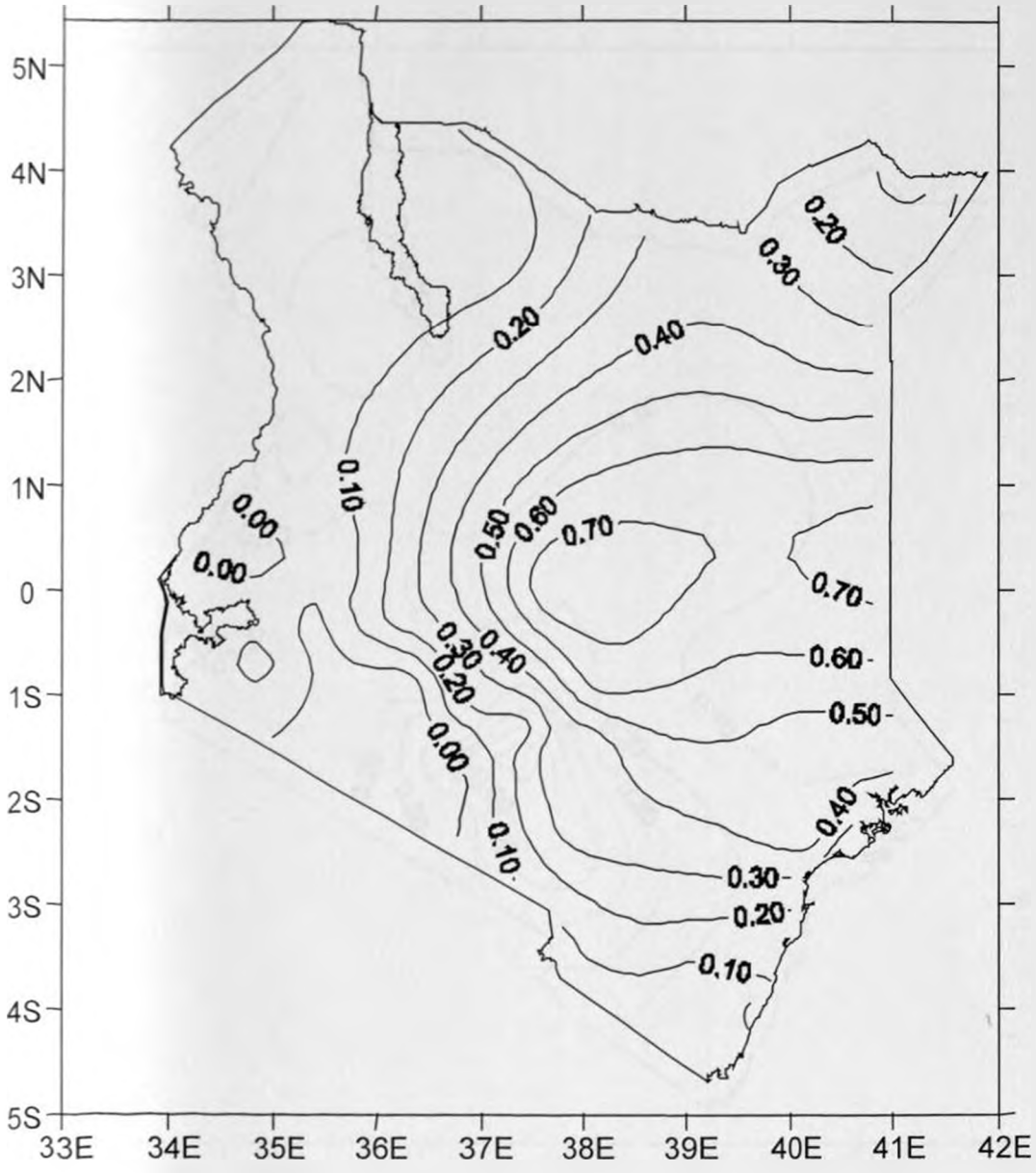

Figure 4.12(b): Spatial patterns of the second rotated principal component during DJF season.

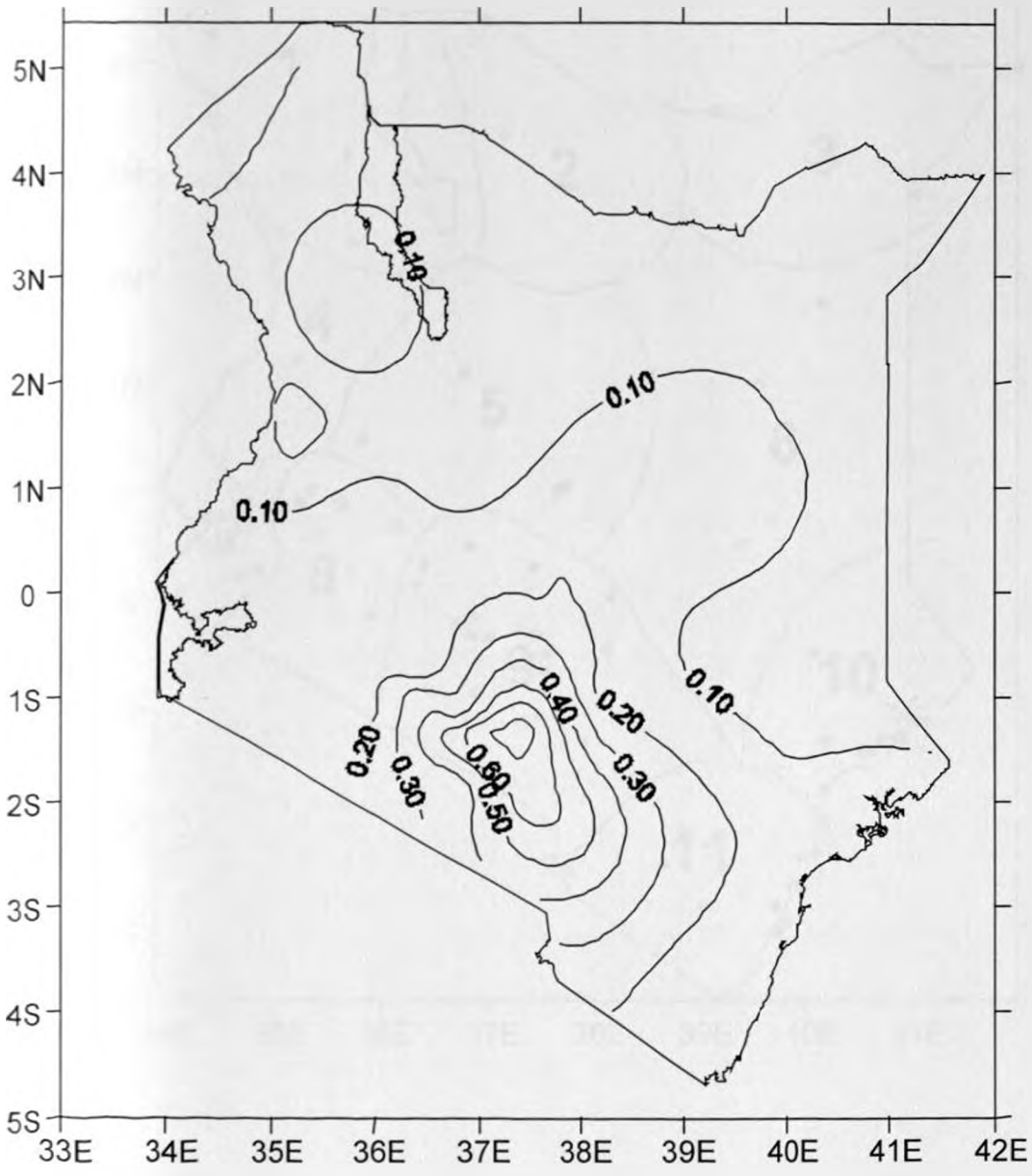

Figure 4.12(c): Spatial patterns of the third rotated principal component during DJF season.

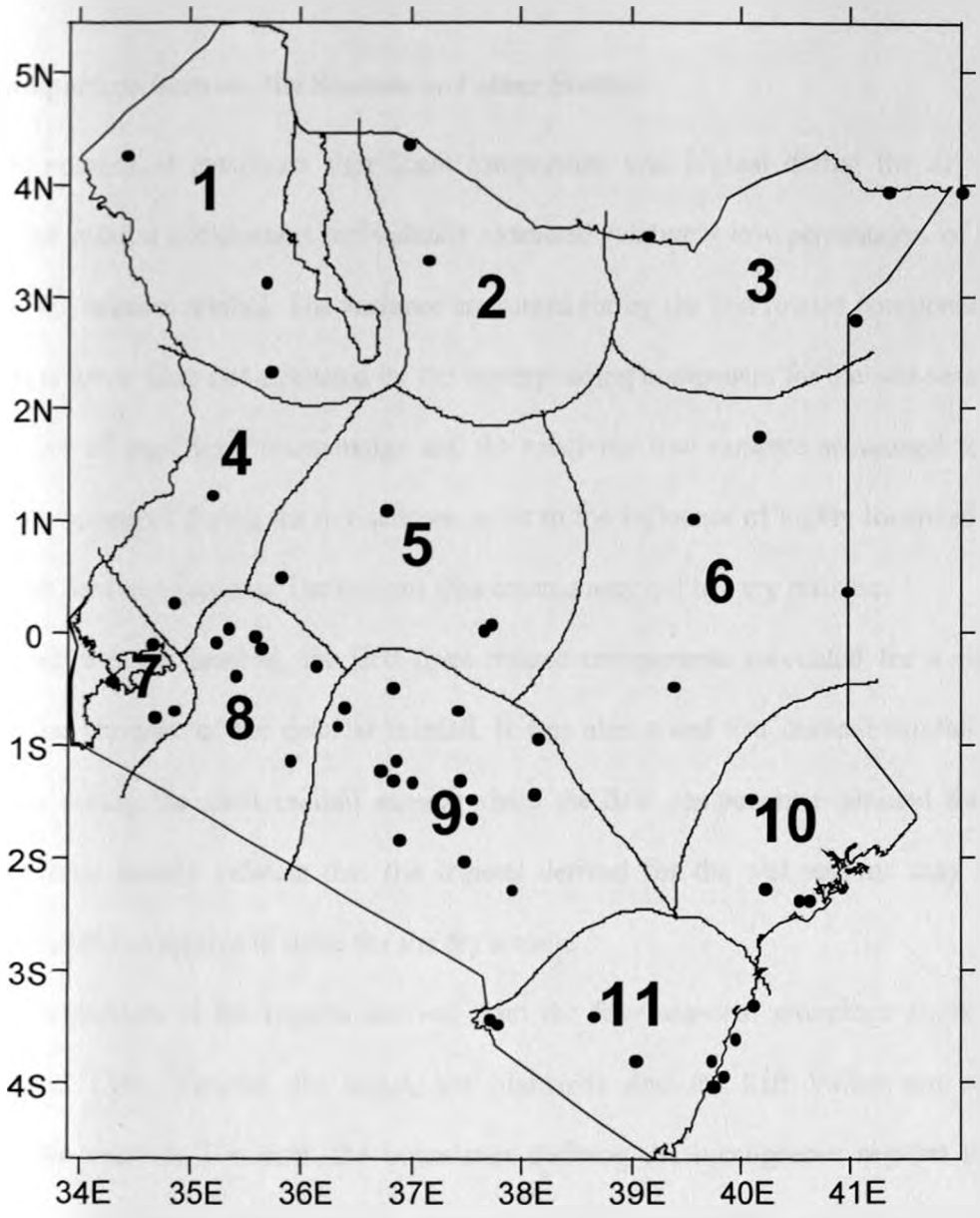

Figure 4.13: Homogenous divisions of the 60 stations derived from the DJF seasonal RPCA patterns.

The results of the four seasons are compared to each other and also to other similar studies in the next section.

4.2.1.5 Comparison between the Seasons and other Studies

The number of maximum significant components was highest during the dry seasons. However, the rotated components individually extracted relatively low percentages of the total variance of the dekadal rainfall. The variance accounted for by the first rotated component for the dry seasons is lower than that extracted by the corresponding component for the wet seasons. The higher number of significant components and the relatively low variance accounted for by the individual components during the dry seasons point to the influence of highly localized systems in the rainfall for these seasons. The regions thus created may not be very realistic.

During the wet seasons, the first three rotated components accounted for a significant amount of the variance of the dekadal rainfall. It was also noted that dekadal rainfall is more homogenous during the short rainfall season where the first component explained the highest variance. These results indicate that the regions derived for the wet seasons may be more physically realistic compared to those for the dry seasons.

A comparison of the regions derived from the four seasonal groupings show that the region around Lake Victoria, the coast, the highlands and the Rift Valley are consistent throughout the seasons. However, the boundaries defining the homogenous regions shift with seasons reflecting the complexity of the seasonal rainfall characteristics over the study region. These could arise from the interplay between the large- and synoptic-scale systems and the local factors like topography. Detailed characteristics of the various systems that control rainfall over the region has been outlined in section 1.3.2.

Other researchers have also, using different time scales, regionalized the study region. The complexities of the spatial rainfall have also been noted in these previous studies. Barring (1988) used daily rainfall to derive eleven annual regions over the study area. Most of these

regions are comparable to the regions derived in this study except for the areal extents. For example, this study divides the northern part into three regions while Barring (1988) has two.

Ogallo (1989) used monthly data to group seasonal and annual climatic regions for East Africa. His seasonal map combines the northern section into one region and has several smaller regions in the central areas. The annual map, however, has only five regions demarcated over Kenya. In this case the area around Lake Victoria is the only one which is similarly demarcated in both studies. Indeje *et al.* (2000), using monthly data for East Africa, demarcated five annual climatic regions over the study region. The region around Lake Victoria is delineated in both studies while the coastal zone is lumped into one region by Indeje *et al.* (2000). It is evident from these studies that the spatial patterns of rainfall are more homogenous at monthly and seasonal time scales than in the lower time scales. While the monthly and seasonal time scales give cumulative rainfall totals for the specific periods, the daily and 10-day time scales include the impacts of spatial migrations of the rainfall producing systems including the ITCZ.

The next section presents results of regionalization of the study area using satellite-derived records.

4.2.2 Results from Regionalization using Satellite-Derived Data

This section presents and discusses results from the regionalization of the study area using PCA of mean dekadal Total Precipitable Water (TPW) derived from satellite information. As in the case of the dekadal rainfall, only rotated solutions are presented. TPW maybe defined as the total amount of moisture present in a given column of air expressed as the depth of water that would accumulate at the base of the column if all the water vapor could be condensed into water (Zeng, 1999).

PCA was performed on the three available layers of TPW (surface – 700 mb, 700 – 500 mb, 500 – 200 mb). Only one component was significant for the highest layer in all the seasons. For the middle layer two components were significant for the first three seasons while the DJF season had three significant components. In the surface-700 mb layer, more than three components were declared significant in all seasons indicating the influence of several factors in this layer. Due to the need of incorporating as many influencing factors as possible, for example local, regional as well as synoptic factors, in the regionalization, the study therefore concentrated only on the lowest layer.

Results from Kaiser's criterion, Scree's and North *et al.* sampling error tests all declared four components significant above noise levels for MAM, SON and JJA seasons accounting for 94.9, 92.1 and 92.5% of the total variance in the dekadal surface – 700 mb layer of TPW, respectively. The tests identified six components, accounting for 90.4% of the total variance, for the DJF season. Four components were retained for rotation for MAM, SON and JJA seasons while six were rotated for DJF season. A summary of these results is presented in Table 4.6.

Figure 4.14 displays the spatial distribution of the first rotated component, which accounts for 85.1% for MAM, 83.6% for SON, 84.4% for JJA and 74.5% for DJF seasons. The distribution of this component may be as a result of the prevailing mean synoptic patterns over the region during the various seasons.

Figures 4.14 (a) and (b) show the spatial distribution of the TPW content of the wet seasons of MAM and SON respectively. There is a striking similarity in the TPW content of these two seasons with the components being generally dominant over most of the study area with a small area with low factor loadings. This general dominance maybe due to the presence of the ITCZ in the area at these times, accompanied by widespread predominantly convective rainfall. According to an earlier study by Tuller (1968), areas of low TPW over the continents are

associated with low temperatures, continental interiors far from oceanic sources of moisture, and/or at high elevations. Hastenrath (1991) also discusses the decreasing TPW with altitude in the tropical regions that are dominated by convective type of precipitation. This would explain the area of low component loadings that is seen in the distribution of the first rotated component for both seasons. This area corresponds to the area covered by the Western and Central highlands as may be seen in the topography map shown in Figure 2. The rest of the study region is generally at low altitude with relatively high temperatures and may be influenced by either Lake Victoria or the Indian Ocean. This similarity can also be observed for the dry seasons of JJA and DJF in Figures 4.14 (c) and (d) respectively. In this case the dominance is a reflection of the relatively dry atmospheres during these seasons. However, the highland areas are still clearly identified in these seasons as well.

Seven homogenous regions were derived for MAM season and these are shown in Figure 4.15(a). The corresponding regions derived from rainfall records were eleven (Figure 4.4). This implies that TPW may be more monogenous than the rain gauge-recorded rainfall. The regions derived from these two sets of data are comparable with the extra regions from the rainfall records being subdivisions of the ones from TPW data. For example, the rainfall data divides the coastal region into two while TPW data has just one whole region. The smaller subdivisions from the rainfall data may be due to some local surface feature that gets averaged out within the lower layer of the TPW data. They may also be the result of errors in the rainfall data and lack of spatial continuity. Similarly, the regions derived for the SON season are also comparable. Seven regions were derived from the TPW data as shown in Figure 4.15(b) while the corresponding regions from the rainfall data were nine (Figure 4.7). In this case the coastal region has expanded further northeastwards but is still one from the TPW data whereas there are two regions from the rainfall data.

The regions derived for the dry seasons of JJA and DJF are shown in Figures 4.15 (c) and (d) respectively. Six regions were derived for the JJA season and eight for DJF season with the corresponding regions from rainfall data being eleven in both cases. The extra regions from the rainfall data are still subdivisions of the regions derived from TPW data. During these seasons, the influence of local topographical features dominates the weather of the study region leading to the several zones demarcated from the rainfall data. The presence of a small raised ground may trigger off rainfall in a small area from the same amount of TPW for a larger area. These influences maybe evened out within the TPW layer resulting in only a few homogenous regions delineated. However, due to the strong influence of local features leading to complex rainfall distribution during these dry seasons, the rest of the study is concentrated on the two wet seasons.

The derived zones (based on both rainfall and TPW records) were compared to the agro-ecological zones of Kenya (Sombroek, *et al.*, 1982). However, the time-scales were different, annual for agro-ecological and seasonal for rainfall/TPW zoning. The zones based on rainfall records were relatively smaller and hence more in number compared to the agro-ecological zones. The TPW zones were closest to the agro-ecological zones in terms of size and numbers, even though the time-scales were different. This indicates that the TPW is more closely linked to crop requirements than simply rainfall amounts. Further work should be done in this line to understand better this relationship.

Table 4.6: Eigenvalue statistics from the PCA of TPW for all the seasons

Component			1	2	3	4	5	6
MAM		Eigenvalue	84.3	6.0	2.6	1.1	*	*
		E_{i+1}-E_i	78.3	3.4	1.5	0.4	*	*
		North's Test	9.6	0.7	0.3	0.1	*	*
	Non Rotated	Variance(%)	85.1	6.1	2.6	1.1	*	*
		Cumulative Variance (%)	85.1	91.2	93.8	94.9	*	*
	Rotated	Eigenvalue	49.3	28.6	14.9	1.1	*	*
		Variance(%)	49.8	28.9	15.0	1.1	*	*
SON		Eigenvalue	82.7	4.2	3.0	1.3	*	*
		E_{i+1}-E_i	78.6	1.2	1.7	0.3	*	*
		North	9.2	0.5	0.3	0.1	*	*
	Non Rotated	Variance(%)	83.6	4.2	3.0	1.3	*	*
		Cumulative Variance (%)	83.6	87.8	90.8	92.1	*	*
	Rotated	Eigenvalue	43.1	28.9	18.0	1.3	*	*
		Variance(%)	43.5	29.2	18.1	1.3	*	*
JJA		Eigenvalue	83.6	4.1	2.7	1.2	*	*
		E_{i+1}-E_i	79.5	1.4	1.5	0.3	*	*
		North	9.5	0.5	0.3	0.1	*	*
	Non Rotated	Variance(%)	84.4	4.1	2.7	1.3	*	*
		Cumulative Variance (%)	84.4	88.5	91.3	92.5	*	*
	Rotated	Eigenvalue	33.4	24.6	28.4	5.1	*	*
		Variance(%)	33.8	24.9	28.7	5.2	*	*
DJF		Eigenvalue	73.8	8.8	3.4	1.9	1.5	1.1
		E_{i+1}-E_i	64.9	5.5	1.4	0.4	0.5	0.7
		North	8.4	1.0	0.4	0.2	0.2	0.1
	Non Rotated	Variance(%)	74.5	8.9	3.4	2.0	1.5	1.1
		Cumulated Variance (%)	74.5	83.5	86.9	88.9	90.4	91.5
	Rotated	Eigenvalue	45.9	23.8	14.1	1.7	3.1	2.1
		Variance(%)	46.4	24.0	14.2	1.7	3.1	2.1

Note: * indicate non-significant principal component

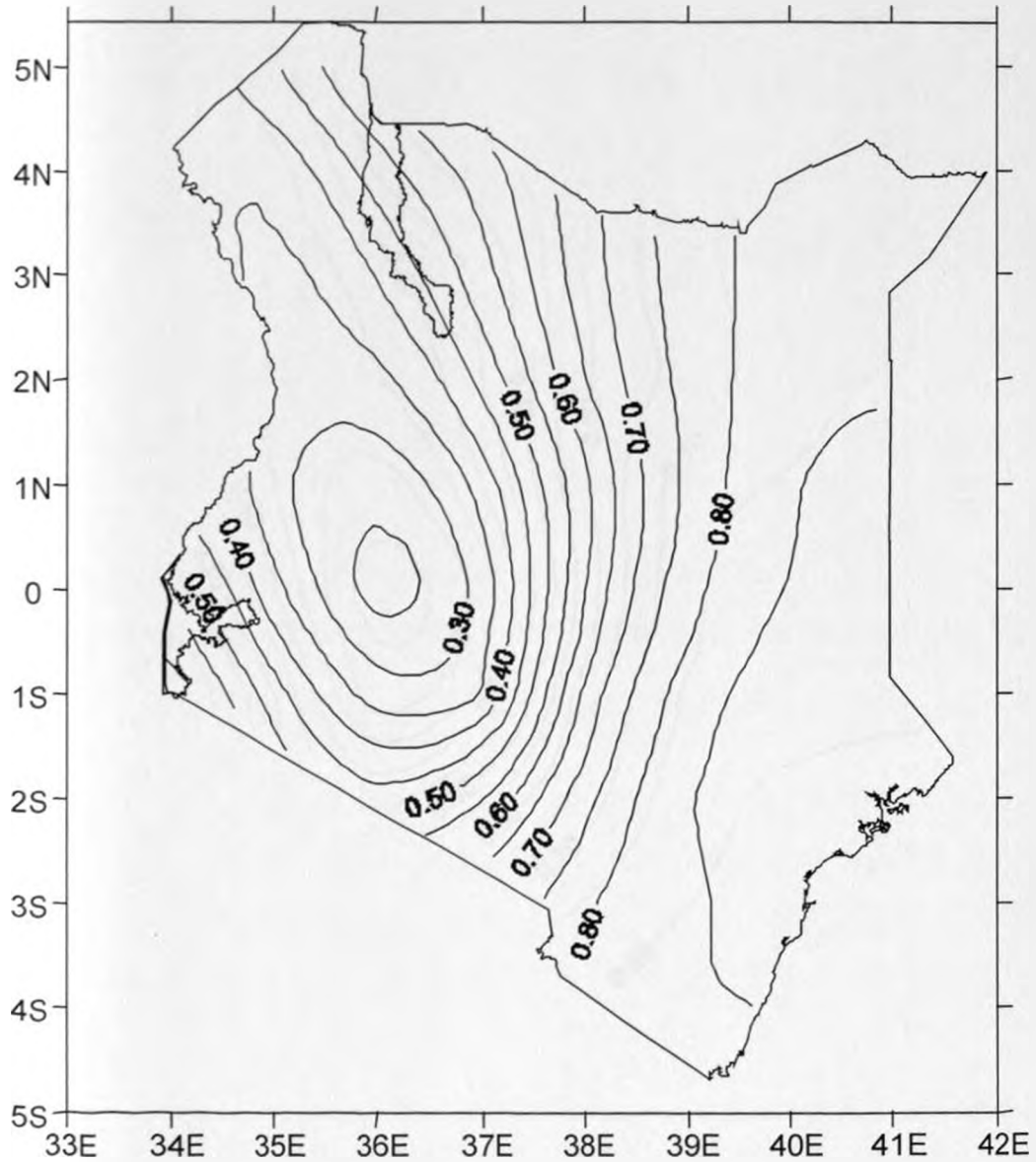

Figure 4.14(a): Spatial patterns of the first rotated principal component for dekadal TPW during MAM season.

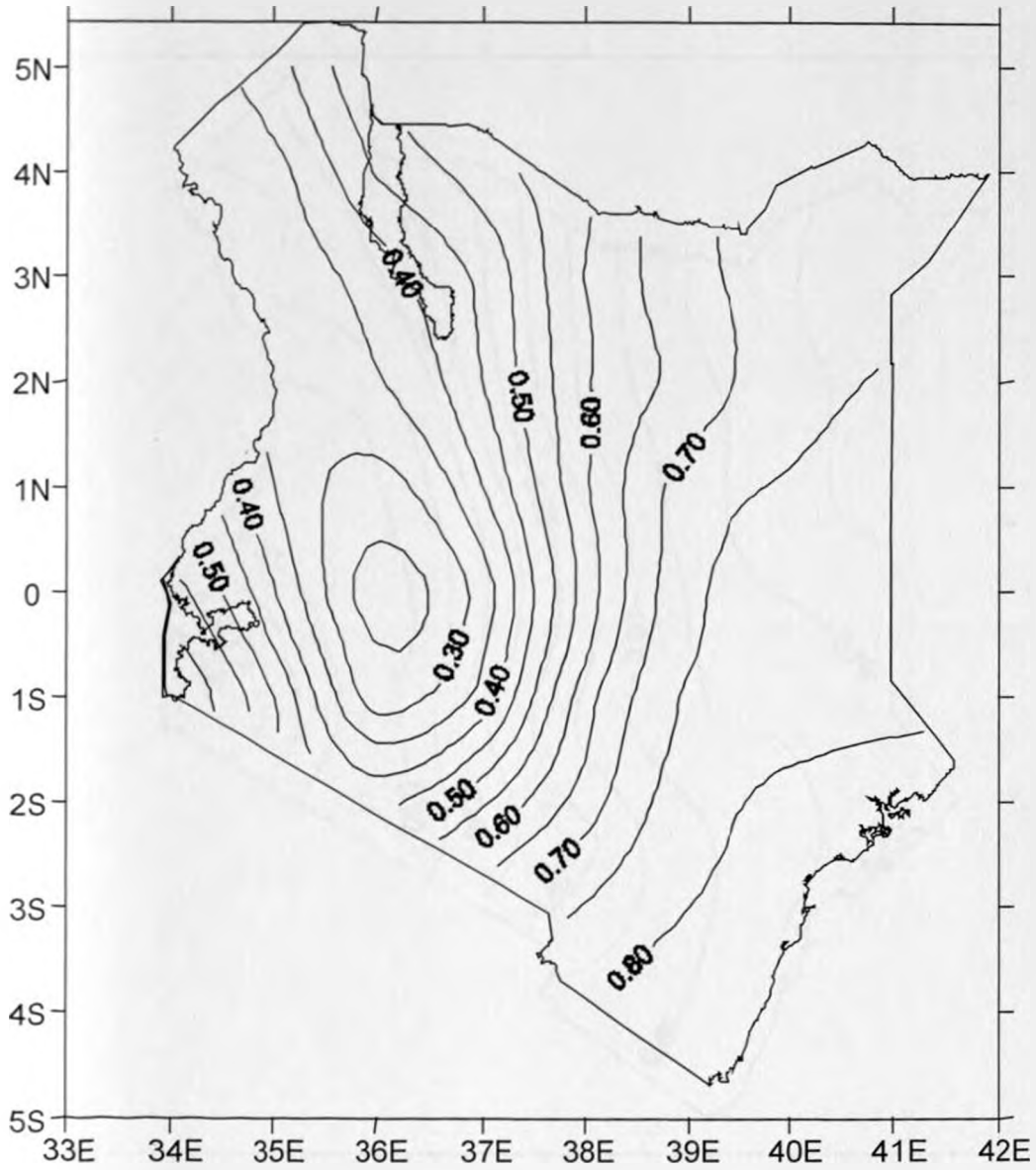

Figure 4.14(b): Spatial patterns of the first rotated principal component for dekadal TPW during SON season.

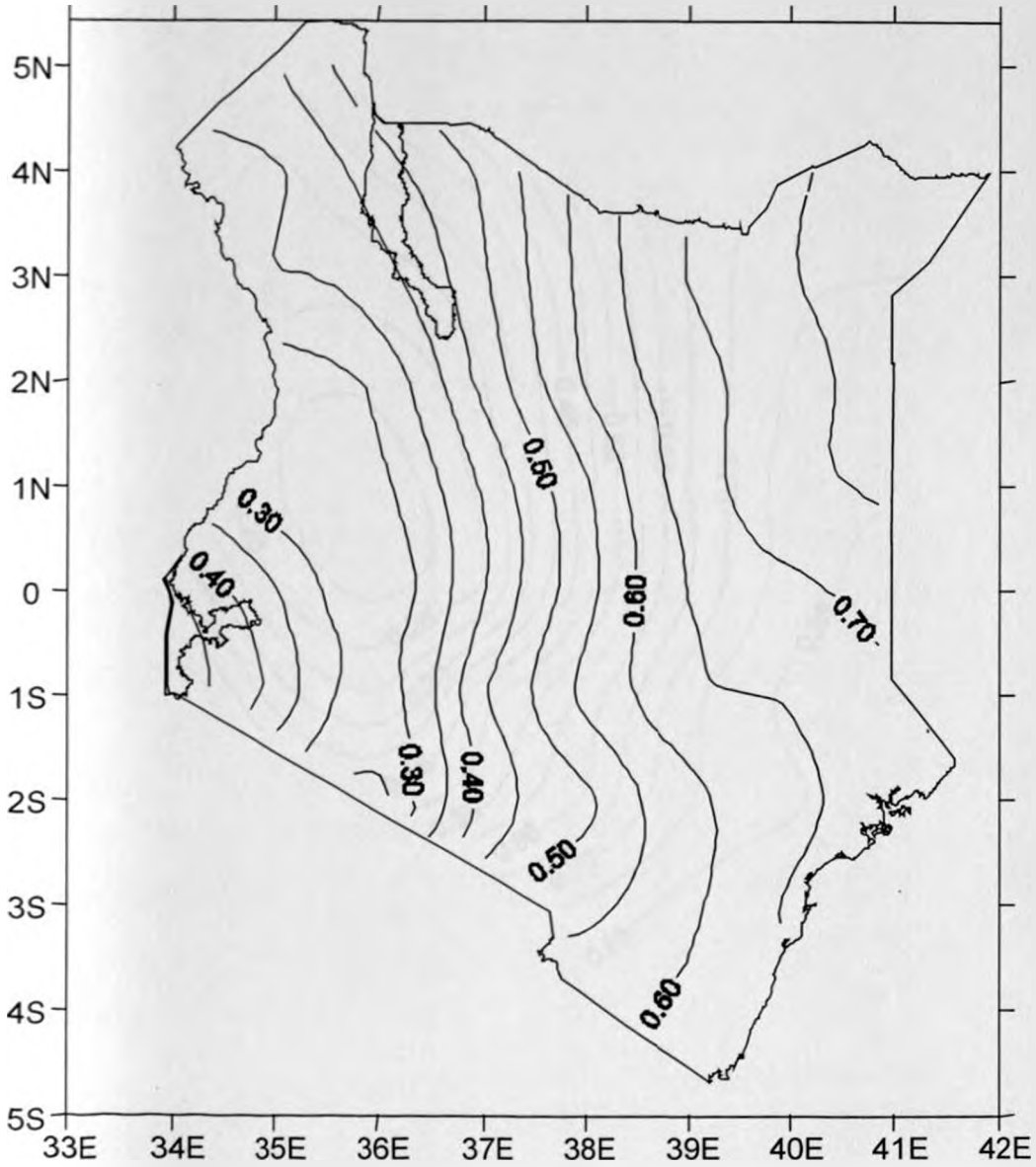

Figure 4.14(c): Spatial patterns of the first rotated principal component for dekadal TPW during JJA season.

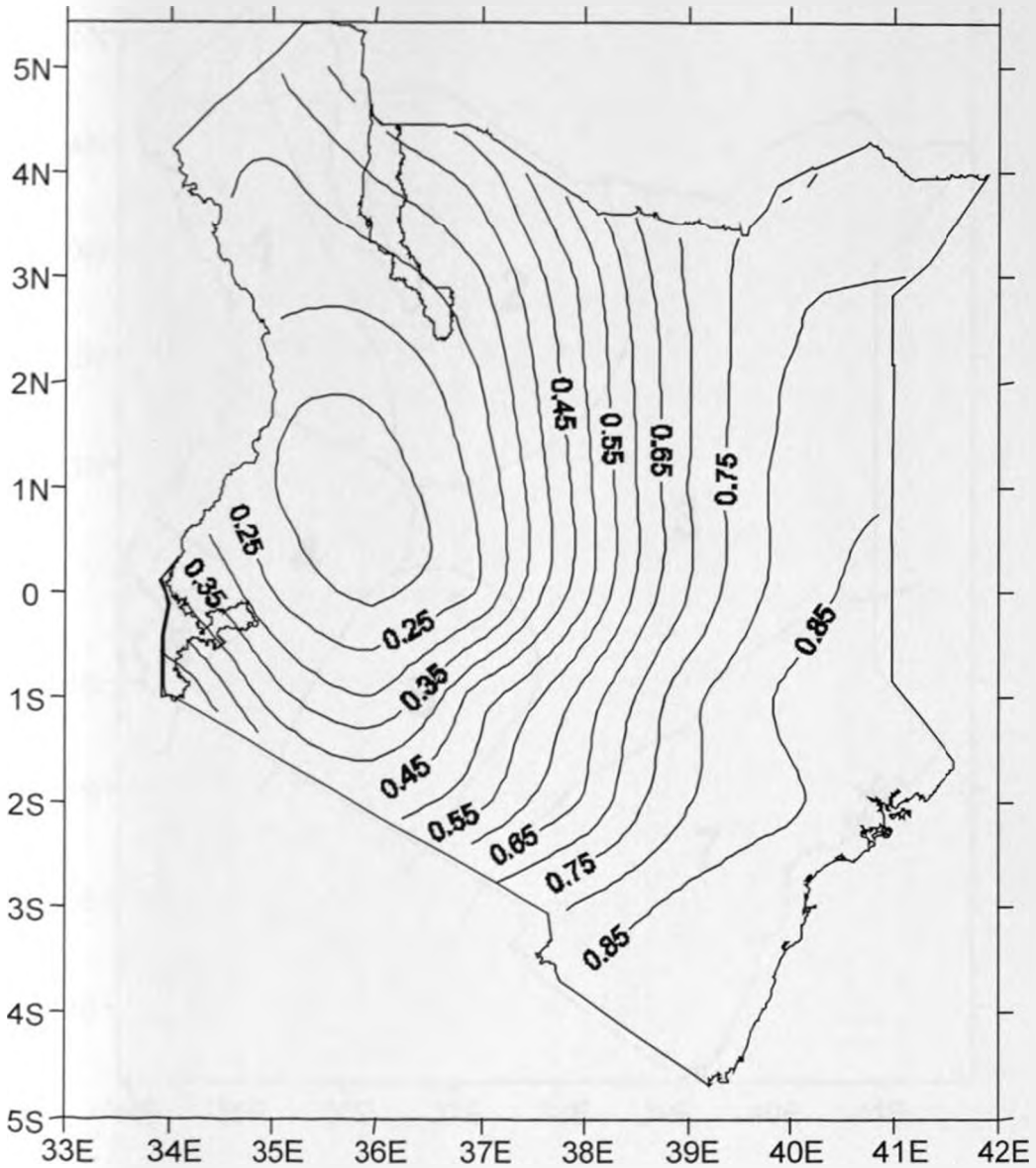

Figure 4.14(d): Spatial patterns of the first rotated principal component for dekadal TPW during DJF season.

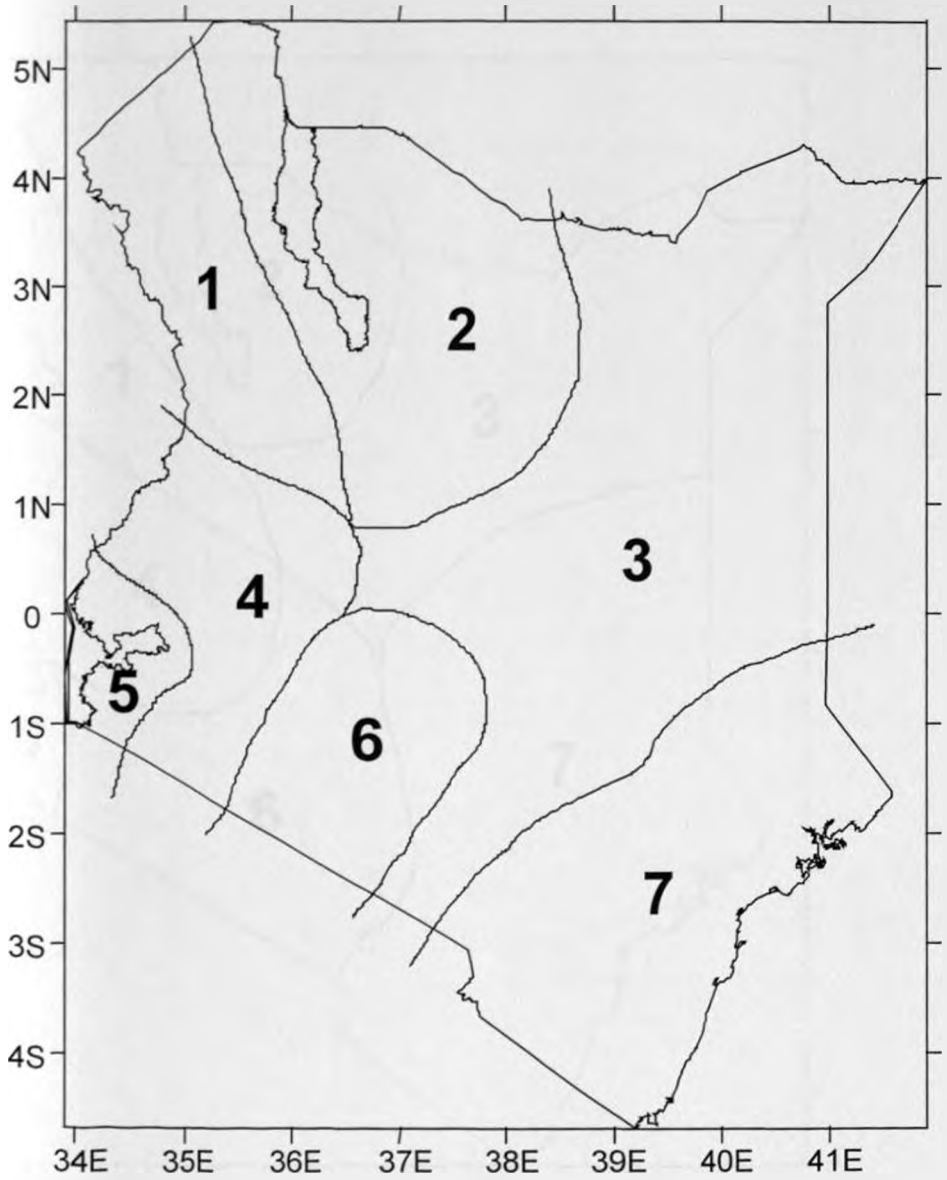

Figure 4.15(a): Homogenous divisions of study region derived from the MAM surface-700mb dekadal TPW seasonal RPCA patterns.

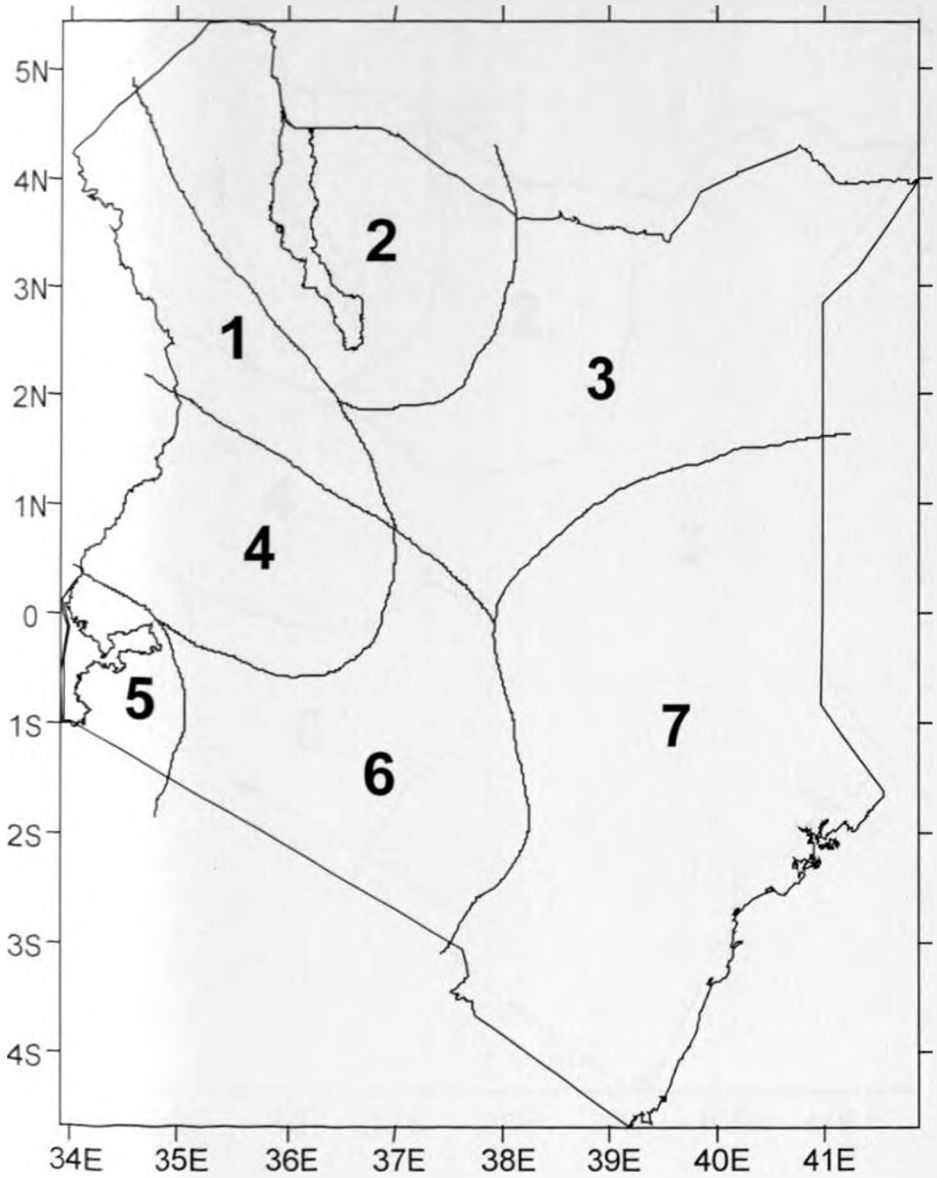

Figure 4.15(b): Homogenous divisions of study region derived from the SON surface-700mb dekadal TPW seasonal RPCA patterns.

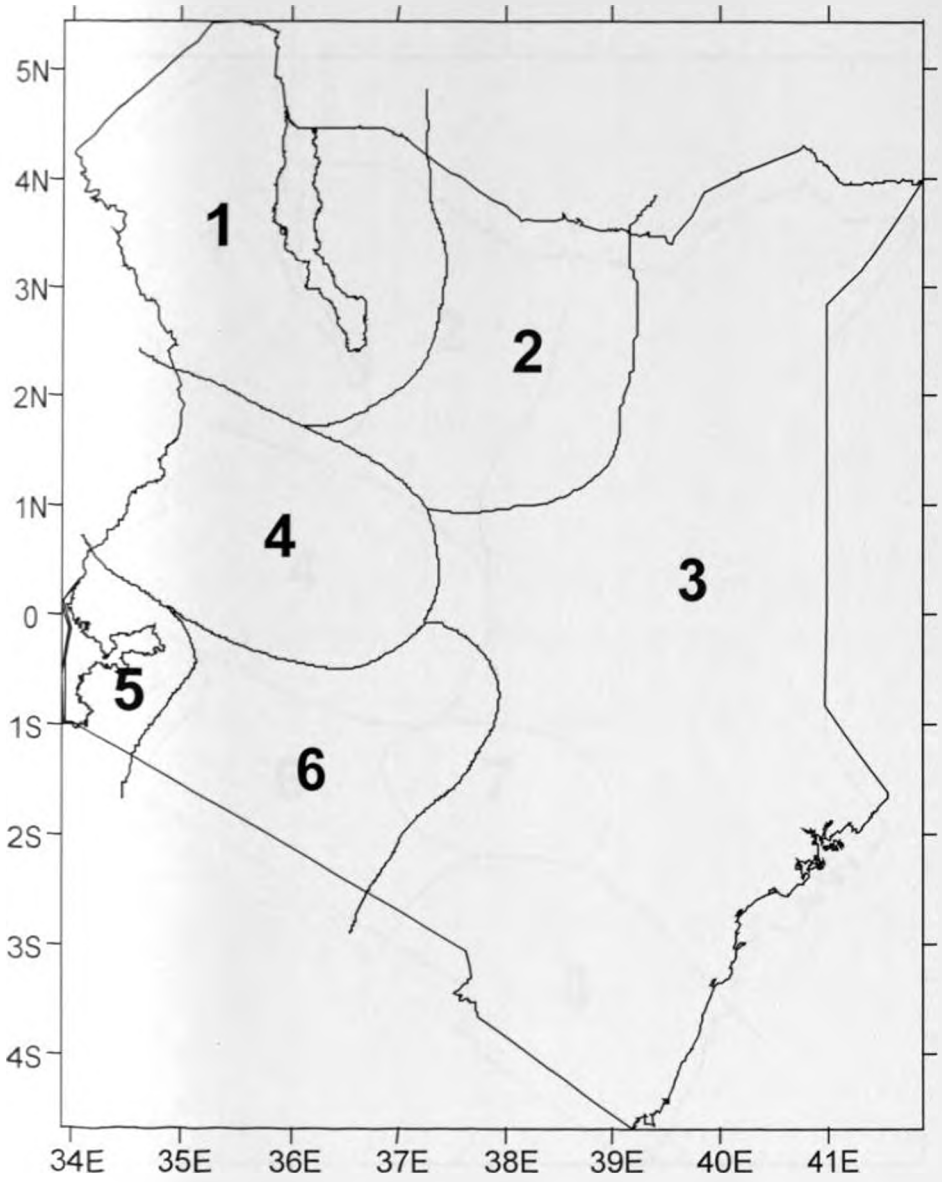

Figure 4.15(c): Homogenous divisions of study region derived from the JJA surface-700mb dekadal TPW seasonal RPCA patterns.

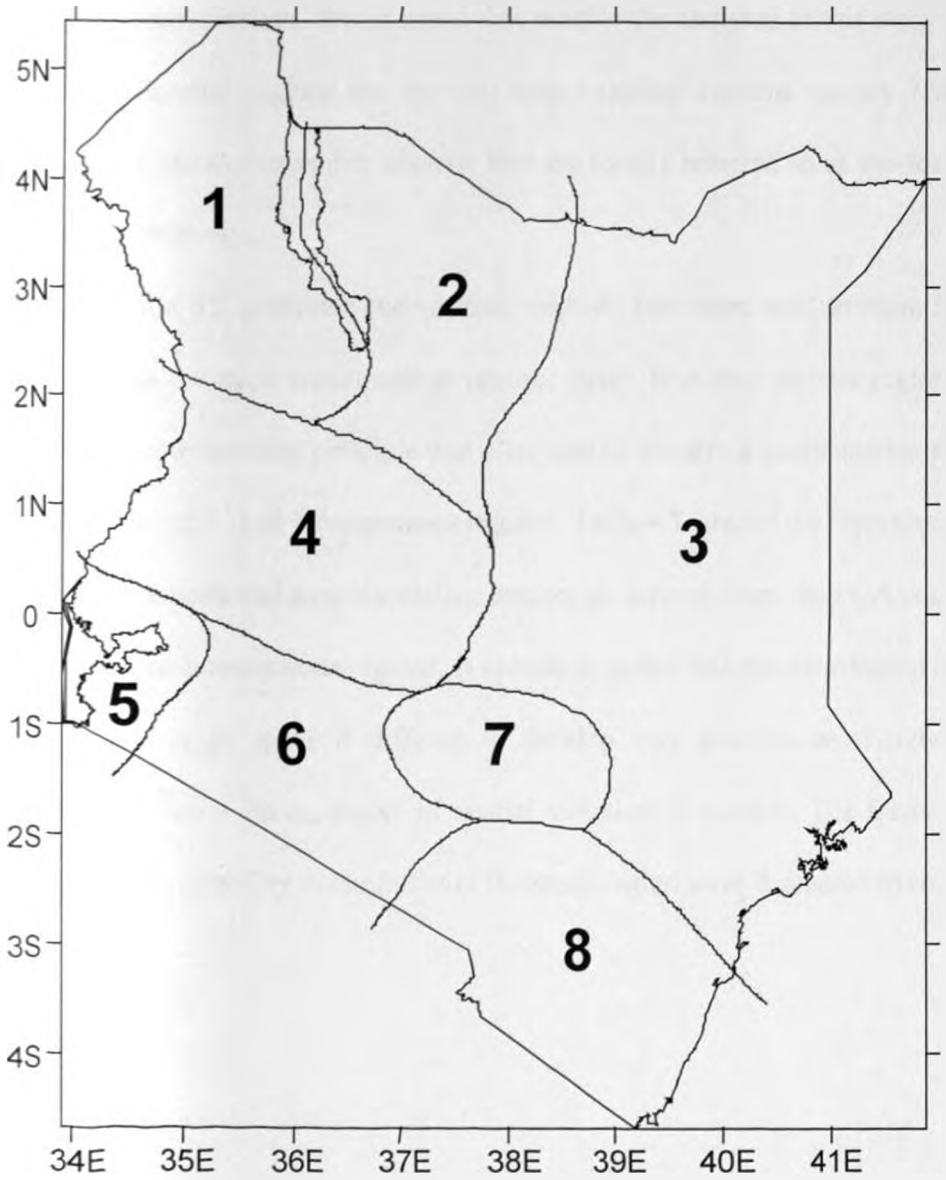

Figure 4.15(d): Homogenous divisions of study region derived from the DJF surface–700mb dekadal TPW seasonal RPCA patterns.

4.3 Representative Records for the Individual Homogeneous Regions

In the previous section we have grouped the area of study into some homogeneous regions for the different seasons. It was noted that most of the analyses in this study concentrated on the specific delineated regions for the two major rainfall seasons namely March-April-May and September-October-November seasons that are locally referred to as the long and short rainfall seasons respectively.

Section 3.2 presented the various methods that were used to identify the representative areal records for each homogeneous region. Apart from the various regionally averaged data, PCA based communality principle was also used to identify a single station that could be used to represent the individual homogeneous regions. Table 4.7 shows the representative stations for the averaging methods and a representative station, as derived from the PCA communality principle, for each of the homogenous regions. It should be noted that the distribution of the stations in the study region might make if difficult to develop very accurate areal indices especially for a variable that has a strong degree of spatial variation as rainfall. The factors that introduce this strong spatial variability in rainfall over the study region were discussed in section 1.3.2.

Table 4.7: Representative stations for each homogenous region for MAM and SON seasons.

SEASON	REGION	REPRESENTATIVE STATION(S)	
		USED WITH ARITHMETIC MEAN AND PCA WEIGHTS METHODS	SELECTED BY PCA COMMUNALITY METHOD
MAM	1	1, 3, 8	1
	2	2, 4	4
	3	5, 6, 7	7
	4	10, 14	14
	5	11	11
	6	9, 12, 13, 19, 34	12
	7	20, 21, 22, 23	20
	8	15, 16, 24, 25, 26, 27, 28, 35	26
	9	17, 18, 29, 30, 31, 32, 33, 36, 37, 38, 39, 40, 41, 42, 43, 44, 46, 47	18
	10	45, 48, 49, 50	48
	11	51, 52, 53, 54, 55, 56, 57, 58, 59, 60	60
SON	1	1,3,8	8
	2	2,4	4
	3	5,6,7,9,12,13,19	5
	4	10,14,15,16,20,21,22,23,24,25,26,27	23
	5	11,17,18,28,29,30,31,32,33,36,38,39,40,41,42,43,44	39
	6	34,45,48,49,50	48
	7	35,37,46,47	47
	8	51,52	52
	9	53,54,55,56,57,58,59,60	60

4.4 Results from the Correlation Analyses

This is devoted to the results that were obtained from correlation analyses for the specific regions using all the three areally averaged records namely those derived from simple arithmetic, PCA weighting and PCA communality methods. As indicated in section 3.3 the correlation methods examined if there were any significant relationships between rain gauge and satellite-derived data within any specific homogeneous region. The correlation results from CCD and TPW data are discussed independently in the next sections.

4.4.1 Results of Correlation with CCD Data

The correlation coefficient values (r) that were obtained for rain gauge and satellite-derived CCD records at specific regions and seasons are given in table 4.8. Results of the correlation analyses show that the correlation coefficients were all significant at 95% level except for region eleven during the MAM season when using areal averages derived from the PCA weights. Using the representative station derived from the communality method, the coefficients were not significant at 95% level in regions ten and eleven during MAM and in regions one, two and five during SON season. The coefficients for regions ten and eleven were not significant during MAM season when using the arithmetic mean areal averages. The maximum value of significant r was 0.9 for regions five and seven during MAM and SON seasons respectively. The minimum was 0.1 in region five during SON season. Thus the variance of rain gauge rainfall that can be derived from CCD records ranged from 1-81% when considering all the areal averaging techniques. This variation was from location to location and season to season with the correlation coefficients being generally lower for the SON season as compared to MAM season.

Table 4.8: Correlation statistics of rainfall against CCD from the areal records derived using arithmetic mean, PCA weights and the principle of communality.

SEASON	REG-ION	Arithmetic Mean	PCA Weights	Communality
		r	r	r
MAM	1	0.5	0.6	0.6
	2	0.5	0.5	0.8
	3	0.5	0.5	0.7
	4	0.7	0.7	0.8
	5	0.9	0.9	0.9
	6	0.5	0.6	0.6
	7	0.8	0.9	0.7
	8	0.7	0.6	0.5
	9	0.8	0.7	0.7
	10	0.2	0.4	0.3
	11	0.3	0.2	0.3
SON	1	0.4	0.5	0.3
	2	0.6	0.5	0.2
	3	0.7	0.8	0.7
	4	0.6	0.6	0.4
	5	0.5	0.5	0.1
	6	0.8	0.7	0.6
	7	0.7	0.5	0.5
	8	0.6	0.5	0.6
	9	0.7	0.7	0.6

Note: r ≡ Correlation coefficient

Results from ANOVA indicated that the significance level had values less than 0.05 in all the instances where the correlation coefficients were significant for all three areal averaging

methods. However, the F-ratio was consistently highest for the PCA-weighting average method compared to the other two methods indicating that the PCA-weighted averages were better representatives of the areal rainfall estimate when compared with the other two methods. Based on this comparison, the rest of the analyses were done using only the PCA-weighted averages.

4.4.2 Results of Correlation with TPW Data

Results that were obtained with TPW data against PCA-weighted average rainfall data are given in table 4.9. The results show that region one during MAM season, and regions one, two, eight and nine during SON season had no significant relationships at 95% level between areal rainfall and TPW data. The maximum significant value of r was 0.7 for region five during SON season, while a minimum of 0.1 was attained in region nine during SON season. Thus the variance in the rain gauge rainfall that may be explained by the TPW records ranged from 1-49%. This also varied from location to location and from season to season.

In general the results showed that r-values were higher for the relationship between rainfall and CCD than that with TWP. This may be due to the fact that CCD attempts to identify the actual convective clouds, and hence it may have a more direct relationship with the recorded rainfall. TPW, on the other hand, records the total moisture available in the atmosphere regardless of whether there is rainfall or not. The relationship may, therefore, not be as direct as in the case of the CCD.

Table 4.9: Correlation coefficients for the relationship between rainfall and TPW data.

SEASON	REGION	r
MAM	1	0.2
	2	0.3
	3	0.5
	4	0.4
	5	0.4
	6	0.4
	7	0.6
	8	0.6
	9	0.6
	10	0.4
	11	0.5
SON	1	0.2
	2	0.2
	3	0.4
	4	0.3
	5	0.7
	6	0.5
	7	0.4
	8	0.2
	9	0.1

Due to the evident variation in the variance of the rainfall estimates derived from the satellite-derived data, care must be taken while using regression equations that are presented below for some regions and seasons.

4.5 Results from Regression Analyses

In this section, the attempt to develop functional relationship between areal rainfall and the two types of satellite-derived data is discussed. Linear regression models were developed between areal rainfall and CCD data while multivariate regression models were developed for the relationship between the areal rainfall, CCD and the three layers of TPW data.

4.5.1 Results of the Simple Regression Analysis

This section deals with the functional relationship between areal rainfall and CCD data. Linear regression models were developed only in cases where there were significant correlation coefficients. From the results of the correlation analysis, discussed in section 4.3, it can be noted that only region eleven during MAM season had no significant relationships between areal rainfall and the corresponding CCD data. Thus regression models can be developed for estimation of areal rain gauge records from the CCD data in all regions and rainfall seasons except for region eleven during the MAM season. Table 4.10 shows the regression statistics for all homogeneous regions that had significant correlation coefficients during both seasons, while Figure 4.16 gives some examples of scatter plots of the observed relationships.

Table 4.10: The simple regression analyses statistics of rainfall against CCD

SEASON	REGION	α	β
MAM	1	54.3	3.3
	2	67.7	3.3
	3	63.7	5.5
	4	143.6	8.3
	5	38.0	13.5
	6	48.8	12.3
	7	29.0	8.0
	8	38.0	13.5
	9	108.6	14.5
	10	184.6	7.6
SON	1	44.2	8.4
	2	53.2	6.7
	3	74.2	12.3
	4	158.8	5.3
	5	224.0	24.6
	6	153.6	13.1
	7	177.9	26.5
	8	74.4	11.7
	9	160.0	21.3

Note α ≡ Intercept of the regression line
β ≡ Coefficient of the independent variable

The intercepts (α) and slopes (β) given in Table 4.10 can be used to represent a linear regression model for all regions and seasons with significant r-values. For example the linear regression model for region seven during MAM season is of the form given in equation 43 below.

$$RF = 29.0 + 8.0CCD \quad (43)$$

Where RF is the estimated rain gauge rainfall amount and CCD is the satellite data.

The best regression model for estimating rainfall amounts from the satellite data should have a very small intercept implying no rainfall incase of no convective cloud cover. The intercept should, therefore, not be significantly different from zero. The results from the study indicated that, except for regions three, five, six, seven, and eight during MAM season, most of the regions have intercepts significantly different from zero. This may imply that the chosen temperature threshold is too cold while the rain is from relatively warm clouds. It may also reflect that the CCD-rainfall relationships are more complex and cannot be accounted for well by linear models. This may call for the need to use individual threshold temperatures for different seasons and even regions and/or the need to use more complex non-linear models. For example the rainfall experienced in these regions are masked by meso-scale convective rainfall systems that could not be adequately represented by the areal records and the network of stations used in the study. It is well known that part of the region like Lake Victoria, Coastal and the Highland region can generate their own meso-scale convective systems (Mukabana, 1992; Okeyo, 1987). This may be a more plausible explanation since, considering the values of the correlation coefficients given in section 4.3, a substantial variance in the rainfall amounts is not explained by the CCD factor in the estimation model. This reasoning is enhanced by the presence of complex topography over the study region that may give rise to varied rainfall mechanisms in the individual homogeneous regions that may not be adequately explained by a linear relationship.

ANOVA tests show that, in comparison, the results for the SON season had relatively lower levels of statistical significance than the MAM season. Furthermore, the intercepts for SON season are all significantly different from zero. It should however be noted that previous studies have shown that SON season has more homogeneous rainfall with a higher degree of predictability with El Nino-Southern Oscillation (ENSO) and Sea Surface Temperature signals (SST) (Ropelewski and Halpart, 1987; Ogallo, 1988; Semazzi et al., 1996; Indeje et al., 2000). This may be indicative of strong influence of larger scale systems in the rainfall mechanism during this season. The rainfall during the MAM season are however more reliable and extend over a longer period compared to SON season where most of the rains are only centered around October and November months (Ogallo, 1988).

It may be concluded from simple regression analyses results that estimation of rain gauge rainfall records using simple regression models of the -50^0C threshold CCD records is limited to a few regions during the major rainfall seasons of MAM and SON. This highlights the space-time complexity of the convective rainfall systems over the region and the strong modulations by the meso- and local- scale systems.

(a): Region 1 (MAM)

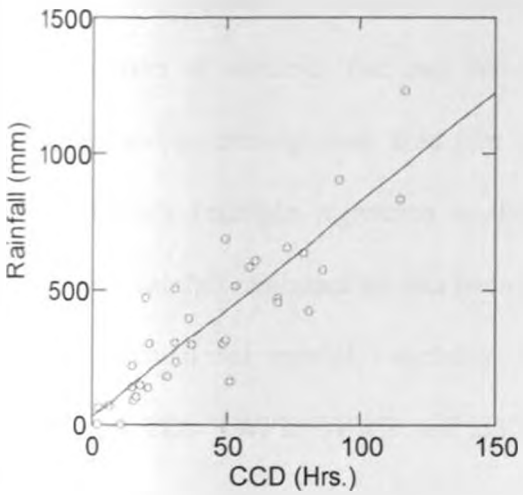

(b): Region 7 (MAM)

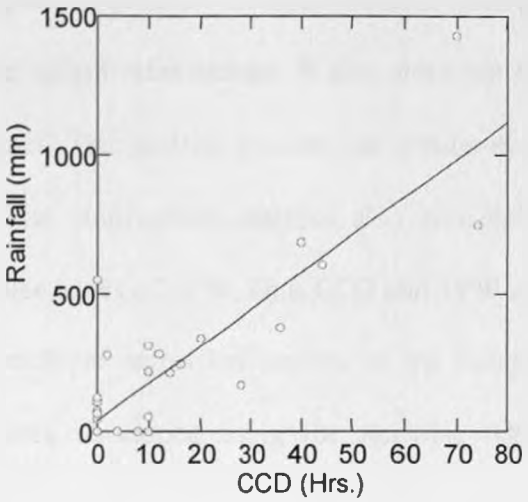

(c): Region 3 (SON)

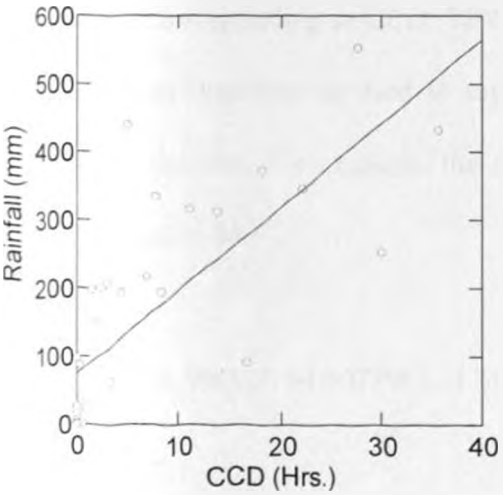

(d): Region 4 (SON)

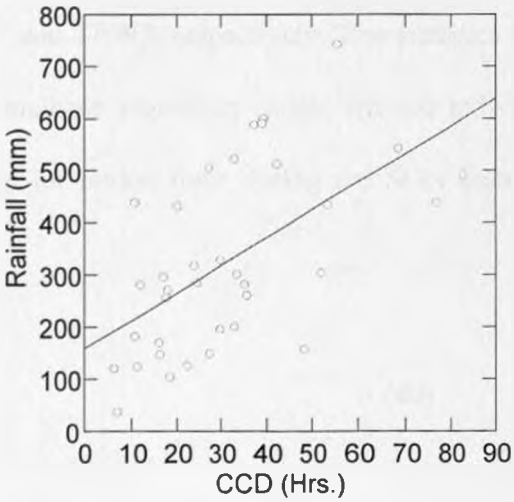

Figure 4.16: Scatter diagrams showing the relationship between rainfall and CCD with the simple regression line included.

4.5.2 Results from Multiple Regression Analyses

As highlighted in section 3.4.1 linear regression does not consider complex interrelations between pairs of variables that may have time lagged relationships. It also does not address interrelationships among more than two variables. This section presents the results that were obtained from multiple regression analyses. The multivariate analyses also considered the variance of rainfall explained by data from the three layers of TPW. Thus CCD and TPW are both used to account for rainfall variability. The multiple regression models of the independent variables CCD, TWP1, TPW2 and TPW3 were developed using the stepwise regression technique.

The analyses were done using standardized values of rainfall and satellite-derived data in order to have comparable values. Table 4.11 shows the regression statistics for the multivariate regressions. The intercept is given by α while β, β_1, β_2 and β_3 are the multiple regression coefficients corresponding to CCD, TPW1, TPW2 and TPW3, respectively. The statistics from table 4.11 can therefore be used to represent a multiple regression model for the individual regions and seasons. For example, the relationship for region three during the SON season is given in equation 44.

$$RF = 0.59CCD + 1.50TPW1 - 1.30 \qquad (44)$$

Where TPW1 refers to the surface to 700 mb layer of TPW. In this case the moisture at the second and third layers had no significant contribution to the precipitation.

Table 4.11: The multivariate regression analyses statistics from the representative records of rainfall against CCD and the three layers of TPW data.

SEA-SON	REG-ION	α	β	β_1	β_2	β_3	V1 (%)	V2 (%)
MAM	1	1.02	0.75	-0.92	NS	1.56	34	39
	2	0.07	0.51	NS	0.54	NS	27	33
	3	-0.83	0.48	1.18	NS	NS	28	37
	4	0.07	1.37	0.61	NS	NS	47	51
	5	0.19	1.50	NS	NS	NS	74	74
	6	-0.76	1.28	1.62	NS	NS	40	48
	7	0.01	1.22	NS	NS	NS	79	79
	8	0.63	0.81	1.51	NS	NS	32	38
	9	-0.27	1.72	0.86	NS	NS	45	50
	10	-1.32	0.40	0.85	NS	NS	13	35
	11	0.00	NS	NS	NS	6.70	5	44
SON	1	0.15	0.29	-0.69	NS	NS	20	37
	2	-0.08	0.44	NS	NS	NS	23	23
	3	-0.02	0.71	NS	NS	NS	58	58
	4	-2.42	0.52	NS	0.92	-6.00	34	58
	5	2.78	0.45	-2.34	1.94	NS	21	34
	6	1.07	0.42	NS	2.34	NS	52	59
	7	0.92	0.41	NS	NS	1.93	24	31
	8	0.25	0.20	0.87	NS	NS	24	36
	9	-1.01	0.55	1.05	NS	NS	53	63

Note: NS ≡ Not statistically significant
β, β_1, β_2 and β_3 ≡ Coefficients of the three independent variables
α has same meaning as in table 4.10
V1 and V2 are percent of variance explained by CCD alone and a combination of CCD and TPW data respectively

A comparison between the results from the linear and the multiple regression models reveal that the additional rainfall variance explained by the inclusion of the TPW data was generally low. These results further show that the moisture in the lowest layer (surface – 700 mb) plays a greater role on the rainfall during the MAM season than that within the other two layers. On the other hand, during the SON season, all the three layers seem to be important in different zones of the study region. The confidence level of the ANOVA results is above 95% for all the

developed models. However, the complexity of rainfall systems as discussed in section 1.3.2 is again confirmed here by the low percentages of variance explained by the multiple regression models in most of the homogeneous regions.

The results from multiple regression analyses further show that the constant terms in the equations were negative and significant in several cases. This is expected since the atmosphere is hardly ever dry. A negative intercept indicates that even when rainfall is zero, there still exists some moisture in the atmosphere. This may be indicative for a need to also have a threshold for TPW data. A comparison of the variances in rainfall explained by the two sets of satellite data indicates that CCD is superior to TWP in estimation of areal rainfall over our region.

4.5.2.1 Tests of Goodness of Fit of the Regression Models

In the previous section, multiple regression models were developed for estimating rainfall from a combination of CCD and TPW records for the individual homogeneous regions and seasons. The model parameters were computed using dekadal data for the period 1989 to 1993. Dekadal data for the period 1994 and 1995, which were not used during the model training period were used to test the skill of the fitted regression models. Table 4.12 shows the summary of some of the ANOVA statistics that were used to evaluate the skill of the fitted models while some graphical examples of the goodness of fit of the models are shown in Figures 4.17(a) and (b).

Table 4.12: The ANOVA for the Estimation Period

Season	Region	MSE	F-Ratio	Significance
MAM	1	0.26	44.08	0.001
	2	1.65	0.79	0.390
	3	0.17	0.27	0.610
	4	0.34	18.22	0.001
	5	0.39	2.83	0.119
	6	0.60	15.25	0.002
	7	0.81	9.60	0.009
	8	0.33	31.04	0.000
	9	0.49	9.01	0.011
	10	0.13	91.05	0.000
	11	2.22	0.03	0.873
SON	1	1.28	0.27	0.609
	2	1.16	1.37	0.257
	3	0.68	24.39	0.000
	4	1.24	2.32	0.144
	5	1.69	0.002	0.967
	6	0.79	2.63	0.121
	7	1.15	0.91	0.351
	8	2.10	1.66	0.214
	9	1.28	2.90	0.105

Note: MSE – Mean Square Error

Results from table 4.12 show that, generally, the skills of the models were better in MAM

than SON season. In regions one, four, six, seven, eight, nine and ten during MAM season, the model results have above 95% confidence level (CL). The models performed poorly in the remaining four regions with the below 90% CL. The worst performance was registered in region eleven with only 13% CL. The poor performance of the models in three of these four regions (two, five, eight and nine) may be due to the low variance that can be accounted for by the models in these regions as has been highlighted in the previous sections. From the correlation analysis results, discussed in section 4.2, it can be noted that region four had no significant relationship between the observed rainfall and CCD. The model for this region was therefore developed using only TPW data. The poor performance reinforces the earlier conclusion that CCD data gives better results in the study region.

The performance of the models was generally poor during the SON season, and for the extreme rainfall occurrences in all seasons. Only in one region, three, did the models have high skill of above 95% CL. The rest of the regions had skills below 90% CL. These observations were quite evident during the training period. These results are reflective of the need for more complex models for estimation and/or different threshold temperatures for CCD and TPW in different homogeneous regions and seasons.

(a): Region 7 (MAM)

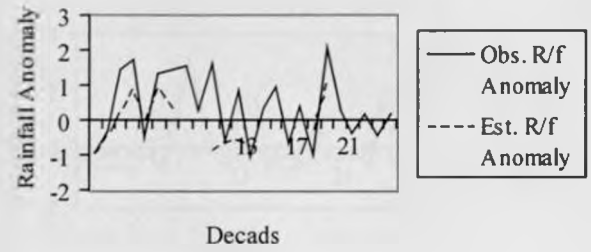

(b): Region4 (MAM)

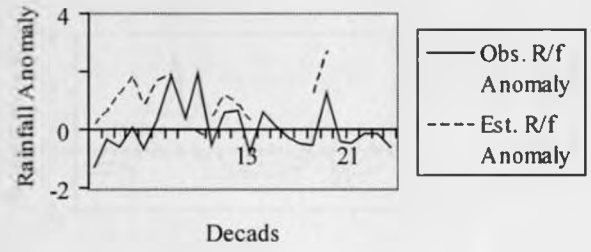

(c): Region 9 (MAM)

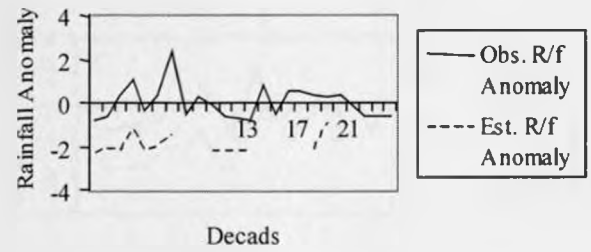

(d): Region 11 (MAM)

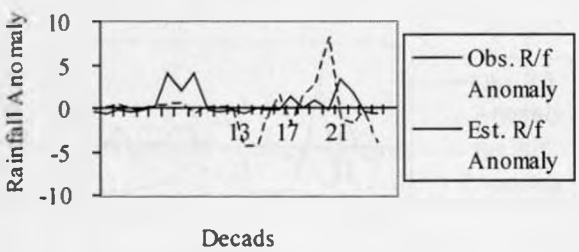

Figure 4.17(a): Plot of the Observed and Estimated Rainfall Anomalies for MAM Season (1994/1995)

(a): Region 2 (SON)

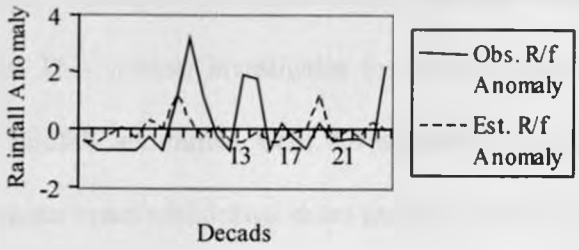

(b): Region 3 (SON)

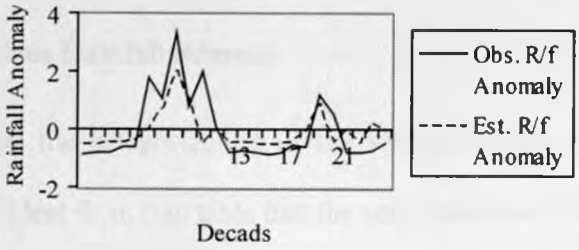

(c): Region 4 (SON)

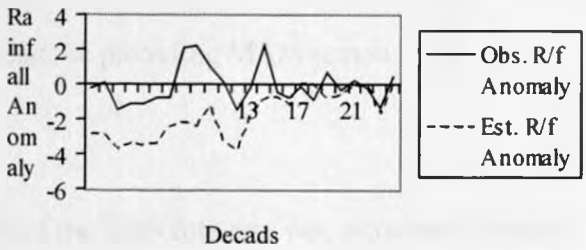

(d): Region 9 (SON)

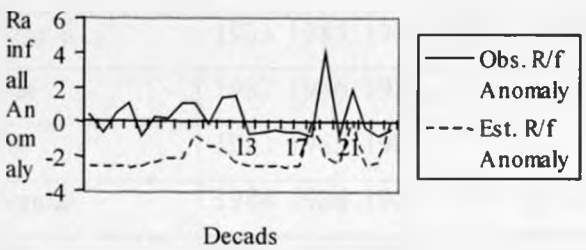

Figure 4.17(b): Plot of the Observed and Estimated Rainfall Anomalies for SON Season (1994/1995)

4.5.2 Results of the Performance of the Regressions during Anomalous Years

In the previous section, attempts were made to derive rainfall estimates from satellite data through regression models. This section investigates the performance of these models during anomalous seasons. The rainfall anomalies were investigated by delineating the anomalous seasons, identifying anomalous onset/withdrawal dates and duration of the seasons. The physical and climate patterns that may be associated with the observed poor or good estimation of rainfall from satellite derived methods during the anomalous seasons are also presented.

4.5.2.1 Observed Anomalous Rainfall Seasons

Table 4.13 presents the categorization of the seasons within the period of study into normal, dry or wet. It is evident from this table that the anomalous wet/dry seasons were recurrent through the study period. The seasonal patterns of these anomalies also varied from year to year. For example, rainfall anomalies during any SON season were not necessarily predetermined by rainfall characteristics during the preceding MAM season.

Table 4.13: Categorization of the years into dry, wet, or normal seasons

Season	Categorization	Years
MAM	Dry	1984 1992 1993
	Normal	1983 1985 1987 1989 1990 1994 1995
	Wet	1982 1986 1988
SON	Dry	1983 1985 1987
	Normal	1984 1986 1988 1989 1990 1992
	Wet	1982 1995 1994

4.5.3.2 Observed Rainfall Onset, Duration and Withdrawal

This section presents the patterns of the onset, withdrawal and duration of the two rainfall seasons as observed from the study. Details of the cumulative curve method used to delineate these events were discussed in section 3.6. The delineated onset, withdrawal and duration for MAM and SON seasons are given in table 4.14 while examples of the cumulative curves that were used to determine the onset and withdrawal dates are shown in Figure 4.18

It is evident from table 4.14 that the onset and withdrawal dates varied significantly from year to year and from season to season. On average the duration for MAM is generally longer, but there were some years in which the SON season duration was equal to or even much longer. For example The SON season of 1989 started on the 26^{th} dekad and persisted for ten dekads while during MAM season of 1985 the duration was only six dekads. It can also be noted from these results that, during the study period, late/early onset and withdrawal dates were not always indicative of poor/good performance of the season. For example some late onsets were sometimes followed by late withdrawals leading to an extension of the rainfall seasons.

Table 4.14: Onset, withdrawal and duration for MAM and SON during the study period

Year	MAM			SON		
	Onset dekad no.	Withdrawal dekad no.	Duration dekads	Onset dekad no.	Withdrawal dekad no.	Duration dekads
1982	6	14	8	28	34	6
1983	7	14	7	35	**	**
1984	7	12	5	28	35	7
1985	8	14	6	29	33	4
1986	6	15	9	27	34	7
1987	9	16	7	30	33	3
1988	6	14	8	30	35	5
1989	7	14	7	26	36	10
1990	6	15	9	27	35	8
1992	9	13	4	30	35	5
1993	10	17	7	*	*	*
1994	7	14	7	30	35	5
1995	6	14	8	27	34	7

Note: * indicates missing data

** indicates season started very late and continued through the end of the year

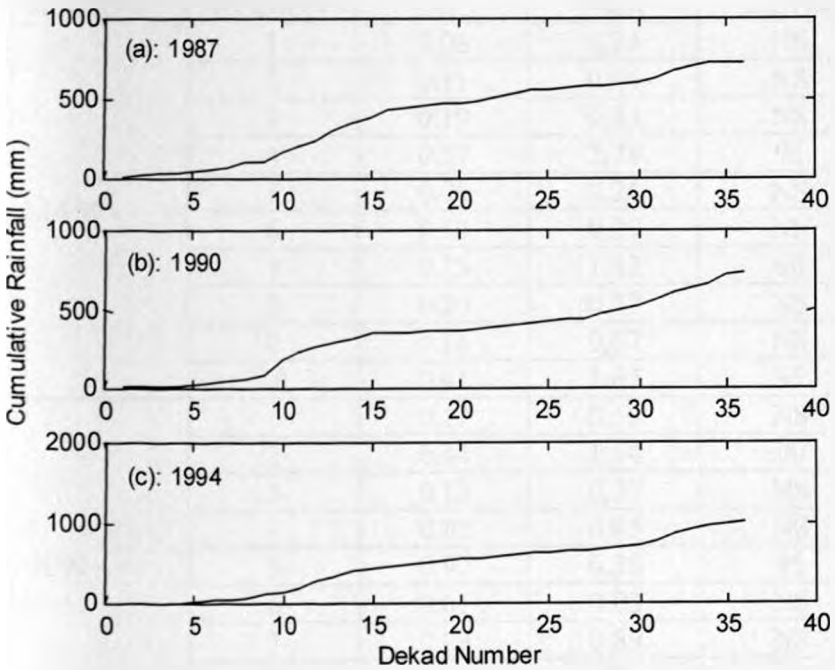

Figure 4.18: Examples of the cumulative curves used to determine the seasonal rainfall onset, withdrawal and duration.

4.5.3.3 Estimates of Rainfall during Anomalous Seasons

Under this section, the regression models that were developed in section 4.4 were used to determine the skill of the models during anomalous dry and wet years. In this regard, satellite-derived data for the anomalous years were independently used to estimate the corresponding rain gauge records. Student t-test was then used to examine the significance of the relationships between the estimates from the satellite-derived data and the rain gauge data during the anomalous dry and wet years. The results that were obtained from these tests are given in Tables 4.15 and 4.16. The correlation coefficient (r) in the tables provide the degree of relationships between rainfall amounts estimated from the satellite data and the rain gauge rainfall.

Table 4.15: ANOVA results and the correlation coefficient, r, for the anomalous dry years.

SEASON	REGION	r	t-test	C.L (%)
MAM	1	0.06	0.24	NS
	2	0.11	0.44	NS
	3	0.19	0.73	NS
	4	0.57	2.78	95
	5	0.06	0.24	NS
	6	0.10	0.39	NS
	7	0.35	1.42	90
	8	0.20	0.77	NS
	9	0.16	0.67	NS
	10	0.41	1.67	95
SON	1	0.17	0.56	NS
	2	0.44	1.54	90
	3	0.12	0.37	NS
	4	0.02	0.05	NS
	5	0.90	6.38	95
	6	0.01	0.03	NS
	7	0.29	0.89	NS
	8	*	*	*
	9	0.11	0.33	NS

Note: * represents regions reporting no rainfall throughout the season
C.L represents confidence levels; NS Not statistically significant

Table 4.16: ANOVA results and the correlation coefficient, r, for the anomalous wet years

SEASON	REGION	r	t-test	CL (%)
MAM	1	0.17	0.46	NS
	2	0.45	1.42	90
	3	0.49	1.49	90
	4	0.41	1.29	90
	5	0.44	1.39	90
	6	0.22	0.63	90
	7	0.53	2.42	95
	8	0.12	0.04	NS
	9	0.33	0.98	NS
	10	0.21	0.56	NS
SON	1	0.26	1.15	90
	2	*	*	*
	3	0.08	0.34	NS
	4	0.13	0.56	NS
	5	0.23	1.16	90
	6	0.09	0.39	NS
	7	0.21	0.96	NS
	8	*	*	*
	9	0.64	3.62	99

Note: * represents regions reporting no rainfall throughout the season
C.L represents confidence levels
NS Not statistically significant

In comparison to the results that were obtained when all the years were used in the analyses (section 4.4), the t-test results given in Tables 4.15 and 4.16 show that the models perform poorly in the anomalous years during MAM season. However during SON, the models perform relatively better during the anomalous years. The models perform relatively better in only five regions during the anomalous wet MAM seasons as compared to seven when all the data were included. The corresponding values for the wet SON seasons are three and only one, respectively. Poor performance of the models during wet periods may be due to the enhanced availability of moisture in the atmosphere during the anomalous wet seasons resulting in the

release of rainfall even at warmer cloud temperatures leading to underestimation of the rainfall from the chosen satellite threshold temperature.

A comparison between the results from anomalous dry seasons and the cases when all the data were included reveal that the models perform well in only three as opposed to seven regions during MAM seasons. The corresponding values for the SON seasons are two and only one, respectively. It is evident that the models also have poor performance during the anomalous dry MAM seasons, but with slightly better performance for the anomalous dry SON seasons. This may be due to the localized nature of rainfall during the dry seasons that may lead to the formation of localized thunderstorm clouds, which are in turn easily identified by the satellite data. The regions with good model performance during the dry seasons include those around and to the north of Lake Victoria, and a region along the coast of Indian Ocean. These regions have moisture sources in Lake Victoria, Congo Basin and the Indian Ocean. However, another region with good model performance is located in the semi-arid northern parts of the study area. The good performance of the models in this region could be due to the existence of many zero or low rainfall and satellite-estimated records that may also induce high correlation values.

4.5.3.4 Circulation Patterns during Anomalous Wet/Dry Seasons

This section presents some composites of the average circulation patterns during the seasons based on the observed anomalous years within the study period. These could be used in explaining the good or bad performance of the satellite data conversion models during the anomalous seasons. Details of the method used in deriving the composites may be found in section 3.6.

Examples of the wind pattern composites are shown in Figures 4.19 and 4.20. One of the major sources of moisture for the study region is the Indian Ocean. It is evident that from Figure

4.19 that during the anomalous wet years the whole region of study is under the influence of the moist southeasterly monsoonal circulation. These strong southeasterly winds carry a lot of moisture from the Indian Ocean into the study region. This may result in the availability of excess moisture that may trigger rainfall from relatively warm clouds that may not be identifiable by the chosen CCD threshold temperature.

During the anomalous dry seasons, a strong southeasterly component is developed in the equatorial flow as shown in Figure 4.20. This diffluent southeasterly flow diverts moisture from the Indian Ocean away from the study region causing a reduction in the amount of moisture reaching most of the study area with the resultant lessening of formation of widespread cumulus clouds. However, the relative good performance of the satellite models during this season in some regions may be due to presence of localized cumulonimbus clouds or low rain gauge/satellite-estimate values as has been explained in section 4.4.3.3.

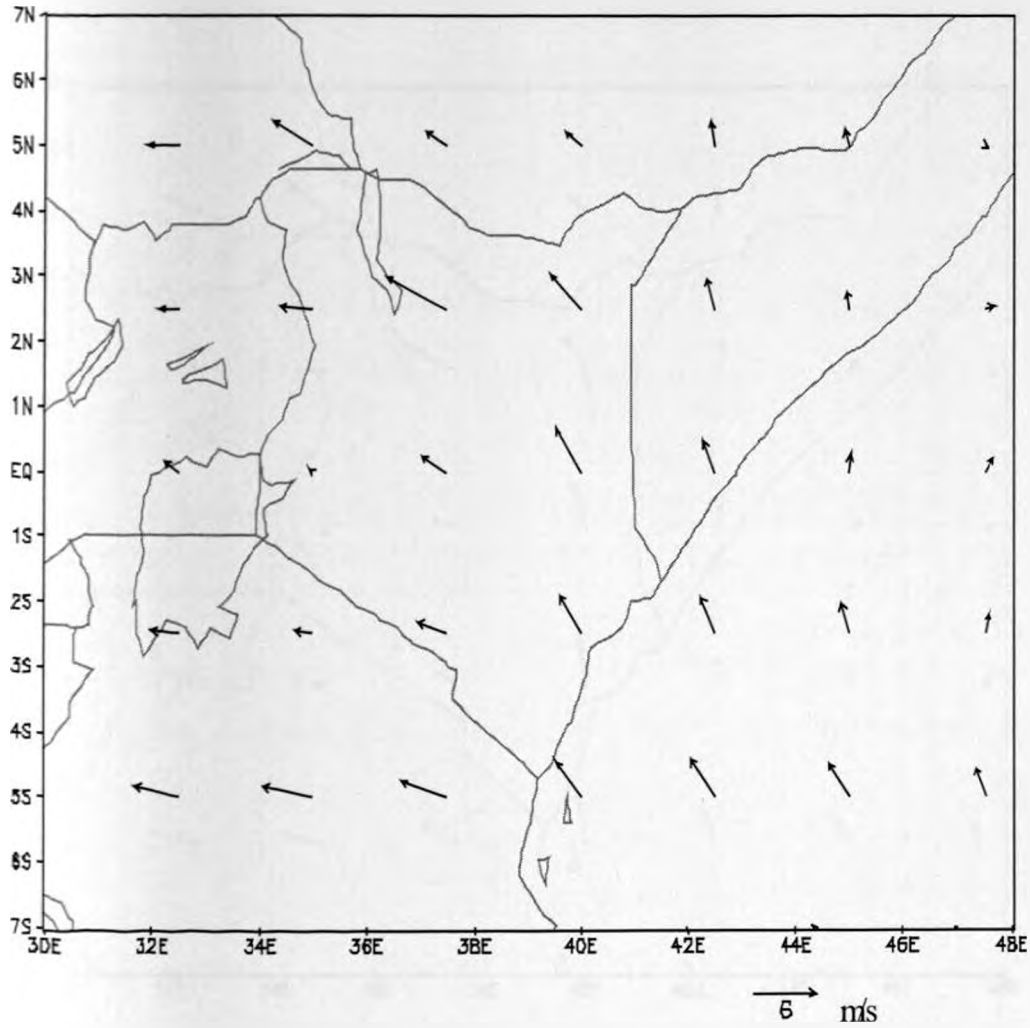

Figure 4.19: Spatial distribution of 850 mb wind during the wet SON season of 1982

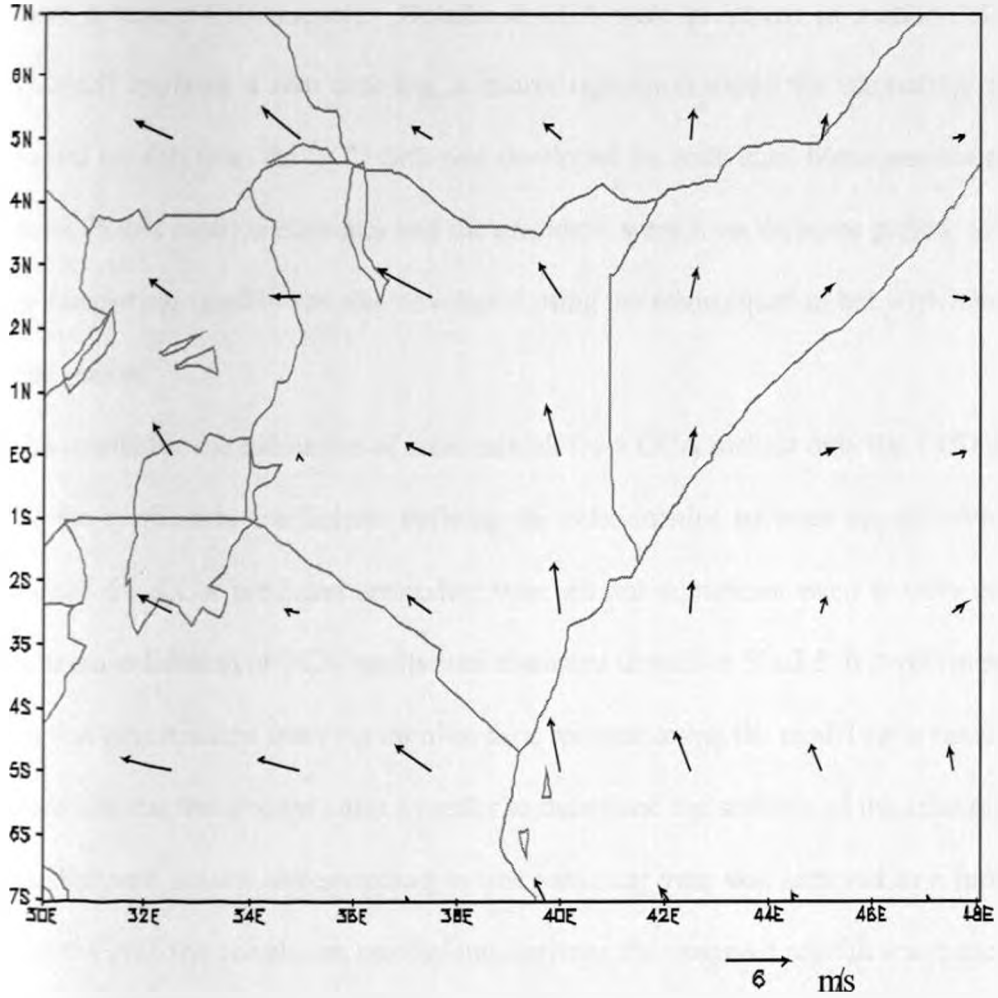

Figure 4.20: Spatial distribution of 850 mb wind during the dry MAM season of 1992

4.5.3 Results from Canonical Correlation Analysis (CCA)

In the previous sections the results of simple linear and multivariate regression models were presented. These models were based on simple and stepwise relations between observed rainfall and the corresponding satellite data. This section presents the results that were obtained by the more complex CCA models. Details of CCA were presented in section 3.4.3. Using equation 22 and applying a zero time lag, a matrix regression model for estimating rain gauge recorded areal rainfall from the CCD data was developed for individual homogeneous regions in both seasons. In this case the estimates and the predictors were from the same period. Similarly, a model for forecasting rainfall was also developed using the same equation but with a built-in lag time of one season.

The results for the estimation of areal rainfall from CCA include only the CCD data. This is because the correlation coefficients defining the relationships between the observed rainfall anomalies and the CCA predicted anomalies were all not significant even at 90% confidence level. The cross-validation of CCA results was discussed in section 3.5.2.5. It involves repeatedly omitting a few observations from the training data, reconstructing the model each time, and then making forecasts for the omitted cases in order to determine the stability of the relations. In this study, data for each season corresponding to one particular year was removed at a time. Tables 4.17(a) and (b) give the correlation coefficients between the observed rainfall anomalies and the resultant predicted values.

Table 4.17(a): Correlation between the observed rainfall and the satellite-derived estimates for MAM season. (Negative correlation coefficients are set to zero)

Year	Homogeneous Regions										
	1	2	3	4	5	6	7	8	9	10	11
1989	0.00	0.00	0.00	0.34	0.00	0.56	0.78	0.00	0.46	0.45	0.27
1990	0.28	0.52	0.02	0.00	0.00	0.00	0.66	0.45	0.39	0.00	0.22
1992	0.00	0.13	0.24	0.39	0.11	0.00	0.00	0.00	0.00	0.20	0.00
1994	0.00	0.00	0.69	0.69	0.73	0.09	0.04	0.00	0.17	0.57	0.00
1995	0.00	0.44	0.33	0.92	0.94	0.22	0.00	0.00	0.91	0.10	0.00
mean	0.28	0.36	0.32	0.59	0.59	0.29	0.49	0.45	0.48	0.33	0.25

Table 4.17(b): Correlation between the observed rainfall and the satellite-derived estimates for SON season. (Negative correlation coefficients are set to zero)

Year	Homogeneous Regions								
	1	2	3	4	5	6	7	8	9
1989	0.00	0.12	0.49	0.00	0.48	0.75	0.67	0.64	0.16
1990	0.19	0.00	0.74	0.13	0.50	0.02	0.41	0.00	0.00
1992	0.27	0.00	0.16	0.44	0.72	0.67	0.51	0.00	0.00
1994	0.10	0.09	0.54	0.00	0.94	0.45	0.23	0.00	0.00
1995	0.44	0.16	0.55	0.10	0.65	0.45	0.02	0.65	0.60
mean	0.25	0.12	0.50	0.22	0.66	0.45	0.34	0.65	0.38

The results show evident significant year to year variations in the relationships at all locations. These variations have often been observed in the year to year rainfall amounts recorded over the study region. On several occasions there were negative relations between the observed rainfall and the estimates, thus large negative/positive anomalies are observed in rainfall while the corresponding estimates were positive/negative respectively. In some years the correlation coefficients were quite low. This shows that the estimation equations may perform better in some years than others.

Several other researchers, including He and Barnston (1996), Prasad and Singh (1996) and Yu *et al.*, (1997), also recorded negative correlation coefficients while cross-validating CCA models. However, in most cases the negative coefficients are set to zero and are then not considered in the working out of the mean skill of the model (He and Barnston, 1996; Yu *et al.*, 1997). In this study, the negative coefficients were also set to zero.

The number of cases estimated every year for each season was at most twelve (every season was composed of four dekads, including the last two dekads of the previous season and the first two dekads of the next season) and the critical value for statistical confidence at 95% level was a correlation coefficient equal to 0.5. Results from the Tables show that the rainfall amounts over regions ten and eleven during MAM and regions three, five and eight during SON seasons were relatively well estimated with a mean skill of 0.50 or higher as is shown at the bottom row of the tables. The estimates were most skillful over region five (0.66) during SON season while the CCA model had the worst skill in region two during the same season.

These results are indicative of some possibility of using CCA to develop an improved model for 10-day rainfall estimation. However, the estimates must be treated with caution because the period of the satellite data available for model development was short. The pre-CCA analysis requires the running of PCA to produce the patterns and reduce redundancy by eliminating the correlated observations. To have stable patterns normally requires a climatological length of data set. In this study the canonical correlation coefficients were different every time a validation year was omitted indicating that the derived patterns were a bit unstable. Figures 4.21 and 4.22 are examples of the relationship between the canonical variable time series and the relationships between the observed anomaly rainfall and the CCA estimates respectively.

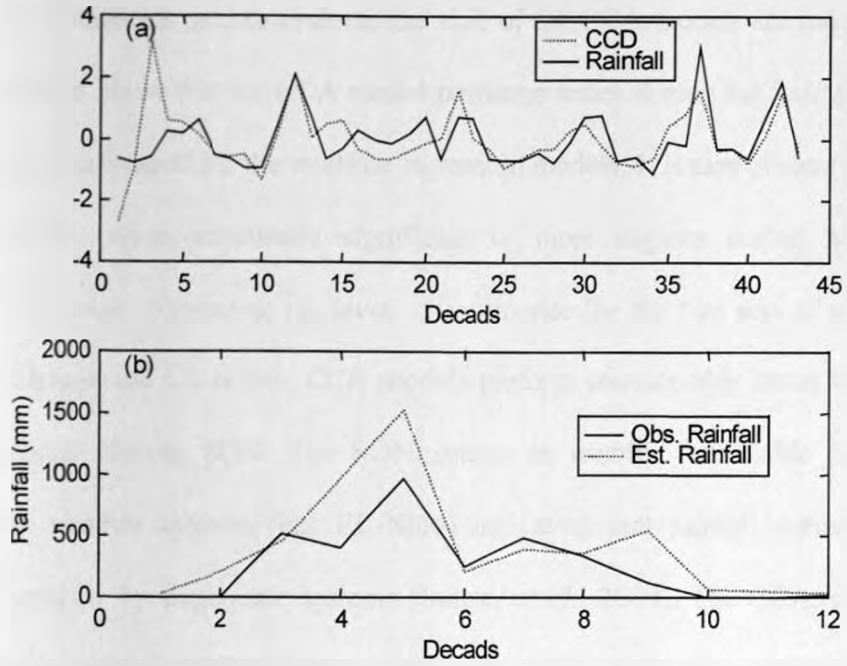

Figure 4.21: Relationship between the observed rainfall and the CCA estimates for MAM season. (a) Canonical component time series in normalized values. (b) Observed rainfall against the CCA model estimated amounts.

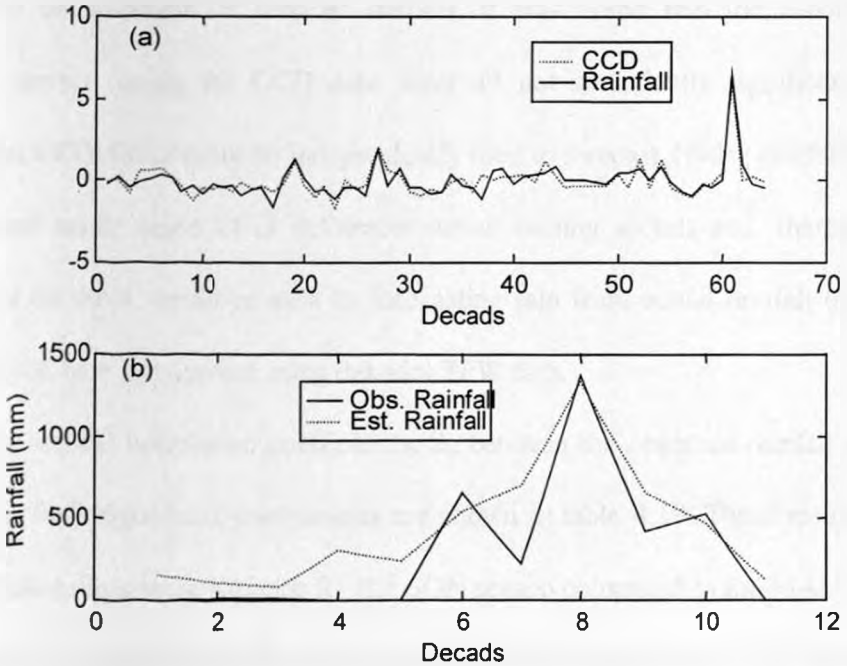

Figure4.22: Relationship between the observed rainfall and the CCA estimates for SON season. (a) Canonical component time series in normalized values. (b) Observed rainfall against the CCA model estimated amounts.

ANOVA statistics used to evaluate the skill of the CCA models are summarized in table 4.18. These results show that the CCA model performs better during the MAM than during the SON season as was evident for the multiple regression models. It is also evident that the multiple regression models were statistically significant in more regions during MAM season in comparison. However, comparing the level of confidence for the two sets of models, it can be noted that, although the CL is low, CCA models perform considerably better than the multiple regression models during SON. The SON season is usually predictable from large-scale, teleconnection weather systems (e.g. EL-Niño) indicating that rainfall during this season is influenced markedly by large-scale systems (Indeje, *et al.*, 2000). The CCA, which deals with patterns, would therefore perform better during the SON season than the multiple regression models.

In the development of forecast models, it was noted that the canonical correlation coefficients derived using the CCD data were all not statistically significant. This may be indicative that CCD data cannot be independently used to forecast 10-day rainfall of an area. This is an expected result since CCD delineates actual raining clouds and, therefore, forecasting rainfall based on them would be akin to forecasting rain from actual rainfall observations. The results presented here are derived using dekadal TPW data.

The canonical correlation coefficients, S_i, between the observed rainfall patterns and the TPW patterns for i significant components are shown in table 4.19. These results show that the canonical relationships were stronger for the SON season compared to the MAM. This is a result consistent with the other studies that have found the short rain season of SON more predictable in the study region (e.g. Indeje *et al.* (2000). The number of data cases used in the development of the CCA matrices were at least one hundred and twenty. The critical correlation coefficient for

significance at 95% CL for such data lengths is 0.19. Only the first mode for SON season was therefore significant while none of the modes for MAM were significant. During SON season in 1993 TPW data were missing.

Table 4.18: The ANOVA for the CCA rainfall estimates

Season	Region	MSE	F-Ratio	Significance
MAM	1	0.47	10.32	0.002
	2	0.56	1.50	0.226
	3	0.22	4.30	0.042
	4	0.95	7.28	0.009
	5	0.51	0.51	0.478
	6	0.94	0.08	0.781
	7	0.78	0.38	0.539
	8	1.03	0.63	0.431
	9	0.69	0.72	0.401
	10	0.76	2.07	0.155
	11	0.67	4.92	0.009
SON	1	0.57	2.21	0.146
	2	1.42	1.43	0.239
	3	0.66	0.75	0.392
	4	1.14	0.05	0.818
	5	0.61	1.25	0.270
	6	0.42	0.36	0.551
	7	1.11	1.07	0.309
	8	1.08	1.40	0.245
	9	0.56	0.29	0.593

Table 4.19: Canonical correlation coefficients between rainfall patterns and TPW patterns

Season	S_i	Years							Mean
		1988	1989	1990	1992	1993	1994	1995	
MAM	S1	0.05	0.07	0.04	0.07	0.07	0.11	0.11	0.07
	S2	0.01	0.04	0.00	0.05	0.00	0.07	0.03	0.03
SON	S1	0.21	0.20	0.28	0.23	-	0.25	0.26	0.24
	S2	0.15	0.07	0.09	0.08	-	0.02	0.14	0.09
	S3	0.03	0.01	0.04	0.01	-	0.01	0.02	0.02

In testing the validation results, the hit and alarm rates were computed in the form of contingency tables for various forecast categories in determining the skill of the forecasts. The hit rate is reflective of correct forecasts while alarm rates indicate rate of the models forecasting extreme large / low values that do not occur. Only the results for SON season are presented in this section. An example of a contingency table for region nine during SON of the hits and alarms is shown in table 4.20. From this table it can be noted that only about 37% were hits. This is a result that is replicated in all the other regions during this season. The low percentages were probably due to the relatively short length of the TPW data as was the case with CCD data in the CCA estimation model.

Table 4.20: Contingency table grouping observed standard anomaly rainfall and CCA estimates from TPW data for region nine during SON season.

	BN (Est)	N (Est)	AN (Est)	Total
BN (Obs)	15	16	15	46
N (Obs)	12	19	15	46
AN (Obs)	19	11	17	47
Total	46	46	47	139

Note:
BN (Obs) observed below normal rain gauge values
N (Obs) observed rain gauge values within normal range
AN (Obs) observed above normal rain gauge values
BN (Est) satellite estimated below normal values
N (Est) satellite estimated values within normal range
AN (Est) satellite estimated above normal values

It can be concluded from these results that CCA can be used to give improved 10-day rainfall estimates from CCD data. There also exists a possibility of deriving dekadal rainfall forecasting models based on the TPW data, especially for the SON season. However, the length of the satellite-derived data needs to be enhanced for better performance.

CHAPTER FIVE

SUMMARY, CONCLUSIONS AND RECOMMENDATIONS

5.0 Summary, Conclusions and Recommendations

This last chapter attempts to provide an overall summary of the thesis. The conclusions drawn from the results of the study, recommendations and suggestions for future extension of the study are also presented.

5.1 Summary and Conclusions

The presentation of this thesis is organized into five chapters. Chapter one provides a general review of the climate of the study region and the major extreme climate events together with the associated impacts. Key issues that are highlighted in this chapter include the spatial and temporal variability of rainfall, with special reference to extreme events such as droughts and floods, and their impacts on the economies of the countries within the region. The problems associated with rainfall monitoring through the existing "in situ" methods and the need for alternative methods of rainfall monitoring are also highlighted. The potential use of satellite-derived data to estimate areal rainfall formed the foundation of this study. The specific objectives that were addressed to meet the overall objective of the study are also presented in chapter one. These include regionalization, using rainfall and satellite-derived data, of the study area into homogeneous climatological zones and the development of empirical functions to investigate the potential use of satellite-derived data in estimating and forecasting areal rainfall at each homogeneous region. The skills of the developed empirical models were also examined. The final part of the study investigated the meteorological factors that may be associated with the good or poor performance of the empirical models during the anomalous dry and wet seasons.

Chapter two presents the data used in the study together with the various methods that were used to examine the quality of the rainfall data. The data used in the study include rain gauge rainfall, satellite-derived and general circulation data. The rain gauge rainfall data consisted of daily records for the period 1982 to 1995 obtained from the Kenya Meteorological Department data archives. The satellite data included Cold Cloud Duration (CCD) information and Total Precipitable Water (TPW) in the atmosphere. The CCD data were obtained from the Regional Center for Services in Surveying, Mapping and Remote Sensing archives in Nairobi, Kenya, while TPW data were obtained from NASA Water Vapor Project data archives. The general circulation data used in the study were the reanalysis data from ECMWF. The last two sets of data were obtained through the Department of Marine, Earth and Atmospheric Sciences, North Carolina State University. Few missing records were estimated using correlation method, while the homogeneity of the data was tested using single mass curves.

The various methods used in attempting to achieve the objectives of the study are presented in chapter three. The first method involved the regionalization of the study region into homogeneous climatological zones that could be used in the development of empirical models for the specific zones. The regionalization was carried out using the S-mode Principal Component Analysis (PCA) method. Both unrotated and rotated solutions were adopted in attempts to delineate the region into zones with similar spatial climatic characteristics. Both the observed rainfall and satellite-derived data were subjected to PCA. The methods that were used to determine the number of significant PCA modes to be retained for rotation included Kaiser's criterion, Scree's test and the sampling of error method.

While the satellite data were in a grid format covering the whole of the study area, the rain gauge records represented point information scattered unevenly across the study region. For a more realistic framework for comparison of the two data sets, areally averaging of each data set

over each homogenous region was required. Three methods were used to derive and compare areal estimates in the study. These included arithmetic mean, PCA-weighted mean and the principle of communality methods.

The development of relationships between the observed rainfall and the satellite-derived data involved the use of correlation and regression methods. While correlation methods present the degree of relationship between the variables, the functional relationships were provided by regression analyses. The three types of regression methods that were used in the study include simple, stepwise and canonical regression analyses. The canonical regression method was also used in forecasting of rainfall from the satellite-derived data. The skill of the fitted models was tested using various methods that ranged from simple mean square error method, χ^2 - and F-test to Kolmogorov-Smirnov test.

Finally, the anomalous wet and dry years were delineated using simple ranking statistics while cumulative curves were used to identify the anomalous onset, cessation and hence duration of the rainfall seasons. Composite maps of the corresponding general circulation patterns were also derived in order to determine the major circulation patterns that were dominant during the specific anomalous periods.

The results that were obtained from the various analyses are presented and discussed in chapter four. It was evident from the data quality control tests that the data used in the study were of good quality. The derived residual mass curves indicated that most of the data, including the few estimated, were not heterogeneous. It should be noted that data were estimated only in cases where less than 10% was missing. This was to minimize errors that may be associated with data estimation. The quality-controlled data formed the fundamental basis of the various analyses carried out in the study.

The regionalization techniques based on PCA of decadal data indicated that the S-mode solutions delineated eleven regions for MAM, JJA and DJF seasons, while only nine were delineated for the SON season from the rainfall data. The derived regions were generally comparable to those delineated by other researchers using daily, monthly and annual data (Barring, 1988; Ogallo, 1989; Indeje *et al.*, 2000). The results from the PCA indicated that the number of significant PCA modes was higher for the dry seasons of JJA and DJF as compared to those from the wet seasons of MAM and SON. However, these components extracted relatively low percentage of total variance in the decadal rainfall. This may reflect the influence of highly localized systems in the rainfall during these dry seasons. The development of regression models for rainfall estimation from satellite data, therefore, concentrated on the wet seasons of MAM and SON. It was further evident that the patterns of the PCA modes highlighted the significant roles of Lake Victoria, Indian Ocean, the Highlands and the Rift Valley in the spatial distribution of rainfall over the study region. The roles of these physical features were consistent throughout all seasons as witnessed from the dominance of unique PCA modes at the specific locations.

When the satellite-derived surface to 700 mb layer of TPW data were subjected to PCA analyses, only seven regions were delineated for MAM and SON seasons while six and eight were delineated for JJA and DJF seasons, respectively. It was evident that fewer regions were demarcated while using these satellite-derived data. This could be probably due to the smoothening of some of the regional features when TPW layer data were used. This was the first time that attempts were being made to derive regional climatic zones based on satellite-derived data. A comparison of the results from the regionalization based on rainfall data to the regions delineated from the satellite-derived TPW data indicate significant large scale similarity in the patterns of the PCA modes. The availability of more satellite-derived data in the coming years

would, however, require similar analyses to be repeated in order to confirm the stability of the satellite-based data derived homogeneous regions.

Results from the comparison of the areal estimates derived from the three different methods indicated that PCA-weighted method provided more realistic areal averaged rainfall at the specific homogeneous regions than the other two methods. PCA-weighted areal estimates were therefore used to develop the areal rainfall indices that were utilized in correlation and regression analyses.

Results from the correlation analyses indicated higher correlation values between rainfall and CCD data as compared to rainfall and TPW data. This was probably due to the fact that CCD identifies the raining clouds and hence having a more direct relationship with the observed rainfall as compared to TPW, which provides the total moisture in the atmosphere regardless of the presence of rain. The results highlighted the potential use of satellite-derived CCD data in providing realistic estimates of areal rainfall. Regression equations were therefore developed for all regions that had significant correlation coefficients.

Linear regression models were developed between rainfall and CCD data, while multiple regression models were developed between rainfall, CCD and the three layers of TPW data. Based on the results of testing the significance of the computed correlation coefficients, linear models were developed for all homogeneous regions during both rainy seasons except for region four in MAM. The developed linear regression models indicated that in general the intercepts of the derived graphs were significantly different from zero. This could be indicative of complex relationships between rainfall and CCD that may not be adequately described by a simple linear model. It could also be due to the use of unrealistic CCD temperature threshold. This calls for future efforts to identify unique individual threshold temperatures for different homogeneous regions and seasons to enable identification of more realistic CCD values. The results of the

study are consistent with results obtained for tropical southern and western Africa (Dugdale and Milford, 1985; 1987; Ouma, 1995). This is the first time that such analyses were carried out for the different homogenous regions of Kenya.

The results obtained from multiple regression analyses indicated that the additional variance explained by the inclusion of TPW data were generally low. However, it was evident that the inclusion of TPW in the estimation models added some skill to the estimated values at some regions. For example, skillful regression for region four during MAM could be derived only after the inclusion of TPW data. The results also showed that, as in the case with the linear models, the constant term in the model equations were even more significantly different from zero. Apart from the reasons already advanced for the linear models, the relatively large constant terms may be indicative of a need to also have a threshold value for TPW data to better discriminate atmospheric moisture amounts that result in rainfall. This is the first time that TPW data have been used in the study region in attempts to improve the accuracy of satellite-derived rainfall estimates. It was hoped that TPW data could capture some of the complex rainfall processes inherent in the study region that could not be adequately represented by the CCD estimates. The linear regression equations used in this study assumed that the CCD and TPW data were independent. Future studies should, however, examine the linkages between these two sets of data. Such information is vital for the improvement of the skill of the developed regression models.

The results presented in section 4.5 of chapter four indicated that the years 1984, 1992 and 1993 could be categorized as dry while 1982, 1986 and 1988 were wet for the MAM season. For the SON season the years 1983,1985 and 1987 were categorized as dry, while 1982,1994 and 1995 as wet. Further, the results from the study indicated that the onset and cessation dates had no significant influence on the outcome of a season within the study period. Thus, although

rainfall started late in some years, such rains extended beyond the normal withdrawal dates. There were also cases of early onsets and withdrawal leading to poor rainfall seasons.

Finally, the study examined the skill of the regression models for areal rainfall estimation using satellite data during anomalous dry/wet periods. The results from the regression models showed that the skills of such models were generally lower during the anomalous wet seasons, but slightly better during the anomalous dry seasons. The prevailing circulation patterns for the anomalous periods showed that during the dry seasons, a strong westerly component was dominant in the equatorial winds. This would minimize the supply of moisture from the Indian Ocean and lead to reduction in the amount of moisture available inland, especially east of the highlands. It may therefore be assumed that the good performance of the regression models during these dry seasons may be due to the dominance of the isolated localized heavy rainfall during the dry season. The better performance could also be due to the existence of many zero rainfall events with corresponding low satellite-derived values that could force some of the observed high correlation values.

Circulation patterns for the anomalous wet seasons showed enhancement of the southwesterly flows inland, which would increase the inland moisture influx from the Indian Ocean. The resultant enhancement of moisture availability in the atmosphere could trigger precipitation even from relatively warm clouds. This may lead to underestimation from the chosen satellite threshold temperature and hence the poor skills of the models during these periods.

The last part of the study examined the skill of more complex relationship regression models in estimating and forecasting rainfall based on satellite-derived data. In this regard the Canonical Correlation Analysis (CCA) that is based on regional pattern recognition was adopted. A comparison of the CCA models results to those of the multiple regression revealed that the

CCA models performed considerably better during the SON season. This could be due to the strong response of the SON seasonal rainfall patterns to large-scale teleconnection systems (Indeje *et al.*, 2000; Ogallo, 1988). These results, however, showed that better areal rainfall forecasts were derived from TPW data. It may, therefore, be concluded from the study that TPW data provided enhanced rainfall prediction signals, especially for SON season. Such a conclusion should, however, be taken cautiously since the satellite data used in the development of the models were of relatively short duration. With the availability of more satellite records, more studies will be required to determine the stability of these predictors.

Inadequacy of data has been a major problem during the weather forecasting procedures leading to major portions of the study region, especially the remote regions, receiving inadequate information. Hydrologists have also had problems in quantifying the rainfall component of their models due to the inadequate rainfall station network. This study has shown the possibility of using satellite-derived information in the estimation and forecasting of areal rainfall. This information may be used to augment the existing observation station network.

In conclusion, the study has for the first time provided some useful information regarding the enormous potential use of satellite-derived data in the estimation of 10-day areal rainfall for specific regions in Kenya. The results from the PCA regionalization show that the satellite-derived data can be used to delineate large-scale spatial anomalies in the rainfall over the study region. Accurate delineation of these anomalies is vital in drought monitoring, flash flood forecasting and general preparedness against extreme weather events.

The recommendations arising from the results of the study are presented in the next section.

5.2 Recommendations and Suggestions for Further Work

The recommendations of this study are targeted towards scientists, policy makers and various professionals in all sectors that are affected by rainfall anomalies leading to too little or too much water. Such sectors include meteorology, hydrology, agriculture, industries, energy, and researchers among many others.

5.2.1 Recommendations to Policy Makers

The source of water for all basic use, including agriculture, domestic and other water resource activities, is rainfall. The planning and management of all rainfall-dependent socio-economic activities rely on accurate projections of rainfall patterns of a given region. The effect of extreme rainfall anomalies can be devastating as is illustrated by the impacts of the 1997/98 El Nino floods and 1998 – 2000 La Nina droughts in Kenya. The results of the study could be used to enhance policies for monitoring of the past and present rainfall patterns together with the projection of future expectations that are vital in early warning and disaster preparedness.

With the launch of new generation of satellites, for example the METEOSAT Second Generation (MSG), a large volume of very useful high-resolution data will become available that would further enhance the skill of the rainfall diagnostic and prognostic models. There is a need for the country to develop the capacity to fully utilize this data and those that are currently available. The capacity development involves the setting up of institutions, the relevant computer hardware and the training of personnel to develop the required software.

Due to the expected varied applications of the satellite-derived data, the government should set up a National Coordinating Office charged with the task of coordinating all efforts in application of the satellite-derived data. The functions of this office would include:

- Receiving and releasing, to the relevant sectors, all the early warning information emanating from the various institutions dealing with satellite applications.

- Running campaigns to sensitize the policy makers and the public about the benefits of satellite-derived information by emphasizing the role of these information in the monitoring of the environmental degradation, climate variability and change, and applications to socio-economic activities among others.
- Coordinate capacity building programs and technological achievements in the use of satellite-derived data.
- Get into alliances with neighboring countries to form a regional organization with the objective of launching a meteorological/environmental satellite for the region.

5.2.2 Recommendations to Meteorology and Hydrology Sectors

The existing rainfall observation station network is not optimally adequate to give a complete coverage of the study area. Some remote and inaccessible areas do not have any representative stations. The weather forecasts have, therefore, been made for large representative homogenous regions. The rainfall component in the hydrological models has also been difficult to quantify for the same reason as above. The results of the study indicate the viability of utilizing satellite-derived data to give a measure of the rainfall. It is recommended that in developing models for meteorological and hydrological applications, including the monitoring of droughts and catchment floods, meteorologists and hydrologists should incorporate the satellite derived information for improved accuracy.

5.2.3 Recommendations to Agriculture Sector

Currently the most commonly utilized satellite-derived data by the agricultural sector are the Normalized Vegetation Indices (NDVI). This research indicates that CCD data could also be used to monitor cumulative rainfall deficits that could provide vital indices for the monitoring of agricultural droughts.

5.2.4 Recommendations to Researchers

One of the major problems in this study stemmed from the relatively short duration of satellite data. For a more complete study, a longer duration of data is desirable. Using a longer duration of satellite data, regionalization should be comprehensively done so as to have better homogeneous zones derived and the development of more stable regression models.

From the results of the skill of the models it can be noted that the variance in rainfall explained by the models are relatively low. These low variances could be related to the poor knowledge of the linkages between rain gauge rainfall, CCD and TPW data. They could also be due to the use of a single threshold temperature for CCD data for the whole study region and period. This study used a climatological approach in discussing the results. However there are certain cloud characteristics that control the precipitation processes. These include cloud time scales, cloud vertical velocities, cloud liquid-water content, cloud temperature, and cloud turbulence (Cotton and Anthes, 1989). A future study, that incorporates the physical and dynamical aspects of clouds, should incorporate all these characteristics in a bid to improve the model skills.

Finally, with the advent of the second generation of satellites, more information with better spatial and temporal resolutions will become available. More studies, especially with reference to TPW, should be taken regarding the potential applications of satellite-based methods. This may lead to higher skills in the derived indices that could improve the monitoring of positive and negative stress that may be associated with too much and/or too little water and other extreme climatic events that often have some socio-economic impacts in Kenya.

6.0 ACKNOWLEDGEMENT

My sincere appreciation goes to my supervisors, Prof. L. A. Ogallo and Dr. N. J. Muthama, for their advice, corporation and valuable guidance during the duration of this research. Further gratitude is extended for their constant reading of the manuscripts and offering of very valuable suggestions.

I am most grateful to DAAD (German Academic Exchange Service) and the University of Nairobi for providing the scholarship that made the pursuance of this study possible. I am also indebted to the World Meteorological Organization (WMO) for providing a fellowship that enabled me to travel and stay in North Carolina State University (NCSU) while accessing and extracting the remote sensing data used in the study. My appreciation is also extended to Prof. F. Semazzi of Department of Marine, Earth and Atmospheric Sciences, NCSU, for arranging for computer time and office space during this visit. I would also like to thank Mr. E. Mukolwe, the permanent representative to WMO of Kenya, for arranging for this fellowship.

My appreciation is also extended to the Kenya Meteorological Department, for providing the rainfall data, and the Regional Center for Services in Surveying, Mapping and Remote Sensing for the provision of the Cold Cloud Duration data.

I would also like to thank my colleagues and all members of staff in the Department of Meteorology, University of Nairobi for the many useful discussions and support during the period of this study.

Last, but not least, I wish to convey special gratitude to my wife, Victoria, and our daughter, Ginger, for their encouragement, patience and support during the entire duration of this study.

7.0 REFERENCES

Adler, R. F., Huffman, G. J. and Keehn, P. R. (1994): Global rain estimates from microwave adjusted geosynchronous IR data. *Remote Sensing Rev.*, **11**, 125-152.

Adler, R.F and Mack, R.A. (1984): Thunderstorm cloud height- rainfall rate relations for use with rainfall estimation techniques. *J. Clim. Appl. Meteor.*, **23**, 280 - 296.

Adler, R.F and Negri, A.J. (1988): A satellite infrared technique to estimate tropical convective and stratiform rainfall. *J. Appl. Meteor.* **27**, 30 - 51.

Akaike, H. (1973): Information theory as an extension of the maximum likelihood principle. *Proc.* 2nd *Int. Symp. On Information Theory. Akademiai Kindo, Budapest.*

Allison, L., Rodgers, E., Wilheit, T. and Fett, R. (1974): tropical cyclone rainfall as measured by the Nimbus 5 ESMR. *Bull. Amer. Met. Soc.* 55, 1074 - 1089.

Alusa, A. L. and Mushi, M. T. (1974): A study of the onset, duration and cessation of the rains in East Africa. *Int. Trop. Meteorol. Meeting, Amer. Meteorol. Soc.*, 3-14.

Ambenje, P. G., Atheru, Z. K. and Degefu, W. (1993): An overview of the rainfall patterns in Eastern and Southern Africa during the period March 1991 to September 1992. *Proc.* 1st *Int. Conf. Of African Meteorol. Soc.*, 482-492.

Arkin, P. A. and Ardanuy, P. E. (1989): Estimating climatic-scale precipitation from space: A review. *J. Climate.* **2**, 1229-1238.

Arkin, P.A and Meisner, B.N. (1987): The relationship between large-scale convective rainfall and cold cloud cover over the Western Hemisphere during 1982-84. *Mon. Wea. Rev.*, **115**, 52 - 74.

Asnani, G. C. (1993): Tropical meteorology. *Noble Printers Pvt. Ltd., Pune*-411002 (*India).* 1202pp.

Austin, G.L (1981): Combining satellite and radar data for the short range forecasting of precipitation. *Proc. IAMAP Symp. on Satellite Hydrology, Hamburg,* 25 - 28 *Aug.* 1981.*(ESA SP-165), June* 1981.

Barnett, T. P. and Preisendorfer P. (1987): Origins and levels of monthly and seasonal forecast skill for United States surface air temperatures determined by canonical correlation analysis. *Mon. Wea. Rev.*, **115**, 1825-1850.

Barnston, A. G. and Smith, T. M. (1996): Specification and prediction of global surface temperature and precipitation from global SST using CCA. *J. Climate* **9,** 2660-2697.

Barrett E.C. (1980): Satellite improved rainfall monitoring by cloud indexing methods: operational experience in support of locust survey and control. *Proc. AWRA Symposium on Satellite Hydrology, Sioux Falls, S.D, June*, 1979.

Barrett, E.C. and D'Souza, G. (1986): An objective monitoring method for African rainfall based on METEOSAT visible and infrared images. *Proc. ISLSCP Conf., Rome, Italy,* 2 - 6 *Dec.* 1985. *(ESA SP*-248, *May* 1985*).*

Barrett, E.C., D'Souza, G., Kidd, C. and Palmer, H. (1989a): Rainfall monitoring by passive microwave satellite, radar and rain gauge: results from Kenya and the British Isles. *Annual Rept to the U.S Dept of Commerce under Co-operative Agreement No.*_NA86AA-H-RA001 (*Amendment No.* 4).

Barrett E.C., Kidd, C. and Bailey, J. O. (1987): The use of SMMR data in support of the Bristol/NOAA Interactive Scheme (BIAS) for satellite-improved rainfall monitoring. *Annual Rept. to the U.S. Dept. of Commerce under Co-operative Agreement No.* NA86AA-H-RA001.

Barrett E.C., Kidd, C. and Palmer, H. (1989b): A passive microwave satellite technique for rainfall monitoring over the British Isles and Surrounding Seas. *Satellite Remote Sensing in*

Hydrology and Water Management, Stage III, *Part* 2: *Rept. To the US dept. of Environment.*

Barrett, E.C. and Martin, D.W. (1981): The use of satellite data in rainfall monitoring. *Academic Press, London* (1981). 340 pp.

Barring, L. (1988): Regionalization of daily rainfall in Kenya by means of common factor analysis. *J. Climatol.*, **8**, 371-389.

Barring, L. (1987): Spatial patterns of daily rainfall in central Kenya: Application of principal component analysis, common factor analysis and spatial correlation. *J. Climatol.*, **7**, 267-289.

Basalirwa, C. P. K. (1991): Rain gauge network designs for Uganda. *Ph.D. Thesis, Dept. Meteorol., University of Nairobi, Kenya.*

Basalirwa, C. P. K. (1990): Estimation of areal rainfall in some catchments of Upper Tana River. *MSc. Thesis, University of Nairobi, Kenya.*

Basalirwa, C. P. K., Odiyo, J. O., Mngodo, R. J. and Mpeta, E. J. (1999): The climatological regions of Tanzania based on the rainfall characteristics. *Intl. J. Climatol.* **19**, 69-80.

Bates, J. J. (1991): High-frequency variability of SSM/I derived wind speed and moisture during intraseasonal oscillation. *J. Geophys. Res.*, **96**, 3411-3423.

Battan, A.J. (1973): Radar observation of the atmosphere. *The University of Chicago Press, Chicago and London.* 324pp.

Beltrando, G. (1990): Space-time variability of rainfall in April and October-November over East Africa during the period 1932-1983. *Intl. J.Climatol.*, **10**, 691-702.

Bengtsson, L., Kanamitsu M., Kallberg P. and Uppala S. (1982): FGGE 4-dimensional data assimilation at ECMWF. *Bull. Amer. Meteorol. Soc.*, **63**, 29-43.

Birch, M. W. (1964): A new proof of the Pearson-Fischer theorem. *Ann. Math. Stat.*, **35**, 818-824.

Burnham, K. P. and Anderson D. R. (1998): Model selection and inference.: A practical information-theoretic approach. *Springer-Verlag, New York Inc.* 353pp.

Callis, L. S. and LeComte, M..D. (1987): Operational use of satellite imagery to estimate rainfall in the Sahelian Countries of Africa. *Proc. 5th. Joint Meeting Incorporating the 18th. Conference on Agricultural and Forest Meteorology and the 8th. Conference on Biometeorology and Aerobiology, Dept.* 15 -18, 1987, *West Lafayette.*

Cattell, R.B. (1966): The Scree test for the number of factors. *Multivar. Behav. Res.*, **1**, 245-259.

Cattell, R.B. (1958): Extracting the correct number of factors in factor analysis. *Edu. Psychol. Meas.* **18**, 791-837.

Cavalieri, D. J., Crawford, J. P., Drinkwater, M. R., Eppler, D. T., Farmer, L. D. and Jentz, R. R. (1991): Aircraft, active and passive microwave validation of sea ice concentration from Defense Meteorological Satellite Program (SSM/I). *J. Geophys. Res.*, **96**. C12, 21989-22008.

Cherna, E., Bellon, A., Austin, G.L and Kilambi, A. (1985): An objective technique for the delineation and extrapolation of thunderstorms from GOES satellite data. *J. Geophysical Res.*, **90**, 6203 - 6210.

Cherry, S. (1996): Singular value decomposition analysis and canonical correlation analysis. *J. Climate*. **9**, 2003-2009.

Child, D. (1990): The essentials of factor analysis. *Cassell Educational Ltd., Second Edition.* 120pp.

Chiu, L. S. (1988): Rain estimation from satellites: Areal rainfall - rain area relations. *Proc. 3rd. Conference on Satellite Meteorology and Oceanography, Feb* 1 - 5, 1988, *Anaheim, Ca.*

Clarke, G. M. and Cooke, D. (1992): A basic course in statistics. *Educational Low Priced Books Scheme.* 3rd *Edition.*451pp.

Cochran, W. G. (1967): Statistical methods. *Oxford and IBH Publishing Co.* 593pp.

Cohen S.J. (1983): Classification of 500-mb height anomalies using obliquely rotated principal components. *J. Clim. Appl. Meteorol.*, **22**, 1975.

Cotton, W. R. and Anthes, R. A. (1989): Storm and cloud dynamics. *Academic press, Inc., International Geophysics Series.* 883pp.

Craddock, J.M. and Flood, C.R. (1969): Eigenvectors for representing the 500-mb geopotential surface over the Northern Hemisphere. *Quart. J. Roy. Meteorol. Soc.*, **95**, 576.

Davies, T. D., Vincent, C. E. and Beresford, A. K. C. (1985): July-August rainfall in west-central Kenya. *J. Climatol.* **5,** 17-33.

Degene, T. (1999): Seasonal rainfall prediction over Ethiopia for March-May 1999 using empirical statistical methods. *DMCN: Proc. 1st. Capacity Building and Training Workshop for the Greater Horn of Africa.* 11 January – 5 February, 1999, Nairobi, Kenya.

DeGroot, M. (1986): Probability and statistics. 2nd *Edition. Addision-Wesley Publishing Company, Reading, Massachusetts.* 723pp.

Dingman, H. F., Miller, C. R. and Eyman, R. K. (1964): A comparison between two analytic rotational solutions where the number of factors in indeterminate. *Behav. Sci.* **9**, 76 – 80.

Doneaud, A. A., Miller, R. J., Vonder-Haar, T.H. and Laybe, P. (1987): The Area-Time-Integral technique to estimate convective rain volumes over areas applied to satellite data - a preliminary investigation. *J. Clim. Appl. Meteor.*, **26**, 156 - 169.

Dugdale, G. (1990): METEOSAT pixel geometry. *FAO training workshop on estimating rainfall over IGADD region using remote sensing techniques. February, 1990, Nairobi, Kenya.*

Dugdale, G., Flitcroft, I.D. and McDougall, V. D. (1987): The calibration and interpretation of METEOSAT based estimates of the Sahelian rainfall. *EUMETSAT; Proc. 6th. METEOSAT User's Meeting, Amsterdam, Nov.*, 1986.

Dugdale, G and Milford, J. R. (1985): Rainfall estimation over the Sahel using METEOSAT thermal infrared data. *Proc. Conference on Parameterization of Land Surface Characteristics, ISLSCP, Rome, Dec.*, 1985.

Dugdale, G. and Milford, J. R. (1987): Rainfall mapping over Southern Africa in 1987. *Rept. to F.A.O of the United Nation, Remote Sensing Center, AGR Division Project* GCP/INT/432/NET.

Ehrendorfer, M. (1987): A regionalization of Austria's precipitation climate using principal component analysis. *J. Climat.*, **7**, 71-89.

Ferraro, R. R. (1997): Special Sensor Microwave Imager derived global rainfall estimates for climatological applications. *J. Geophys. Res.*, **102**, D14, 16715-16735.

Ferraro, R. R. and Marks, G. F. (1995): The development of SSM/I rain-rate retrieval algorithms using ground-based radar measurements. *J. Atmos. And Oceanic Techn.*, **12**, 755-770.

Ferriday, J. G. and Avery, S. K. (1994): Passive microwave remote sensing of rainfall with SSM/I: Algorithm development and implementation. *J. Appl. Meteorol.*, **33**, 1587-1596.

Folland, C. K. (1983): Regional scale inter-annual variability of climate: A northwest European perspective. *Meteorol. Mag.*, **112**, 163-187.

Follansbee, W. A. (1973): Estimation of daily precipitation from satellite cloud photographs. *NOAA Tech. Memo., NESS* 44, *Washington D.C*, 39pp.

Fremming, D. (1970): Notes on Easterly disturbances affecting East Africa. *E.A. Met. Dept. Tech. Memo.*, No. 13.

Goodberlet, M. A., Swift, C. T. and Wilkeson, J. C. (1989): Remote sensing of ocean surface winds with the SSM/I. *J. Geophys. Res.*, **94**, 14547-14555.

Greenwald, T. J., Stephens, G. L., Vonder-Haar, T. H. and Jackson, D. L. (1993): A physical retrieval of cloud liquid water over the global oceans using SSM/I observations. *J. Geophys. Res.*, **98**, 18471-18488.

Grody, N. C. (1991): Classification of snow cover and precipitation using the Special Sensor Microwave/Imager (SSM/I). *J. Geophys. Res.*, **96**, D4, 7423-7435.

Grody, N.C. (1984): Precipitation monitoring over land from satellites by microwave radiometry. *Proc. International Geoscience and Remote Sensing Symposium (AGERSS, 1984), Strasbourg*, ESA SP - **215**, 417 -423.

Gruber, A. (1973): Estimating rainfall in areas of active convection. *J. Appl. Meteor.*, **12**, 110 - 118.

Harman, H. H. (1967): Modern factor analysis. *University of Chicago Press, Chicago and London*, 474pp.

Hastenrath, S. (1991): Climate dynamics of the tropics. *Atmospheric Sciences Library. Kluwer Academic Publishers.* 488pp.

Hastenrath, S., Nicklis, A. and Greischar, L. (1993): Atmospheric-hydrospheric mechanisms of climate anomalies in the Western equatorial Indian Ocean. *J. Geophys. Res.*, **98**, 20219-20236.

He, Y. and Barnston, A. G. (1996): Long-lead forecasts of seasonal precipitation in the tropical Pacific Islands using CCA. *J. Climate*, **9**, 2020-2035.

Hogg, R. V. and Craig, A. T. (1970): Introduction to mathematical statistics. 4th *Edition, Macmillan Publishing Co., New York.* 438pp.

Hong, Y., Wilheit, T. T. and Russell, W. R. (1997): Estimation of monthly rainfall over oceans from truncated rain-rate samples: Application to SSM/I data. *J. Atmos. And Oceanic Techn.* **14**, 1012-1022.

Huffman, G. R., Adler, R. F., Rudolf, B., Schneider, U. and Keehn, P. R. (1995): Global precipitation estimates based on a technique for combining satellite-based estimates, rain gauge analysis and NWP model precipitation information. *J. Climate*, **8**, 1284-1295.

Indeje, M., Semazzi, F.H.M., and Ogallo, L.J (2000): ENSO signals in East African seasons. *Intl. J. Climatol.*, **20**, 19-46.

Ininda, J. M. (1994): Numerical simulation of the influence of the sea surface temperature anomalies on the East African seasonal rainfall. *Ph.D. Thesis, Dept. Of Meteorol., University of Nairobi, Kenya.*

Jolliffe, I.T. (1986): Principal component analysis. *Springer-Verlag, New York.*

Jolliffe, I. T. and Sarria-Dodd, D. E. (1994): Early detection of the start of the wet season in tropical climates. *J. Climatol.*, **14**, 71-76.

Kaiser, H.F. (1959): Computer program for Varimax rotation in factor analysis. *Educ. Psych. Meas.*, **19**, 413 -426.

Kendall, M. G. and Stuart, A. (1961): The advanced theory of statistics, Vol.2: Inference relationship. *Charles Griffin (Ed)*, 676pp, London.

Kidd, C. (1998): On rainfall retrieval using polarization-corrected temperatures. *Int. J. Remote Sensing*, **19**, 981-996.

Kidd, C. and Barrett, E.C. (1990): The use of passive microwave imagery in rainfall monitoring. *Remote Sensing Reviews*, **4**, 415 - 450.

Kidder, S. Q. and Vonder-Haar, T. H. (1995): Satellite meteorology: An introduction. *Academic Press*, 456pp.

Kullback, S. and R. A. Liebler (1951): On information and sufficiency. *Annals of Mathematical Statisitics*, **22**, 79-86.

Kite, G. W. (1978): Frequency and risk analyses in hydrology. *Water Resources Publications, Fort Collins, Colorado, USA*, 2nd *Printing*. 224pp.

Kuo, H. L (1965): On formation and intensification of tropical cyclones through latent heat by cumulus convection. *J. Atmos. Sci.*, **22**, 40 - 63.

Kutzbach, J. E (1967): Empirical eigenvectors of sea-level pressure, surface temperature and precipitation complexes over North America. *J. Appl. Meteorol.* **6**, 791-802.

Liu, G. and Curry, J. A. (1992): Retrieval of precipitation from satellite microwave measurement using both emission and scattering. *J. Geophys. Res.*, **97**, D9, 9959-9974.

Lorenz, E.N. (1956): Empirical orthogonal functions and statistical weather prediction. *Sci. Rep. No.* 1, *Statist. Forecasting Proj., Dept. Meteorol., MIT*, 49pp.

Martin, D.W. and Howland, M.R. (1986): A geostationary satellite technique for estimating daily rainfall in the tropics. *J. Clim. Appl. Meteor.*, **25**, 184 -195.

Martin, D.W. and Scherer, W. D. (1973): Review of satellite rainfall estimation methods. *Bull. Amer. Met. Soc.*, **54**, 661 - 674.

Matarira, C. H. and M. R. Jury (1992): Contrasting meteorological structure of intra-seasonal wet and dry spells in Zimbabwe. *Int. J. Climat.*, **12**, 165-176.

Mitchel, W. and Smith, E. A. (1987): Precipitation discrimination from satellite infrared temperatures over the CCOPE Mesonet region. *J. Clim. Appl. Meteor.*, **26**, 687 -697.

Mishra, D. K., Kalsi, S. R. and Jain, R. K. (1988): The estimation of heavy rainfall using INSAT-1B satellite data. *Mausam*, **39**, 383 - 392.

Morrison, D. F. (1976): Multivariate statistical methods. *McGraw Hill*, 415pp.

Mugnai, A. and Smith, E. A. (1988): Radiative transfer to space through a precipitating cloud at multiple microwave frequencies, Part I: Model definition. *J. Appl. Meteor.*, **27**, 1055 - 1073.

Mukabana, J. R. (1992): Numerical simulation of the influence of the large-scale monsoon flow on the weather patterns over Kenya using a three-dimensional limited area model. *Ph.D. Thesis, Dept. Of Meteorol., University of Nairobi, Kenya.*

Mukabana, J. R. and Pielke, R. A. (1996): Investigating the influence of synoptic-scale mosoonal winds and mesoscale circulation on diurnal weather patterns over Kenya using a Mesoscale Numerical Model. *Mon. Wea. Rev.* **124**, 224-243.

Muruyama, T., Nitta, T. and Tsuneoka, Y. (1986): Estimation of monthly rainfall from satellite observed cloud amount in tropical Western Pacific. *J. Met. Soc. of Japan*, **64**, 147 - 153.

Negri, A.J and Adler, R.F (1987a): Infrared and visible satellite rain estimation. Part I: A grid cell approach. *J. Clim. Appl. Meteor.*, **26**, 1553 - 1564.

Negri, A.J and Adler, R.F (1987b): Infrared and visible satellite rain estimation. Part II: Cloud model approach. *J. Clim. Appl. Meteor.*, **26**, 1565 - 1576.

Njau,L.N (1982): Tropospheric wave disturbances in East Africa. *M.SC. Thesis, Dept. of Met., University of Nairobi.*

North, G.R., Bell, T. L., Cahalan, R. F. and Moeng, F.J (1982): Sampling errors in estimation of empirical orthogonal functions. *Mon. Wea. Rev.*, **110**, 699-706.

Nyakwada, W., Gathura, J. G. and Kariuki, J. M. (1999): Seasonal rainfall forecast for March-May 1999 over Kenya using empirical statistical models. *DMCN: Proc. 1st. Capacity Building Training Workshop for the Greater Horn of Africa*, 55-77.

Ogallo, L. J. (1989): The spatial and temporal patterns of East African seasonal rainfall derived from principal component analysis. *Int. J. Climatol.*, **9**, 145-167.

Ogallo, L. J. (1988): Relationship between seasonal rainfall in East Africa and the Southern Oscillation. *J. Climate*, **8**, 31-43.

Ogallo L. J. (1987): Climate data processing. *Paper presented during Regional Training Seminar for National Instructors of RA IV*, 26 *October* – 6 *November* 1987, *Niamey, Niger).*

Ogallo, L. J. (1983): Temporal fluctuations of seasonal rainfall patterns in East Africa. *Mausam*, **35**, 175 - 180.

Ogallo L. J. (1982): Homogeneity of the rainfall records over East Africa. *Kenya Met. Dept. Research Rep. No.* 4/1981.

Ogallo L. J. (1980): Regional classification of East African rainfall stations into homogeneous groups using the method of Principal Component Analysis. *Stat. Climatology. Devel. In Atmos. Sci.* **13**, 255-266.

Ogallo, L. J., Okoola, R. E. A. and Wanjohi, D. N. (1994): Characteristics of quasi-biennial oscillation over Kenya and their predictability potential for seasonal rainfall. *Mausam*, **45**, 57-62.

Okeyo, A. E. (1987): The influence of Lake Victoria on the convective activities over the Kenya highlands. *J. Meteorol. Soc. Japan*, special volume, 689-695.

Okoola, R. A. E. (1999): A diagnostic study of the Eastern Africa monsoon circulation during the Northern Hemisphere spring season. *Intl. J. Climatology*, **19**, 143-168.

Okoola, R. A. E. (1998): Spatial evolutions of the active convective patterns across the equatorial Eastern Africa region during the northern hemisphere spring season using outgoing long wave radiation records. *Meteorol. and Atms. Phys.*, **66**, 51-63.

Okoola, R. E. A. (1996): Space-time characteristics of the ITCZ over equatorial eastern Africa during anomalous rainfall years. *Ph.D. Thesis, Dept. of Meteorol., University of Nairobi, Kenya.*

Opere, A. O. (1998): Space-time characteristics of streamflow in Kenya. *Ph.D. Thesis, University of Nairobi, Kenya.*

Oort, A. H. (1983): Global atmospheric circulation statistics, 1958-1973. *NOAA Professional Paper No.* 14, 180pp.

Ouma, G.O. (1988): Estimation of areal rainfall from satellite data. *M.SC. Thesis, Dept. of Met., University of Nairobi.*

Ouma, G. O., Kumar, O. S. R. U. B. and Ogallo, L. J. (1995): Satellite remote sensing estimates of point and areal rainfall over some parts of East Africa. *J. Afri. Meteorol. Soc.*, **2**, 80-92.

Prasad, K. D. and Sing, S. V. (1996): Forecasting the spatial variability of the Indian monsoon rainfall using canonical correlation. *Int. J. Climat.*, **16**, 1379-1390.

Purdom, J.F.W (1981): Combining satellite and conventional data for very short range forecasting purposes. *Proc. IAMAP Symposium, Hamburg,* 25-28 *June (ESA SP-165, June,* 1981*).*

Randel, D. L., Vonder-Haar, T. H., Ringernd, M. A., Stephens, G. L., Greenwald, T. J. and Combs, C. L. (1996): A new global water vapor data set. *Bull. Amer. Meteorol. Soc.*, 77, 1233-1246.

Reale, A. L., Goldberg, M. D. and Daniels, J. M. (1989): Operational TOVS soundings using a physical approach. *Proc. IGARRS* 1989 12th *Canadian Symp. On Remote Sensing, Vancouver, B. C., Canada, IGARRS,* 2653-2657.

Reynolds, R. W. (1988): A real-time global sea surface temperature analysis. *J. Climate,* **1**, 75-86.

Richman, M. B. (1986): Rotation of principal components. A review article. *J. Climatol.*, **6**, 293-335.

Richman, M. B. (1981): Obliquely rotated principal components: An improved meteorological map typing technique? *J. Appl. Meteorol.*, **20**, 1145-1159.

Ropelewski, C. F. and Halpert, M. S. (1987): Global and regional scale precipitation patterns associated with El-Nino/Southern Oscillation. *Mon. Wea. Rev.*, **115**, 1606-1626.

Schubert, S. D., Rood, R. B. and Pfaendner, J. (1993): An assimilated data set for earth science applications. *Bull. Amer. Meteorol. Soc.*, **74**, 2331-2342.

Scofield, A. R. (1987): The NESDIS operational convective precipitation estimation technique. *Mon. Wea. Rev.*, **115**, 1773 - 1792.

Semazzi, F. H., Burns, B., Lin, N. H. and Schemm, J. K. (1996): A GCM study of the teleconnection between the continental climate of Africa and global sea surface temperature anomalies. *J. Climate*, **9**, 2480-2497.

Short, D. A., Wolf, D. B., Rosenfeld, D. and Atlas, D. (1989): A rain gauge, radar and satellite simulation study of the estimation of convective rainfall by Area-Time- Integrals. *Proc. 4th. Conference on Satellite Meteorology, May* 1989, *San Diego, Ca.*

Simpson, J. and Wiggert, V. (1969): Models of precipitating cumulus towers. *Mon. Wea. Rev.*, **97**, 471 - 489.

Smith, W. L. and Woolf, H. M. (1984): Improved vertical sounding from amalgamation of polar and geostationary radiance observations. *Proc. Conf. On Satellite Meteorology/Remote sensing/Applications. Clearwater Beach, FL., Amer. Meteorol. Soc.*, 45-48.

Sombroek, W.G., Braun H.M.H. and Van der Pouw, B.J.A (1982): Exploratory soil and agro-ecological zone map of Kenya. *Exploratory soil survey report E*1, *Kenya Soil Survey, Nairobi.*

Stephens, G. L., Jackson, D. L. and Bates, J. J. (1994): A comparison of SSM/I and TOVS column water vapor data over the global oceans. *Meteorol. Atms. Phys.* **54**, 183-201.

Stone, M. (1974): Cross-validatory choice and assessment of statistical predictors. *J. Roy. Stat. Soc.*, **B36**, 111-147.

Thompson, B.W. (1957): Some reflections of equations and tropical forecasting. *E.A Met. Dept. Tech. Memo.*, No. 7

Tjemkes, S. A., Stephens, G. L. and Jackson, D. L. (1991): Spaceborne observation of columnar water vapor: SSM/I observations and algorithm. *J. Geophys. Res.*, **96**, 10941-10954.

Tsonis, A. A. and Isaac, G. A. (1987): On a new approach for instantaneous rain area delineation in the mid-latitudes using GOES data. *J. Clim. Appl. Meteor.*, **24**, 1208 - 1218.

Tuller, S. E. (1968): World distribution of the mean monthly and annual precipitable water. *Mon. Wea. Rev.*, **96**, 785-797.

Turpenein, O. M., Abedi, A. and Belhouane, W. (1987): Determination of rainfall with ESOC Precipitation Index. *Mon. Wea. Rev.*, **115**, 52 - 74.

Ward, M. N. (1992): Provisionally corrected surface wind data, worldwide ocean-atmosphere surface fields, and Sahelian rainfall variability. *J. Climate*, **5**, 454-475.

Webster, P. J. (1994): The annual cycle and the predictability of the tropical coupled ocean-atmosphere system. *Meteorol. and Atmos. Phys.* **56**, 33-35.

Weng, F. and Grody, N. C. (1994): Retrieval of cloud liquid water using the Special Sensor Microwave Imager (SSM/I). *J. Geophys. Res.*, **99**, D12, 25535-25551.

Weng, F., Ferraro, R. R. and Grody, N. C. (1994): Global precipitation estimates using Defense Meteorological Satellite Program F10 and F11 Special Sensor Microwave Imager data. *J. Geophys. Res.*, **99**, D7, 14493-14502.

Werbowtzki, A. (1981): Atmospheric sounding user's guide. *NOAA Tech. Rep. NESS* 83, *US Dept. Of Commerce, Washington, D.C.*, 82pp.

Wilheit, T. T., Chang, A.T.C., Rao, M. S. V., Rodgers, E. B and Stone, J. S. (1977): A satellite technique for quantitatively mapping rainfall rates over the oceans. *J. Appl. Meteor.*, **16**, 551 - 560.

Wilheit, T. T., Theon, J., Shenk, W., Allison, L. and Rodgers, E. (1973): Meteorological interpretation of the images from Nimbus 5 ESMR. *J. Appl. Meteor.*, **15**, 168 - 172.

Wilks, D. S. (1995): Statistical methods in the Atmospheric Sciences: An introduction. *Academic Press, New York*, 453pp.

WMO (1974): Guide to hydrological practices. *Third Edition, WMO* 168. *Secretariat of WMO, Geneva, Switzerland.*

Wu, R., Weinman, J. A. and Chin, R. T. (1985): Determination of rainfall rates from GOES satellite images by a pattern recognition technique. *J. Atmos. and Oceanic Technology*, **2**, 314 - 330.

Wylie, D. P. (1979): An application of a geostationary satellite rain estimation technique to an extratropical area. *J. Appl. Meteor.*, **18**, 1640 - 1648.

Xubin, Z. (1999): The relationship among precipitation, cloud-top temperature and precipitable water over the tropics. *J. Climate*, **12**, 2503-2514.

Yevjevich, V. (1972): Probability and statistics in hydrology. *Water Resources Publications, Fort Collins, Colorado, USA.* 303pp.

Yin X. and Nicholson, S. E (2000): On the feasibility of using a lake water balance model to infer rainfall: an example of Lake Victoria. *Hydrol. Sci. J.*, **45**, 75-96.

Yu, Z. P., Chu, P. S. and Schroeder, T. (1997): Predictive skills of seasonal to annual rainfall variations in the US affiliated Pacific Islands: Canonical correlation analysis and multivariate principal component regression approaches. *J. Climate*, **10**, 2586-2599.

Zeng, X. (1999): The relationship among precipitation, cloud-top temperature, and precipitable water over the tropics. *J. Climate*, **12**, 2503-2514.